ABSTRACT

WANG, CONGJIAN. Exact-to-Precision Generalized Perturbation Theory for Nuclear Reactor Analysis. (Under the direction of Dr. Hany S. Abdel-Khalik.)

This dissertation is devoted to developing a unified framework under the name of exact-to-precision generalized perturbation theory (E_PGPT) which combines perturbation theory with reduced basis methods and range finding algorithms for reactor analysis and design calculations. This framework places high premium on reducing the associated computational overhead via the reduced basis methods in order to enable the use of perturbation theory in routine reactor calculations. For this work, E_PGPT will be used to evaluate the variations in the neutron flux due to various perturbations such as cross sections perturbations, enrichment variations, poison loading, temperature, etc., at the lattice physics level, often referred to as assembly level calculations. To ensure that the E_PGPT predications are robust, range-finding algorithm is utilized to make quantitative bounding statements about the errors in the predications of responses for all possible model perturbations. In contrast to traditional generalized perturbation theory, E_PGPT allows one to efficiently calculate higher orders of variations for the responses of interest with very inexpensive computational cost.

The major focus of this research is to develop an efficient computational algorithm employing the E_PGPT to address the explosion in dimensionality whether at the input parameter level or at the response level. Although the proposed algorithm is only demonstrated by using radiation diffusion/transport models for the purpose of reactor design analysis, it can be applied to many different problems because of it is generic in nature. By way of examples, these new developments could be employed in core simulation to accurately estimate the few-group cross sections variations resulting from perturbations in neutronics and thermal-hydraulics core conditions. These variations are currently being

described using a look-up table approach, where thousands of assembly calculations are performed to capture few-group cross sections variations for the downstream core calculations. Other applications include the efficient evaluation of surrogates for applications that require repeated model runs such as design optimization, inverse studies, uncertainty quantification, and online core monitoring.

Exact-to-Precision Generalized Perturbation Theory for Nuclear Reactor Analysis

by
Congjian Wang

A dissertation submitted to the Graduate Faculty of
North Carolina State University
in partial fulfillment of the
requirements for the Degree of
Doctor of Philosophy

Nuclear Engineering

Raleigh, North Carolina

2013

APPROVED BY:

_____	_____
Dr. Hany S. Abdel-Khalik Committee Chair	Dr. Paul J. Turinsky
_____	_____
Dr. John Mattingly	Dr. Ralph C. Smith

DEDICATION

This work is dedicated to my devoted wife Yannan. Throughout this process you have supported me, encouraged me, and always believed in me. This work is also dedicated to my wonderful daughter Lingyu who brings all joys to me.

BIOGRAPHY

Congjian Wang, born on October 31st, 1986, is the second of three siblings of his father Xiangjin Wang and his mother Cuiying Li. He has one older brother and one younger sister. His hometown, Lianyungang, Jiangsu, China, has gotten its reputation from a fictionalized novel, *Journey to the West*, published in 1590 A.D. by Cheng'en Wu. In Wu's legendary stories, the beautiful wild mountain, Huaguoshan meaning *Flowers and Fruits Mountain* located in Lianyungang, was described as the home of a magic monkey transformed from a stone, Wukong Sun also commonly known as the Monkey King, and nourished by Five Elements (i.e. Wood, fire, earth, metal and water), who learns the art of the 72 polymorphic transformations, combat and secrets of immortality. Inspired by Monkey King, Congjian believes that "where there is a will, there is a way".

Congjian left his hometown and went to Tsinghua University for undergraduate study in Beijing in 2005. He graduated from Tsinghua University in 2009 and received his Engineering Bachelor's Degree from the Department of Engineering Physics. His thesis was on Synchronous Circuit Analysis and Design, under the supervision of Professor Yi Wang.

Congjian began his graduate study in the Nuclear Engineering Department at North Carolina State University in August, 2009, working as a research assistant under the supervision of Dr. Hany S. Abdel-Khalik.

Congjian was married to Yannan Bu in April, 2009. His first daughter Lingyu A. Wang was born in April, 2012.

Congjian has won the scholarship of Tsinghua University for the years 2006 and 2007. He has been awarded with “Best Student Paper Award” during the PHYSOR 2012 conference held in Knoxville, Tennessee.

ACKNOWLEDGEMENTS

I would like to express my deep and sincere appreciation to my advisor, Dr. Abdel-Khalik. I have the greatest respect for you as a mentor, teacher, and advisor. Throughout my doctoral program, you were the person I could trust to come to with questions or concerns and somehow you always knew how to make things right. I continue to be impressed by the quality and quantity of patient and constructive feedback; and I have no doubt that my research, writing and overall work are much the better for these.

I would like to thank my committee members: Dr. Mattingly, Dr. Smith, and Dr. Turinsky for their valuable helps and insight comments.

I would like to extend my gratitude and appreciation to Dr. Bang, Dr. Cyrus and Dr. Wu. Thank you for being supports in my journey toward attaining a doctorate and in developing as a professional. I would also like to thank my friends and colleagues for listening, sharing, and laughing with me.

I am deeply grateful to my wife, Yannan. Thank you for tolerating the many late nights and weekends I could not share with you and my devoted daughter. This work would not have been possible without your understanding, patience, encouragement, support, love and taking care of everything at home while I was in school. Thank you is just not enough to express my gratitude and all the sacrifices you made to help pursue this goal.

Finally I must thank my parents, Xiangjin Wang and Cuiying Li, for their love and support through the years. That has always meant the most to me, and helped me when I needed it most.

TABLE OF CONTENTS

LIST OF TABLES

LIST OF FIGURES

CHAPTER 1. INTRODUCTION

1.1 Overview and Motivation for Research

The role of scientific computing has been heavily promoted in many fields to improve understanding the physics of complex engineering systems via computational models in recent years. This is because conducting the experiments can be time-consuming, inflexible, expensive and difficult to repeat, especially for nuclear reactor systems. From an engineering point of view, a computational model is a mathematical representation of the physical system of interest. The model is represented by a set of mathematical equations whose solution can be used to measure the performance of the system. Generally speaking, there are three key elements for a computational model, i.e., parameters, state or state variables, and responses of interest. The parameters, on the other hand, are the inputs of the model; the state describes the basic physical quantity that is calculated by the numerical solution, e.g., flow velocity distribution, temperature distribution, atom displacement, etc.; the responses of interest, in general, are functions of the state and the parameters. In reactor physics analysis, one can use neutron transport/diffusion equation to describe the motions and interactions of neutrons with materials within the reactor core. For this model, the input parameters involve atom densities, microscopic cross sections, and fission yields; the state is denoted as the neutron flux; and the power distributions across the core can be considered as the responses of interest.

Reactor design calculations are mainly focusing on the determination of the neutron flux and power generated inside the reactor core. Given the complex nature of the physics

governing the neutron transport, one must execute reactor calculations many times to characterize the impact of various core conditions on the responses of interest. This proves to be a computationally demanding task given the heterogeneity of reactor design deliberately introduced in support of economical and safety considerations. In nuclear engineering literature, abundance of examples indicates that perturbation theory can be employed to complete this analysis in a computationally efficient manner. That is achieved with the help of an adjoint model - the mathematical dual of the forward model - that calculates an importance function, called the adjoint solution. The adjoint solution calculated at reference condition allows one to estimate the variations in the responses of interest to a given order without re-executing the forward model. A first-order perturbation theory allows one to calculate the linear variations in responses resulting from perturbations in core conditions, often characterized by perturbations in input parameters such as fuel enrichments, cross sections, temperatures, etc. Perturbation theory has also been extended to calculate higher orders of variations when first order of variations is not enough to accurately estimate response variations. The following is a list of typical problems for which the use of perturbation theory has been attempted with varying level of success:

1. Fuel management optimization, e.g., fuel evolution and shuffling analysis, equilibrium cycle optimization;

2. Sensitivity analysis for reaction rates ratios and reactivity coefficients, whose results can be used in uncertainty quantification and data assimilation;

3. Accelerator driven system (ADS) analysis;

4. Control rod worth calculations;

5. Shielding design, i.e., in deep penetration neutron-photon transport calculations;

6. Boundary condition perturbation theory in assembly calculations.

Despite the great theoretical advances recorded in the literature, perturbation theory has not realized its full potential in practice. This is because existing perturbation theory faces two challenges which prohibit its use for real-world reactor calculations. First, to render accurate estimation of response variations for general nonlinear cases, perturbation theory must be able to calculate higher orders of variations for the response of interest. This proves to be as computationally demanding as executing the forward model repeatedly, thereby defeating the use of perturbation theory. Second, because the adjoint solution is intimately tied to the response of interest (as will be shown later), e.g., the total power produced in a given fuel pin, one must independently execute the adjoint model for each response of interest.

This dissertation aims to address these two challenges via a new mathematical framework that combines existing perturbation theory with reduced basis methods used in reduced order modeling and range finding algorithms from linear algebra. This framework will be referred to as Exact-to-Precision Generalized Perturbation Theory (E_PGPT). The idea is that although reactor calculations are inherently complex, our past experience has shown that they depend on few degrees of freedom (DOFs). When properly determined, these DOFs can be used to recast existing perturbation theory into one that efficiently calculates higher orders of variations and be independent of the responses of interest. Range finding algorithms

are employed to determine these DOFs, while reduced basis methods help recast the adjoint model in terms of the identified DOFs rather than the responses of interest. Finally, the descriptive 'Exact-to-Precision' implies the capability to estimate errors in response variations, rather than the order of the variations which can be misleading, especially for nonlinear models.

In the context of reactor calculations, this framework will be used to evaluate the variations in the neutron flux due to various perturbations such as control rod insertion, enrichment variations, poison loading, temperature, etc., at the lattice physics level, often referred to as assembly level calculations. In typical assembly calculations, one executes the flux solver a number of times in the order of 10^5 to capture the impact of all possible variations on the few-group cross sections used in downstream calculations, e.g. if the reactor core is divided into 20 layers for the axial geometry, and one only considers 30 assembly types for each axial layer during 60 depletion time steps. Providing 2 control rods variations (in or out), and 3 different fuel temperatures for all assembly types, the total required number of assemblies calculations would be $20\times30\times60\times2\times3=2.16\times10^5$. The use of our developed framework will significantly minimize this computational cost.

The goal of this dissertation is to enable the completion of engineering analyses which require repeated execution of the models with high accuracy and computational efficiency. Applications like sensitivity analysis (SA), uncertainty quantification (UQ), data assimilation, design optimization, and homogenization techniques could benefit greatly from E_pGPT. The specific objectives of this dissertation are:

1. To develop an efficient perturbation theory algorithm that recognizes the explosion in both the input parameters and responses spaces for reactor physics models;

2. To calculate the exact (with user-defined precision) variations in the responses of interest, rather than estimating a certain order of variation;

3. Enable efficient propagation of non-Gaussian uncertainties through nonlinear models;

The use of EPGPT to achieve these objectives is expected to be advantageous to state of the art techniques for the following reasons:

First, the number of adjoint evaluations needed by EPGPT to capture higher orders of variations is independent of the size of the state phase space. They are determined using a statistical approach that employs only the forward model simulations.

Second, the adjoint model is not dependent on the number or type of responses or the number of input parameters.

Third, unlike existing reduced basis methods, an upper error bound could be established to describe the accuracy of the response variations as they compare to exact response variations calculated using direct forward model perturbations. Moreover, different error bounds for different responses could also be defined by the user depending on the design specifications.

1.2 Literature Review

This dissertation employs EPGPT theory, a hybrid methodology combining the perturbation theory, the reduced basis methods, and the range-finding algorithms to reduce

the computational cost required to calculate the exact responses' variations in support of nuclear reactor design calculations. These three classes of methods have been widely employed by scientists and practitioners from a variety of scientific backgrounds. This section provides a literature review of the state-of-the-art in these three areas, highlighting their advantages, and the limitations to be addressed by the EPGPT theory.

1.2.1 Previous Work on Perturbation Theory

First-order perturbation theory is able to bypass the evaluation of the perturbed state by solving an adjoint model that is related to the unperturbed model, meaning that the adjoint model needs to be executed only once to calculate adjoint function. Response variations with respect to all input parameters could then be evaluated using simple inner product relations involving the forward and adjoint solutions of the unperturbed model. This aspect of perturbation theory has given it a competitive advantage over forward perturbation methods when the number of input parameters is larger than the responses of interest. During the last fifty years, it has been successfully applied to reactor design calculations, e.g., reactor critical calculations, depletion calculations, shielding design, and kinetics problems.

Wigner is often credited as the first to introduce the use of perturbation theory in nuclear engineering calculations (Wigner 1992). As acknowledged by Wigner, additional contributions were introduced by (Usachev 1964). These early contributions were further developed for nuclear applications by (Lewins 1965), (Pomraning 1965), (Gandini 1967), (Stacey 1974), (Cacuci et al. 1980), (Rahnema 1981) and others. Perturbation theory, or its

generalization, i.e., generalized perturbation theory or GPT, has been widely used to perform sensitivity analysis in reactor physics and shielding problems (Abdel-Khalik 2012, Ball 2012, Cacuci 1981a, Rearden 2004). Moreover, it has found its way into standardized computer codes that are available for routine reactor calculations; see for example the computer package SCALE 6.0 (Jessee, Williams & Dehart 2009). The objective of sensitivity analysis is to evaluate the sensitivity coefficients that represent the percentage effect on the response of interest to a percentage perturbation in the nuclear reaction probabilities or cross sections. The sensitivity coefficients could be then used in conjunction with the uncertainties in the cross section data, the cross section covariance data, to determine the uncertainty in the response of interest due to uncertainties in the nuclear cross section library.

It is noteworthy to mention that several GPT formalisms have appeared in the literature. As mentioned by (Gandini 2001), the three most prominent formalisms are: (a). Heuristic generalized perturbation theory (HGPT), first adopted by (Usachev 1964) and then extensively developed by (Gandini 1967); (b). Variational formalism adopted by (Lewins 1965) and (Stacey 1974); (c). Differential formalism proposed by (Oblow 1978) and including the matrix formalism further developed by (Cacuci et al. 1980). An introduction to these three formalisms is given:

(a). Heuristic Generalized Perturbation Theory

(Usachev 1964) developed the perturbation theory, making exclusive use of importance conservation concepts, for linear responses of neutron flux in a reactor working under steady-state conditions. The neutron importance function is corresponding to the contribution of a

given particle, inserted at a given time and a given point of the phase space, to the response of interest. Usachev's formulation was extended to calculate the bilinear responses of the forward and adjoint fluxes, e.g., reactivity worth, reaction ratios and prompt neutron lifetimes, by (Gandini 1967). This approach was then extensively developed by (Gandini 1978a, 1978b, 1981, 1988, 1990, 2001) in static problem, time-dependent problem and nonlinear subcritical, accelerator driven systems, and named as Heuristic Generalized Perturbation Theory (HGPT) by (Gandini 2001).

(b). Variational Formalism

The variational approach, based on variational principles, was developed by (Lewins 1965), (Pomraning 1965), (Stacey 1974) and (Williams 1978). Variational approach provides a strong theoretical basis for generalized perturbation theory, and has a much wider application in reactor physics. (Slesarev, Sirotkin 1971) introduced the variational principles into the finite-difference schemes to solve the neutron transport equation. (Pomraning 1986) employed the variational approach to accurately calculate the mixed boundary conditions for the equilibrium diffusion equation of radiative transfer. This approach was also applied to stochastic radiation transport problems to estimate the average of linear responses of interest by (Su, Pomraning 1994), as well as boundary conditions perturbations in steady state neutron transport calculations (Gheorghiu, Rahnema 1998).

(c). Differential Formalism

The differential approach, based on a formal differentiation of the response considered, was proposed by (Oblow 1976) and extensively developed by (Cacuci et al. 1980). The initial

applications were made in the thermal-hydraulic field by (Oblow 1978). The results, compared with the response surface technique, confirm the expectation on its computational efficiency. A more rigorous formalism of differential approach for the perturbation theory was established, in particular the matrix approach was developed making the use of the same principles employed in differential approach to obtain the importance function (Cacuci et al. 1980). Based on this formalism, (Cacuci, Ionescu-Bujor & Navon 2005) proposed two modern sensitivity analysis approaches, i.e., the adjoint sensitivity analysis procedure and the global adjoint sensitivity analysis procedure, which were successfully applied to two-phase flow models to simulate the thermal-hydraulic characteristics of light water nuclear reactors, and radiative convective model for climate simulation.

It is important to reaffirm that all the formalisms described above lead to identical expressions of the sensitivity coefficients (Greenspan 1975). Each of the above methods has its own merit, variational and differential formalisms provide a strict mathematical framework; while HGPT is a physics oriented approach based on importance conservation concepts. Although a difference in the specific treatment of boundary conditions in these three formalisms can result in one approach being somewhat advantageous in certain type of problems. As also mentioned by (Cacuci et al. 1980), it has always been inherently assumed that they all lead to identical expressions for the sensitivity coefficients. In addition, although the matrix and operator formalisms may lead to adjoint difference equations that are not identical, both formalisms solve consistent numerical approximations of the adjoint differential equation.

Perturbation theory has also been extended by many scientists to account for higher orders of variations when input parameters perturbations are too large to render the accuracy of first-order approach acceptable in reactor design calculations. (Mitani 1973) derived a higher-order perturbation technique for evaluating the reactivity effects consequent to given alterations of reactor system. (Gandini 1978b) developed an explicit higher-order perturbation method in terms of input parameters perturbations for static neutron transport problems. This work was further exploited by (Gandini 1978a) for time dependent systems, e.g., reactor kinetics calculations, depletion calculations. (Greenspan, Gilai 1978) presented a second-order GPT formulation with explicit expressions for the general responses, using the differential sensitivity theory proposed by (Oblow 1978), for altered source-driven systems. This approach was subsequently implemented to evaluate the non-linear effects in cross section sensitivity analysis (Greenspan, Kami & Gilai 1979). (Dubi, Dudziak 1981) provided a general explicit expression for the *n*th-order derivative of neutron flux that utilizes the unperturbed flux, adjoint flux, and a detailed Green's function, all from the unperturbed problem, everywhere in the region of the perturbation. (White, Swanbon 1990) developed an explicit second-order GPT formulation, using a direct correlation technique to obtain a first-order approximation of the perturbed flux distribution, for the perturbed powers in two group diffusion problem. (Kropaczek, Turinsky 1991) introduced a second-order GPT for nodal power prediction during stochastic optimization, (Maldonado, Turinsky & Kropaczek 1995) extended its basis to an advanced nodal method, and furthermore, (Moore, Turinsky 1998) used it to perform perturbed BWR loading pattern calculations that correctly addresses the

strong nonlinear feedbacks of two-phase flow. (Van Geemert 2001) combined the parallelism and higher-order depletion GPT, developed by (Williams 1978), that yields the exact perturbation in the equilibrium cycle solution. In his subsequent study, polynomial function was utilized to approximate the localized flux variation with higher-order accuracy (Van Geemert, Tani 2005). Additionally, higher-order perturbation theory has also been introduced into reactor physics for boundary condition variations since 1999 (McKinley, Rahnema 1999), which is mainly devoted to cross section homogenization to improve the coarse-mesh nodal accuracy (McKinley, Rahnema 2000, McKinley, Rahnema 2002, Rahnema, McKinley 2002).

Classically, there have been three basic approaches for obtaining higher-order approximations for the response variations. In the first approach, one attempts to estimate the perturbed flux explicitly to some higher-order accuracy. The basic idea is to represent the perturbed flux as $\phi = \sum_n \beta_n \Psi_n$, where the sum over n refers to the order of the series expansion, β_n are the coefficient, and the Ψ_n functions are successive higher-order approximations, e.g. eigenfunctions of neutron diffusion/transport equation, Green's functions, polynomial functions, etc. (Gandini 1978b, Dubi, Dudziak 1981, Van Geemert, Tani 2005). The second approach bases on a formal derivation of second-order GPT proposed by (Greenspan, Gilai 1978). It couples the importance functions of first-order GPT with an expression for the first derivative of the flux with respect to the perturbed quantity. This flux derivative is usually expressed as the solution to a generalization fixed-source problem. The third approach, based on iterative scheme, can be employed to acquire the

higher-order accurate to exact results for the perturbed flux (Moore, Turinsky 1998, McKinley, Rahnema 2000, McKinley, Rahnema 2002).

Unfortunately, as higher orders of variations are sought, the computational cost becomes dependent either on the number of input parameters, or the dimension of the space used to describe the forward solution, as one can observe from Table 1-1 (Gandini 1978b, McKinley, Rahnema 2002, Cacuci 2003, Williams 1986). This challenge has limited the use of perturbation theory to linear models and investigative studies only.

Table 1-1. Computational Cost of Perturbation Theory

Perturbation Theory		Method	Number of Simulations
Forward-based	1st-order	Direct Calculation GFM FSAP	$k+1$
	2nd-order	Direct Calculation	$k\times(k+1)/2$
Adjoint-based GPT	1st-order	ASAP	m
	2nd-order or higher-order	(Gandini 1978b)	n
		(Greenspan, Gilai 1978)	$m\times(k+1)$
		(McKinley, Rahnema 2002)	n

- GFM: Green's function method, FSAP: forward sensitivity analysis procedure, ASAP: adjoint sensitivity analysis procedure.
- k: number of input parameters, m: number of responses of interest, n: dimension of system or number of points in the phase space.

Another challenge of perturbation theory is the difficulty in calculating multi-responses or distributed responses. This is based on the fact that the evaluation of the adjoint function is traditionally based on a given single response, implying that a separate adjoint function must be evaluated for each desired response. If the responses are distributed in time and space,

e.g., the space and time-dependent fluxes, power density, etc., the associated computational burden becomes overwhelming if one treats each point in the phase space as a separate response. Two primary approaches have been suggested in the past to address distributed responses. First, instead of treating each point in the phase space as a single response, responses could be averaged over coarse regions and the averaged values are employed as responses (Williams 1986). Second, one could employ a multi-modal approach to express distributed responses. Multi-modal techniques are based on the observation that any smooth function could be expanded using a set of modes, i.e., basis functions. If the number of terms in the expansion is low, one could employ the coefficients of the expansion as responses. If parameters perturbations are small enough, the variations in the responses everywhere in the phase space could be approximated by variations in the expansion coefficients. This idea has been employed in many scientific fields. For example, (Cacuci 1981b) used a generalized Fourier expansion to describe responses distribution in space and time in the field of nuclear engineering. In this approach, the number of adjoint model executions becomes dependent on the number of terms in the expansion rather than on the number of points in the phase space. For sufficiently smooth distributed responses and with a proper choice of the basis functions, this could lead to tremendous computational savings. In practical engineering calculations, however, the distributed responses are often non-smooth, e.g., severe flux gradients across the interface between two significantly different fuel assemblies or the flux change following the insertion of a control rod. Another obstacle that faces multi-modal techniques is that input parameters perturbations could be large enough where the number of terms in the expansion

is no longer enough to accurately capture the responses variations. Also, depending on the type of variations, the optimum basis functions for the perturbed case may not be the same as those employed at reference unperturbed conditions. Therefore, the applicability of multi-modal methods is limited to problem with smooth distributed responses only, and extending this approach to estimate higher orders of variations becomes more difficult as the functions employed in the expansion could in general be perturbation-dependent.

1.2.2 Reduced basis methods and reduction error analysis

Historically, reduced basis methods have been built upon underlying finite element discretizations. Reduced basis discretization is, in brief, a Galerkin projection on a *K*-dimensional approximation space that focuses on the parametrically induced manifolds. Moreover, many different kinds of reduced basis methods have been devised to reduce the computational cost associated with the simulation of complex models, especially when repeated evaluations are required for supporting engineering analyses such as SA and UQ. In spite of the startling growth in computer power over the past few decades, the simulation of complex systems is still considered computationally challenging, which keeps reduced basis methods at the forefront of modeling and simulation research. The fundamental idea of reduced basis methods is to represent the response/state space, often belonging to a high dimensional space, by much fewer DOFs described mathematically by a subspace. A subspace is an abstract notion used by most reduced basis methods. For example, in Euclidean geometry, a 2D plane passing through the origin is considered a subspace in a 3D

space. The subspace has two DOFs, i.e., one degree of freedom less than the 3D space. Any two independent vectors are said to form a basis for the subspace, implying that any vector in the subspace can be described by a linear combination of the basis vectors. Subspaces are abstract notions which generalize the Euclidean picture of a hyper-plane into high dimensional spaces. The idea is that one can describe points in high dimensional spaces by much fewer DOFs.

Reduced basis methods first appeared in 1970s tackling linear/nonlinear structural analysis (Almroth, Brogan & Stern 1978), and since then have been employed and further developed by many researchers from different scientific backgrounds, e.g., fluid dynamics, nuclear physics, and quantum mechanics (Porsching 1985, Ito, Ravindran 1998, Bang 2012, Rozza 2011). Furthermore, these techniques were introduced into discretized stochastic systems by (Nair, Keane 2000) and further extended to efficiently compute response uncertainty for non-Gaussian models via combining with polynomial chaos expansions (Sachdeva, Nair & Keane 2006).

The essential approach utilized to explore the best basis functions is known as proper orthogonal decomposition (POD) or POD of snapshots in temporal domain. A snapshot is usually denoted as the state of a model at a particular point in time. In this dissertation, we will also use the snapshot to denote the solution of a set of partial differential equations that describes the behaviors of examined computational model, corresponding to a given perturbation in input parameters. According to (Lumley 1970), the POD was rediscovered independently by Kosambi (1943), Loève (1945), Karhunen (1946), Pougachev (1953) and

Obukhov (1954) in a variety of disciplines under a variety of different names, e.g. Principal Component Analysis (PCA), Karhunen-Loève Decomposition (KLD), or Empirical Orthogonal Function (EOF),. The POD/POD of snapshots did not gain much attention until the mid 80's due to its computational requirements. To date, it has gained recognition as a powerful and elegant tool for complex model reduction aimed at obtaining low-dimension approximate description of a high-dimension state space. In the last thirty years, the POD/POD of snapshots has been successfully applied to image processing, signal analysis, data compression, structure dynamics, fluid flows, oceanography, etc. (Holmes, Lumley & Berkooz 1996, Kappagantu, Feeny 2000, Georgiou, Schwartz 1999, Rowley 2005, Kerschen et al. 2005).

In addition, there are three essential properties of POD/POD of snapshots which are well described by (Liang et al. 2002, Rathinam, Petzold 2004). First, the POD/POD of snapshots provides an orthonormal basis for the modal decomposition of an ensemble of systems, such as data obtained in the course of experiments or numerical simulations, in a certain least square optimal sense. The optimal basis (also called empirical eigenfunctions, empirical basis functions, empirical orthogonal functions, proper orthogonal modes, or basis vectors) it yields is the most attractive feature of POD/POD of snapshots, because it provides the most efficient way of capturing the dominant components of a high-dimension state space with only a small number of basis vectors. Second, the modal decomposition of POD is completely independent on the data obtained by experiments or numerical simulations. It does not assume any prior knowledge of the system that generates the data, while it can also

help in identifying patterns in data that will reveal some insight into the underlying system. Third, the POD/POD of snapshots does not neglect the nonlinearities of the original system, although this approach always looks for linear subspace instead of curved sub-manifolds. This is because if the original system is nonlinear, then the resulting POD reduced order model will also typically be nonlinear.

However, early approaches mainly focus on low-dimensional parameter domains and the approximated subspaces tended to be local (Porsching 1985, Noor, Peters 1981a, Noor, Peters 1981a, Noor, Peters 1981b). Moreover, the POD of snapshots has found most application in the time domain, i.e., a single dimension (Bui-Thanh, Damodaran & Willcox 2003, Willcox, Peraire & Paduano 2002). The application of POD of snapshots into high dimensional parameter space seems impracticable, since in high-dimension – even three-dimension – parameter space simple tensor-products are computationally intractable. Hence, many efforts have been devoted to devise efficient sampling strategies to obtain the best representative snapshots in order to gain large computational reduction. Recently, there has been a surge of interest in the sparse grid stochastic collocation method in order to reduce the dimensionality of input parameter space (Ganapathysubramanian, Zabaras 2007, Nobile, Tempone & Webster 2008a, Nobile, Tempone & Webster 2008b), whereas the practical applications are limited to a small dimension of input parameter space at present, e.g., $O(10)$. One of the most promising approaches is a greedy sampling method proposed by Rozza and his colleagues (Rozza 2011, Rozza, Veroy 2007, Patera, Rozza 2007). This method makes use of a posteriori error bound to construct the hierarchical Lagrange reduced basis space, i.e.

the basis elements are the snapshots of the given model. Another promising approach is the efficient subspace method (ESM) introduced by (Abdel-Khalik 2004). ESM is originally used to find low rank approximations to the very large, dense sensitivity matrices which are generally rank-deficient. ESM employs randomized perturbations in the input parameter space to identify the efficient subspace for the vectors of multi-responses sensitivity coefficients. Typically, the dimension of input parameter space for BWR core simulations is larger than 10^6. ESM was employed to reduce the number of lattice physics calculations by an order of magnitude in cross section adjustment (Jessee 2008).

For reduced basis methods to be effective, response/state variations calculated from the full space should be approximately equal to those calculated from the subspace of reduced basis. The discrepancies between the two are referred to hereinafter as reduction errors. Many approaches have been devised to identify the subspace that minimizes reduction errors. Early studies mainly focus on priori error analysis (Porsching 1985, Fink, Rheinboldt 1985, Rheinboldt 1993). Previously, (Porsching 1985, Fink, Rheinboldt 1985) proposed a priori error estimator for single parameter problems; while (Rheinboldt 1993) worked on a priori error estimator for multi-parameter problems. However, priori error estimators, as provided by the standard error analysis for finite-element or finite-different methods, are often insufficient and unstable, since the overall accuracy of the numerical approximations is deteriorated by local singularities, e.g., control rod movement, or burnable poison rod insertion in a nuclear reactor system. (Noor, Peters 1983) first investigated posteriori error analysis by computing the residual norms with the solution from the reduced system of

equations. However, this is a pretty rough error estimator without any stability consideration. For realistic large-scale systems, many thousands of simulations are needed to obtain reliable results. In the past few years, many scientists have proposed several heuristic estimators for the reduction errors. (Galbally et al. 2010) employed an average relative error norm of outputs over a set of test parameters:

$$\varepsilon_{rel} = \underset{\alpha \in \Im}{\text{mean}} \frac{\left\| \phi(\alpha) - \phi_r(\alpha) \right\|_2}{\left\| \phi(\alpha) \right\|_2}$$

where $\left\| \bullet \right\|_2$ is Euclidean norm, $\Im$ denotes the test set, ϕ_r is the POD approximation for ϕ employing r basis vectors. (Chaturantabut, Sorensen 2010) shown that the average error bound satisfies the following inequality:

$$\frac{1}{l} \sum_{i=1}^{l} \left\| \phi(\alpha) - \phi_r(\alpha) \right\|_2 \le C \sigma_{r+1}$$

where C is a constant, and σ_{r+1} is $(r+1)^{\text{th}}$ singular value of the snapshot matrix $\mathbf{Q}$, and l is the number of snapshots and r is the number of optimal basis vectors.

From a practical viewpoint, these error estimators provide reasonable qualitative approximations of the expected errors. However, these quantities cannot make quantitative bounding statements about the reduction errors for all possible model parameters perturbations. To overcome this challenge, Rozza and his colleagues devised a rigorous a posteriori error estimator based on a greedy sampling method in order to explore much larger subsets of parameter spaces in search of most representative basis functions (Rozza 2011, Rozza, Veroy 2007, Patera, Rozza 2007). In this dissertation we take advantage of recent

developments in randomized linear algebra community. In particular, we employ range-finding algorithms in conjunction with reduced basis methods to reliably quantify the errors resulting from the reduction.

Range-finding algorithms have been developed in the linear algebra community over the past several decades (Golub, Van Loan 1996). They are designed to identify patterns in large data sets which can be used to identify the reduced basis spaces. Past research in the nuclear engineering community has shown that ESM could be employed to find subspaces for the ranges of general rectangular matrices (Abdel-Khalik 2004). In recent years, this algorithm has been rigorously proved by applied mathematicians; it has been shown that randomized operations could be used to approximate the range of matrix operators with high probability (Halko, Martinsson & Tropp 2011). The idea has been further extended to identify the range of nonlinear operators by (Bang, Abdel-Khalik & Hite 2012).

In particular, the range-finding algorithm used in this dissertation is a probabilistic posteriori error estimator employing a small number of oversampling to obtain a reliable error bound. Consequently, the computational savings provided by range-finding algorithm were typically significant. Additionally, the range-finding algorithm can also be organized such that each iteration processes a block of samples simultaneously. This attractive feature of range-finding algorithm can lead to dramatic improvements in speed if one exploits parallel processors. Furthermore, we note here that range-finding algorithm are similar in objective to, but very different in approach from, greedy sampling methods; the former

utilizes a set of random samples in the parameter space, while the latter employs a set of nested samples in the parameter space.

CHAPTER 2. BRIEF INTRODUCTION OF MATHEMATICAL METHODS

This chapter outlines the mathematical theory and methods for EPGPT. We begin with general preliminaries. The purpose of the general preliminaries is to review the background material on which the rest of this dissertation shall rest. We discuss the basic elements of EPGPT analysis: fundamental subspaces; inner product and norms; proper orthogonal decomposition of snapshots; adjoint operators; neutron diffusion/transport theory; generalized perturbation theory; and finally range-finding algorithm.

2.1 Preliminaries

Let $\mathbb{Z}$ denote the scalar field for real number, and $\mathbb{R}$ denote the vector space over $\mathbb{Z}$. An integer n is denoted by lowercase italic letter $n \in \mathbb{Z}$. A vector q of n components is also denoted by a lowercase letter: $q \in \mathbb{R}^n$, where $\mathbb{R}^n$ is an n dimensional vector space over $\mathbb{Z}$. This should lead to no confusion as the integers will mainly represent the dimensions of the various vector spaces. To distinguish between a vector and its components, the notation $[q]_i$ will be used to denote the i^{th} component of the vector q. If vector has a single component, it will be represented by an uppercase italic letter, e.g., R is a real number representing a single value or a single-valued functional.

Matrices will be denoted by bold capital letters. The matrix $\mathbf{A} \in \mathbb{R}^{m \times n}$ belongs to the space of matrices of m rows and n columns. To reference the element at the intersection of

the i^{th} row and the j^{th} column of matrix $\mathbf{A}$, the following notation is adopted: $[\mathbf{A}]_{ij}$. In addition, operators will also be denoted by bold capital letters since the numerically-discretized operators are in the form of matrices.

Subspaces will be denoted by $\mathbb{C}$. If $\mathbb{C}$ is also a vector space over $\mathbb{Z}$ using the same addition and scalar multiplication operations and $\mathbb{C} \subseteq \mathbb{R}$, then $\mathbb{C}$ is called a subspace of $\mathbb{R}$. That is, $\mathbb{C}$ is a subspace of $\mathbb{R}$ if and only if

$$\mathbb{C} \subseteq \mathbb{R};\ x, y \in \mathbb{C} \Rightarrow x + y \in \mathbb{C} \tag{2.1.1}$$

and

$$\mathbb{C} \subseteq \mathbb{R};\ x \in \mathbb{C} \Rightarrow Ax \in \mathbb{C} \text{ for all } A \in \mathbb{Z} \tag{2.1.2}$$

The complementary subspace of $\mathbb{C}$ is denoted by $\mathbb{C}^{\perp}$. In this dissertation, two fundamental subspaces will be used, that are the range space and the nullspace. For a given matrix $\mathbf{A} \in \mathbb{R}^{m \times n}$, the range space $R(\mathbf{A})$ of $\mathbb{R}^m$ is defined as:

$$R(\mathbf{A}) = \{\mathbf{A}x \mid x \in \mathbb{R}^n\} \subseteq \mathbb{R}^m \tag{2.1.3}$$

and the nullspace $N(\mathbf{A})$ of $\mathbb{R}^n$ is defined as:

$$N(\mathbf{A}) = \{x \in \mathbb{R}^n \mid \mathbf{A}x = 0\} \subseteq \mathbb{R}^n \tag{2.1.4}$$

A linearly independent spanning set, i.e., $\{q_1, q_2, \cdots, q_r\} \subseteq \mathbb{C}^r$, for a vector subspace $\mathbb{C}^r$ is called a basis for $\mathbb{C}^r$. The size of the subspace $\mathbb{C}^r$ is defined to be the number of vectors in any basis for $\mathbb{C}^r$.

Vector and matrix Euclidean norm or 2-norms will be denoted by $\| \ \|_2$, for a vector $x \in \mathbb{R}^n$, the norm of x is defined to be:

$$\|x\|_2 = \sqrt{\left(\sum_{i=1}^{n} [x]_i^2 \right)} = \sqrt{x^T x} \tag{2.1.5}$$

where the superscript '^{T}' denotes the transpose of vector x. The norm of a matrix **A** is defined to be:

$$\|\mathbf{A}\|_2 = \max_{\|x\|_2 = 1} \|\mathbf{A}x\|_2 \tag{2.1.6}$$

The inner product of two vectors is defined to be

$$\langle x, y \rangle = x^T y = \sum_{i=1}^{n} [x]_i [y]_i \in \mathbb{Z} \tag{2.1.7}$$

If the inner product of two vectors $\langle x, y \rangle = 0$, then the two vectors are said to be orthogonal. The set $\{q_1, q_2, \cdots, q_r\} \subseteq \mathbb{C}^r$ is called an orthonormal set whenever $\|q_i\|_2 = 1$ for each i, and $q_i \perp q_j$ for all $i \neq j$. In other words,

$$\langle q_i, q_j \rangle = \begin{cases} 1 & \text{when } i = j, \\ 0 & \text{when } i \neq j, \end{cases} \tag{2.1.8}$$

An orthogonal matrix is defined to be a real matrix $\mathbf{Q}^{n \times r} = [q_1 \ q_2 \ \cdots \ q_r]$ whose columns constitute an orthonormal basis for the subspace $\mathbb{C}^r$.

Similar to the inner product on vectors that uses a sum over corresponding components, the inner product on functions is defined as an integral over the domains of functions. For example, let $\psi(\alpha)$ and $\phi(\alpha)$ both be functions of the same variables, represented by

general symbol $\alpha \in \mathbb{R}^k$; the *inner product* of these two continuous functions is then expressed and defined by

$$(\psi,\phi) \equiv \langle \psi,\phi \rangle = \int_{\alpha_1}^{\alpha_2} \psi(\alpha)\phi(\alpha)\, d\alpha \tag{2.1.9}$$

where the integration is carried over the whole accessible range of the variables.

A functional is defined as a function whose arguments are themselves functions. For example, the responses of interest considered in this dissertation are functions of input parameters and state, and the state is a function of input parameters, thus the responses of interest is called functionals of the input parameters and state.

2.2 POD of Snapshots

The main idea of the POD of snapshots is to find a set of ordered orthonormal basis vectors in a subspace where a random vector takes its value, such that the samples space $\{y_j\}_{j=1}^{p}$ can be expressed optimally using the selected first r basis vectors $\{q_i\}_{i=1}^{r}$, and the basis set $\{q_i\}_{i=1}^{r}$ is the solution to the minimization problem:

$$\min_{\{q_i\}_{i=1}^{r}} \sum_{j=1}^{p} \left\| y_j - \sum_{i=1}^{r} \langle y_j, q_i \rangle q_i \right\|_2^2 \tag{2.2.1}$$

The POD of snapshots approach is summarized as follows:

POD of Snapshots Approach

Given $y_1, \cdots, y_p \in \mathbb{R}^n$. Define $y_i \equiv$ snapshot i, $\forall i$. Let $R(\mathbf{Q}) = span\{y_1, \cdots, y_p\} \subset \mathbb{R}^n$;
Given $r \leq p$, POD generates a set of orthonormal basis of dimension r, which minimizes:

$$\min_{\{q_i\}_{i=1}^r} \sum_{j=1}^{p} \left\| y_j - \tilde{y}_j \right\|_2^2, \text{ where } \langle q_i, q_j \rangle = \delta_{ij}, \text{ and } \tilde{y}_j = \sum_{i=1}^{r} \langle y_j, q_i \rangle q_i$$

It is well know that the solution to Eq. (2.2.1) is provided by the set of the left singular vectors of the snapshot matrix $\mathbf{Y} = \begin{bmatrix} y_1 & \cdots & y_p \end{bmatrix} \in \mathbb{R}^{n \times p}$. In particular, suppose that the singular value decomposition (or in short, SVD) of $\mathbf{Y}$ is

$$\mathbf{Y} = \mathbf{Q}\mathbf{\Sigma}\mathbf{V}^T \tag{2.2.2}$$

where $\mathbf{Q} = \begin{bmatrix} q_1 & \cdots & q_r \end{bmatrix} \in \mathbb{R}^{n \times r}$ and $\mathbf{V} = \begin{bmatrix} v_1 & \cdots & v_r \end{bmatrix} \in \mathbb{R}^{p \times r}$ are orthogonal matrices and $\mathbf{\Sigma} = diag(\sigma_1, \cdots, \sigma_r) \in \mathbb{R}^{r \times r}$, with $\sigma_1 \geq \sigma_2 \geq \cdots \geq \sigma_r > 0$. The rank of $\mathbf{Y}$ is $r \leq \min\{n, p\}$. The optimal solution of Eq. (2.2.1) is $\{q_i\}_{i=1}^r$. The minimum 2-norm error from approximating the snapshots using the POD basis is then given by

$$\sum_{j=1}^{p} \left\| y_j - \sum_{i=1}^{l} \langle y_j, q_i \rangle q_i \right\|_2^2 = \sum_{i=l+1}^{r} \sigma_i^2 \tag{2.2.3}$$

It is noteworthy to remark that in POD of snapshots method, the subspace employed for reduction is identified via a predetermined set of state solutions typically at different points in time which form a basis for the subspace. This allows the subspace to be tailored more intimately, compared to response surface methods, to the model. Despite its success, it is hard to guarantee that the evolution of the reference solution at different times is

representative of all possible variations that may be induced by all possible input parameters perturbations.

2.3 Neutron Diffusion or Transport Theory

For nuclear reactor analysis and design, the central problem is how to determine the space, angle, energy, and time-dependence of the neutron distributions in the reactor. Because the neutron distributions can be used to determine the nuclear reaction rates, power distributions occur within the reactor core. Traditionally, neutron diffusion/transport theory can be employed to calculate the distribution of neutrons in the core. Neutron transport theory is much more fundamental and exact description of the neutron population in the reactor compared to neutron diffusion theory. The neutron transport equation is a linear version of the Boltzmann equation having seven independent variables. Considering the complex geometries of nuclear reactors and the resonant behaviors in energy of many cross sections, the detailed solution of the neutron transport equation for the full-core calculations requires lots of computational resources so that one usually employs a two-level computational scheme, which is based on the fact that the reactor is an assembly of pin-cells or assemblies built in a lattice layout. The first level, denoted as lattice calculation, involves the calculation of the neutron transport equation over the pin-cell or assembly using numerical techniques with multi-group cross sections as input parameters. At the end of a lattice calculation, the homogenized and condensed cross sections are stored for the second level full-core calculation. A simplified transport equation, such as diffusion equation or the

simplified P_n equation, will be utilized to generate the neutron flux and reaction rates over the complete reactor core. In this section, we will briefly introduce the neutron diffusion and transport theories, and recommend the reader to (Bell 1979, Duderstadt, Hamilton 1976) for the detailed descriptions.

The neutron transport equation is obtained by the phase-space (i.e., generally space, angle, energy and time) balance relation for the neutron flux by which a neutron can be gained or lost from an arbitrary volume within the system. In steady-state conditions, it is written as

$$\begin{aligned}&\Omega\bullet\nabla\phi(r,\Omega,E)+\Sigma_t(r,E)\phi(r,\Omega,E)-\int_{4\pi}d\Omega'\int_0^\infty dE'\Sigma_s(r,\Omega',E'\to\Omega,E)\phi(r,\Omega',E')\\&=\frac{1}{4\pi}\chi(r,E)\int_{4\pi}d\Omega'\int_0^\infty dE'\nu(r,E')\Sigma_f(r,E')\phi(r,\Omega',E')+Q_{\text{ex}}(r,\Omega,E)\end{aligned}\tag{2.3.1}$$

where $\phi(r,\Omega,E)$ is the neutron angular flux, $\Sigma_t(r,E)$ is the total cross section, $\Sigma_s(r,\Omega',E'\to\Omega,E)$ is the differential-scattering cross section, $\chi(r,E)$ is the fission spectrum, $\nu(r,E)$ is the averaged neutron yield per fission, and $\Sigma_f(r,E)$ is the fission cross section. While the phase-space is denoted by (r,Ω,E), which represents the neutron location, moving direction and energy, respectively. In this dissertation, the equation (2.3.1) is written in a more compact form:

$$\mathbf{P}\phi(r,\Omega,E)=Q_{\text{ex}}(r,\Omega,E)\tag{2.3.2}$$

where **P** denotes the neutron transport operator and defined as

$$\mathbf{P}\phi = \Omega \bullet \nabla \phi(r,\Omega,E) + \Sigma_t(r,E)\phi(r,\Omega,E) - \int_{4\pi} d\Omega' \int_0^\infty dE' \Sigma_s(r,\Omega',E' \to \Omega,E)\phi(r,\Omega',E')$$
$$-\frac{1}{4\pi}\chi(r,E)\int_{4\pi} d\Omega' \int_0^\infty dE' \nu(r,E')\Sigma_f(r,E')\phi(r,\Omega',E')$$

The equation (2.3.2) could be solved subject to given boundary conditions (e.g., vacuum boundaries, reflecting boundaries, periodic boundaries) using numerical techniques such as the finite difference or finite element method.

One can obtain the neutron diffusion equation by employing the Fick's law which is acceptable on the scale of the full-core calculation. It is written as:

$$J_g(r) = -D_g(r)\nabla\phi_g(r) \tag{2.3.3}$$

Skipping over the derivation, the diffusion equation is written as:

$$\begin{aligned} &-\nabla \bullet D(r,E)\nabla\phi(r,E) + \Sigma_t(r,E)\phi(r,E) - \int_0^\infty \Sigma_s(r,E' \to E)\phi(r,E')dE' \\ &= \chi(r,E)\int_0^\infty \nu(r,E')\Sigma_f(r,E')\phi(r,E')dE' + Q_{\text{ex}}(r,E) \end{aligned} \tag{2.3.4}$$

Mathematically, diffusion theory is valid when the following assumptions are satisfied: 1) highly scattering medium; 2) a few mean free paths away from the boundaries or external sources; 3) isotropic scattering. However, diffusion theory is widely used in full-core reactor analysis and it is sufficiently accurate to provide a quantitative prediction. The reason is that one can employ the transport theory to generate the effective averaged cross sections and diffusion coefficients with associated discontinuity factors to create a computational model for which the diffusion theory is valid. Similar to transport equation (2.3.2), the equation (2.3.4) can be written in a more compact form:

$$\mathbf{H}\phi(r,E) = Q_{\text{ex}}(r,E) \tag{2.3.5}$$

where **H** here denotes the neutron diffusion operator and **H** is defined as

$$\mathbf{H} = -\nabla \bullet D(r,E)\nabla\phi(r,E) + \Sigma_t(r,E)\phi(r,E) - \int_0^\infty \Sigma_s(r,E' \to E)\phi(r,E')\,dE'$$

$$-\chi(r,E)\int_0^\infty \nu(r,E')\Sigma_f(r,E')\phi(r,E')\,dE'$$

2.4 Adjoint Operators

The form of the diffusion/transport equation introduced in the preceding section is known as the forward equation, in the sense that neutrons are followed forward in time from their birth to their loss from the nuclear reactor system. A related form of the forward equation is the adjoint form: in the adjoint view, the solution basically tells you that what contribution each part of the problem makes to the response of interest at a given position in the nuclear reactor system. Moreover, the adjoint solutions have a clear physical significance as the "importance" of neutrons within a particular system. This has a couple of uses: for shielding calculations, it can tell you how particles are getting through the shield so that one can add shielding more profitable; for reactor physics analysis, generalized perturbation theory is combined with properties of adjoint operators and equations to calculate the response variations without having to re-solve the entire forward equation.

If $\psi(\alpha)$ and $\phi(\alpha)$ in Eq. (2.1.9) are any "well behaved" functions, in the sense that they satisfy certain boundary and continuity conditions, then a *Hermitian* or *self-adjoint* operator **M** is one for which the inner products $\langle \psi, \mathbf{M}\phi \rangle$ and $\langle \phi, \mathbf{M}\psi \rangle$ are equal, i.e.,

$$\langle \psi, \mathbf{M}\phi \rangle = \langle \phi, \mathbf{M}\psi \rangle \tag{2.4.1}$$

In the treatment of neutron diffusion/transport theory, the operators and the functions on which they operate, e.g., the neutron flux, are real and complex conjugates are not required. However, the operator associated with the diffusion/transport equation is not self-adjoint. If an operator **A** is not self-adjoint, it is possible in the following way to define an operator $\mathbf{A}^*$ that is adjoint to **A**. The operator , $\mathbf{A}^*$, will operate on functions ψ^*, often called *adjoint functions*, which may satisfy boundary conditions different from those satisfied by functions ϕ on which **A** operates. The adjoint operator, $\mathbf{A}^*$, is then defined by the requirement that

$$\langle \psi^*, \mathbf{A}\phi \rangle = \langle \phi, \mathbf{A}^*\psi^* \rangle \tag{2.4.2}$$

for any "well behaved" functions ϕ and ψ^*. The neutron transport operator **P**, as shown by (Bell 1979), is not self-adjoint. In other words, if $\psi(r,\Omega,E)$ and $\phi(r,\Omega,E)$ are functions of (r,Ω,E) satisfying the required continuity and boundary conditions, then

$$\langle \psi, \mathbf{P}\phi \rangle \neq \langle \phi, \mathbf{P}\psi \rangle \tag{2.4.3}$$

As indicated earlier, however, it is possible to define an operator $\mathbf{P}^*$, adjoint to **P**, so that any function $\phi^*(r,\Omega,E)$ fulfilling continuity and boundary conditions, which may be different from those on $\phi(r,\Omega,E)$, will satisfy the relationship

$$\langle \phi^*, \mathbf{P}\phi \rangle = \langle \phi, \mathbf{P}^*\phi^* \rangle \tag{2.4.4}$$

where $\phi^*(r,\Omega,E)$ is sometimes referred to as the adjoint (angular) flux or, more commonly, as the *adjoint function*; $\phi(r,\Omega,E)$ and $\phi^*(r,\Omega,E)$ are any two functions satisfying the appropriate boundary and continuity conditions for the neutron forward and adjoint flux, respectively. By considering the left side of Eq. (2.4.4), it is possible to derive the necessary form for $\mathbf{P}^*$ and the boundary conditions on $\phi^*(r,\Omega,E)$. For simplicity, however, the procedure adopted here will be to write down the expression for the adjoint operator and one can find the proof in many different references (Bell 1979, Duderstadt, Hamilton 1976).

Let us consider the function $\phi(r,\Omega,E)$ satisfies the free-surface boundary conditions; thus, $\phi(r,\Omega,E)=0$ for all r on the convex boundary and all incoming neutron directions. Then the adjoint function will satisfy the boundary conditions that $\phi^*(r,\Omega,E)=0$ for all r on the boundary and for all outgoing directions. Moreover, it is assumed that both $\phi(r,\Omega,E)$ and $\phi^*(r,\Omega,E)$ are continuous functions of space, so that no difficulties arise when their gradients are computed. Then, in accordance with the definition of the adjoint transport operator, $\mathbf{P}^*$, in Eq. (2.4.4),

$$\begin{aligned}\mathbf{P}^*\phi^*(r,\Omega,E) = &-\Omega\bullet\nabla\phi^*(r,\Omega,E)+\Sigma_t(r,E)\phi^*(r,\Omega,E)\\ &-\int_{4\pi}d\Omega'\int_0^\infty dE'\,\Sigma_s(r,\Omega,E\to\Omega',E')\phi^*(r,\Omega',E')\\ &-\frac{1}{4\pi}v(r,E)\Sigma_f(r,E)\int_{4\pi}d\Omega'\int_0^\infty dE'\,\chi(r,E')\phi^*(r,\Omega',E')\end{aligned} \tag{2.4.5}$$

The following differences should be noted between $\mathbf{P}^*$ as given by Eq. (2.4.5) and $\mathbf{P}$ as defined by Eq. (2.3.2): (a) the gradient terms have opposite signs; (b) the before and after parts of the scattering function $\Sigma_s(r,\Omega,E\to\Omega',E')$ have been interchanged, i.e., $\Omega',E'\to\Omega,E$ in $\mathbf{P}$ becomes $\Omega,E\to\Omega',E'$ in $\mathbf{P}^*$; (c) the terms $\nu\Sigma_f$ and χ have been interchanged.

Similarly, the adjoint operator to Eq. (2.3.5) for neutron diffusion theory is written as:

$$\mathbf{H}^* = -\nabla\bullet D(r,E)\nabla\phi^*(r,E)+\Sigma_t(r,E)\phi^*(r,E)-\int_0^\infty \Sigma_s(r,E\to E')\phi^*(r,E')dE' \\ -\nu(r,E)\Sigma_f(r,E)\int_0^\infty \chi(r,E')\phi^*(r,E')dE' \tag{2.4.6}$$

where $\phi^*(r,E)$ is the adjoint flux.

2.5 Generalized Perturbation Theory

In this dissertation, the term "response" refers to an observable output, such as nuclear power density distribution, detector response, or reactivity, of reactor system whose value is to be evaluated in a reactor physics or shielding analysis. There are usually two types of encountered responses: (1) integrals of the neutron flux or (2) ratios of these integrals. Examples are given in the following:

$$R=\left\langle \Sigma_d(r,E),\phi(r,E,\Omega)\right\rangle \equiv \int_V\int_0^\infty\int_{4\pi}\Sigma_d(r,E)\phi(r,E,\Omega)\,d\Omega dEdV \tag{2.5.1}$$

$$R=\frac{\left\langle \Sigma_1(r,E),\phi(r,E,\Omega)\right\rangle}{\left\langle \Sigma_2(r,E),\phi(r,E,\Omega)\right\rangle} \tag{2.5.2}$$

where $\Sigma_d, \Sigma_1, \Sigma_2$ are cross sections, and $\phi(r, \Omega, E)$ is the neutron flux determined by the neutron transport equation (2.3.2) or diffusion equation (2.3.5). Generally, we assume that ϕ is determined by solving an equation of the form

$$\mathbf{A}(\alpha)\phi = Q_{\text{ex}} \tag{2.5.3}$$

where $\mathbf{A}(\alpha)$ is a linear operator, the components of $\alpha \in \mathbb{R}^k$ represent the input parameters and Q_{ex} is an inhomogeneous fixed source. When $\mathbf{A}(\alpha)$ contains space derivatives, Equation (2.5.3) is a boundary value problem (BVP) with specified boundary conditions in order to have a unique solution, examples are the neutron diffusion calculation and neutron Boltzmann transport calculation. When $\mathbf{A}(\alpha)$ contains first-order time derivatives, the equation becomes an initial value problem (IVP) with specified initial time conditions, such as the burnup equation in nuclear reactor depletion calculation and point kinetic equation in nuclear dynamics system. When Q_{ex} is equal to zero, the equation can be an eigenvalue problem, for which the operator $\mathbf{A}(\alpha)$ is singular. Generally speaking, the operator $\mathbf{A}(\alpha)$ depends on input parameters, e.g. cross sections, material compositions, material temperatures, half-lives, etc., and hence the solution ϕ is dependent on the special values of those parameters. Therefore, the responses implicitly depend on all parameters showing in the system equation (2.5.3) for ϕ and explicitly on the parameters appearing in the response functionals, e.g., $\Sigma_d, \Sigma_1, \Sigma_2$ in Eq. (2.5.1) and Eq. (2.5.2). The purpose of perturbation theory is to determine the response variations corresponding to the perturbations in the input

parameters. In particular, the solution ϕ is a function of space, energy, and direction, which is implied but not shown in the operator notation used here. Moreover, numerical technique should be utilized to obtain the solution to the continuous equation (2.5.3). This is because analytical solutions are available only for a few simplified models with very specific geometries. In this dissertation, the numerical solutions for the neutron transport and burnup calculations are obtained using SCALE 6.1 which is originally developed and maintained by Oak Ridge National Laboratory for nuclear safety analysis and design. Hence, the numerical discretization and the application of the approximate boundary conditions lead to a matrix system of the form:

$$\mathbf{A}\phi = q_{\text{ex}} \tag{2.5.4}$$

where $\mathbf{A} \in \mathbb{R}^{n\times n}$ and $q_{\text{ex}} \in \mathbb{R}^n$ are numerically-discretized matrix operator and external source, respectively; in principle, $\phi \in \mathbb{R}^n$ is the numerical solution that approaches the continuous equation (2.5.3) as the phase-space meshes are refined.

2.5.1 Generalized Perturbation Theory for Source-Driven Problem

Consider a source-driven transport model described by:

$$\mathbf{P}(\alpha)\phi = Q_{\text{ex}}(\alpha) \tag{2.5.5}$$

or in the form of discretization scheme:

$$\mathbf{P}\phi = q_{\text{ex}} \tag{2.5.6}$$

where $\mathbf{P}(\alpha)$ is the transport operator defined in Eq. (2.3.2), $Q_{\text{ex}}(\alpha)$ is the external source, and finally both $\mathbf{P}(\alpha)$ and $Q_{\text{ex}}(\alpha)$ depend on the model's k input parameters that are described by a vector α. Next, consider an integral response functional (e.g., a system characteristic) $R(\alpha,\phi)$ that is defined in Eq. (2.5.1). The GPT variational formalism employs an auxiliary functional of the form:

$$K\left[\alpha,\phi,\Gamma^*\right] = R(\alpha,\phi) - \left\langle \Gamma^*, \left(\mathbf{P}(\alpha)\phi - Q_{\text{ex}}(\alpha)\right)\right\rangle \tag{2.5.7}$$

where Γ^* is the Lagrange multiplier associated with the constraint in Eq. (2.5.5). Note that if ϕ is the exact solution to the Eq. (2.5.5), the response becomes equal to the auxiliary functional, i.e., K=R. Similarly, for a given perturbation in the input parameters, the K functional becomes:

$$K \to K'\left[\alpha',\phi',\Gamma^*\right]$$

where the prime superscripts will be used throughout this dissertation to denote the values at perturbed conditions. Like before, with ϕ' being the exact solution to the perturbed system, i.e.,

$$\mathbf{P}(\alpha')\phi' = Q_{\text{ex}}(\alpha') \tag{2.5.8}$$

The perturbed response and auxiliary functional remain equal:

$$K' = R' \Rightarrow \delta K = \delta R$$

Unlike the response $R(\alpha,\phi)$, where ϕ implicitly depends on the input parameters, the functional K_i depends explicitly on all input parameters, as well as ϕ and Γ_i^*. The first-order

GPT proceeds by expanding K' about the unperturbed conditions and neglecting second- and higher-order terms which gives:

$$K' \approx K + \left\langle \frac{\partial K}{\partial \alpha}, \delta\alpha \right\rangle + \left\langle \frac{\partial K}{\partial \phi}, \delta\phi \right\rangle + \left\langle \frac{\partial K}{\partial \Gamma^*}, \delta\Gamma^* \right\rangle \tag{2.5.9}$$

The idea of the variational formalism is to make the auxiliary functional stationary with respect to all variables except the input parameters. This is done by equating the first-order derivatives of the auxiliary functional with respect to the variables ϕ and Γ^* to zero as follows:

$$\frac{\partial K}{\partial \phi} = 0 \Rightarrow \mathbf{P}(\alpha)^* \Gamma^* = \Sigma_d \tag{2.5.10}$$

$$\frac{\partial K}{\partial \Gamma^*} = 0 \Rightarrow \mathbf{P}(\alpha)\phi = Q_{\text{ex}}(\alpha) \tag{2.5.11}$$

Thus, the first-order approximation for the variation in the response reduces to:

$$\begin{aligned} \delta K &\approx \left\langle \frac{\partial K}{\partial \alpha}, \delta\alpha \right\rangle \\ &= \left\langle \frac{\partial R(\alpha,\phi)}{\partial \alpha}, \delta\alpha \right\rangle - \left\langle \frac{\partial \left\langle \Gamma^*, \left(\mathbf{P}(\alpha)\phi - Q_{\text{ex}}(\alpha)\right)\right\rangle}{\partial \alpha}, \delta\alpha \right\rangle \\ &= \left\langle \delta\Sigma_d, \phi \right\rangle + \left\langle \Gamma^*, \left(\frac{\partial Q_{\text{ex}}(\alpha)}{\partial \alpha} - \frac{\partial \mathbf{P}(\alpha)}{\partial \alpha}\phi \right)\delta\alpha \right\rangle \end{aligned} \tag{2.5.12}$$

$$\delta R = \delta K \approx \left\langle \delta\Sigma_d, \phi \right\rangle + \left\langle \Gamma^*, \left(\frac{\partial Q_{\text{ex}}(\alpha)}{\partial \alpha} - \frac{\partial \mathbf{P}(\alpha)}{\partial \alpha}\phi \right)\delta\alpha \right\rangle \tag{2.5.13}$$

The first term $\left\langle \delta\Sigma_d, \phi \right\rangle$ on the RHS of Eq. (2.5.13) can be readily determined since it is a function of the parameters perturbations only, it is referred to as the direct effect. The second

term requires a single solution of the adjoint model defined in Eq. (2.5.10). This term, denoted as the indirect effect, is evaluated as many times as there are perturbations. In practice, even with a large number of parameters perturbations, this cost is very small compared to the cost needed to solve Eq. (2.5.11) for the forward flux or Eq. (2.5.10) for the adjoint flux.

2.5.2 Generalized Perturbation Theory for Critical Eigenvalue Problem

Consider the steady-state radiation transport eigenvalue problem with the appropriate boundary condition over a given domain for the unperturbed system:

$$\begin{aligned}&\Omega\bullet\nabla\phi(r,\Omega,E)+\Sigma_t(r,E)\phi(r,\Omega,E)-\int_{4\pi}d\Omega'\int_0^\infty dE'\Sigma_s(r,\Omega',E'\to\Omega,E)\phi(r,\Omega',E')\\&=\frac{\lambda}{4\pi}\chi(E)\int_0^\infty dE'\nu(r,E')\Sigma_f(r,E')\phi(r,E')\end{aligned}\tag{2.5.14}$$

with boundary condition on the incoming flux $\phi(r,\Omega,E)=\phi_{\text{inc}}(r,\Omega,E)$ and r on the boundary. Rewrite Eq. (2.5.14) in a more compact form

$$\left(\mathbf{L}(\alpha)-\lambda\mathbf{F}(\alpha)\right)\phi=0\tag{2.5.15}$$

or in the form of discretization scheme

$$\left(\mathbf{L}-\lambda\mathbf{F}\right)\phi=0\tag{2.5.16}$$

where $\mathbf{L}(\alpha)$ and $\mathbf{F}(\alpha)$ are operators that describe the radiation transport loss and production operators with appropriate boundary condition, respectively; λ is the smallest eigenvalue (equal to $1/k_{eff}$) associated with the eigenfunction ϕ which denotes the neutron

flux. Finally, the $\mathbf{L}(\alpha)$, $\mathbf{F}(\alpha)$ and λ depend on the k model parameters described by a vector α. The neutron flux is normalized by the following equation:

$$\langle h,\phi\rangle = N \tag{2.5.17}$$

where h is a vector of weights that determine the normalization condition and N is the normalization constant. Without loss of generality, we assume for simplicity that h is independent of α. In practical calculations, the flux is often normalized based on the total power generated hence h is expected to depend on the fission cross sections and energy production per fission.

For the eigenvalue problem, the GPT variational formalism employs an auxiliary functional of the form:

$$K\left[\alpha,\phi,\lambda,N^*,\Gamma^*\right] = R(\alpha,\phi) - N^*\left(\langle h,\phi\rangle - N\right) - \left\langle \Gamma^*, \left(\mathbf{L}(\alpha)\phi - \lambda\mathbf{F}(\alpha)\phi\right)\right\rangle \tag{2.5.18}$$

where $R(\alpha,\phi)$ is given in Eq. (2.5.1), N^* and Γ^* are the Lagrange multipliers associated with the two constraints in Eq. (2.5.17) and Eq. (2.5.15), respectively. Note that if ϕ and λ are exact solutions to the forward model, the response becomes equal to the auxiliary functional, i.e.,

$$K = R$$

Similarly, for a given perturbation in the input parameters, the K functional becomes:

$$K \to K'\left[\alpha',\phi',\lambda',N^*,\Gamma^*\right]$$

As before, with ϕ' and λ' being the exact solutions to the perturbed system, i.e.,

$$\left(\mathbf{L}(\alpha') - \lambda'\mathbf{F}(\alpha')\right)\phi' = 0 \tag{2.5.19}$$

with neutron flux normalized by:

$$\langle h, \phi' \rangle = N \tag{2.5.20}$$

Therefore, the perturbed response and auxiliary functional remain equal:

$$K' = R' \Rightarrow \delta K = \delta R$$

Expanding K' about the unperturbed conditions and neglecting second and higher orders of variations results in:

$$K' \approx K + \left\langle \frac{\partial K}{\partial \alpha}, \delta\alpha \right\rangle + \left\langle \frac{\partial K}{\partial \phi}, \delta\phi \right\rangle + \left\langle \frac{\partial K}{\partial \lambda}, \delta\lambda \right\rangle + \left\langle \frac{\partial K}{\partial \Gamma^*}, \delta\Gamma^* \right\rangle + \left\langle \frac{\partial K}{\partial N^*}, \delta N^* \right\rangle \tag{2.5.21}$$

Let the auxiliary functional be stationary with respect to all variables except the input parameters. This is obtained by equating the first-order derivatives of the functional with respect to the variables $\phi, \lambda, N^*, \Gamma^*$ to zero, thus:

$$\frac{\partial K}{\partial \phi} = 0 \Rightarrow \left(\mathbf{L}(\alpha) - \lambda \mathbf{F}(\alpha)\right)^* \Gamma^* = \Sigma_d - N^* \bullet h \tag{2.5.22}$$

$$\frac{\partial K}{\partial \lambda} = 0 \Rightarrow \left\langle \Gamma^*, \mathbf{F}(\alpha)\phi \right\rangle = 0 \tag{2.5.23}$$

$$\frac{\partial K}{\partial N^*} = 0 \Rightarrow \langle h, \phi \rangle = N \tag{2.5.24}$$

$$\frac{\partial K}{\partial \Gamma^*} = 0 \Rightarrow \mathbf{L}(\alpha)\phi - \lambda \mathbf{F}(\alpha)\phi = 0 \tag{2.5.25}$$

The N^* is determined by requiring the RHS of Eq. (2.5.22) to be orthogonal to the forward neutron flux, i.e.,

$$\left\langle \left(\Sigma_d - N^* \bullet h\right), \phi \right\rangle = 0 \Rightarrow N^* = \frac{\langle \Sigma_d, \phi \rangle}{\langle h, \phi \rangle} \tag{2.5.26}$$

Then the first-order approximation for the variation in the response reduces to:

$$\begin{aligned}\delta K &\approx \left\langle \frac{\partial K}{\partial \alpha}, \delta\alpha \right\rangle \\ &= \left\langle \frac{\partial R(\alpha,\phi)}{\partial \alpha}, \delta\alpha \right\rangle - \left\langle \frac{\partial \left\langle \Gamma^*, \left(\mathbf{L}(\alpha)\phi - \lambda \mathbf{F}(\alpha)\phi\right)\right\rangle}{\partial \alpha}, \delta\alpha \right\rangle \\ &= \left\langle \delta\Sigma_d, \phi \right\rangle - \left\langle \Gamma^*, \left(\frac{\partial \mathbf{L}(\alpha)}{\partial \alpha}\phi - \lambda \frac{\partial \mathbf{F}(\alpha)}{\partial \alpha}\phi \right)\delta\alpha \right\rangle\end{aligned} \tag{2.5.27}$$

$$\delta R = \delta K \approx \left\langle \delta\Sigma_d, \phi \right\rangle - \left\langle \Gamma^*, \left(\frac{\partial \mathbf{L}(\alpha)}{\partial \alpha}\phi - \lambda \frac{\partial \mathbf{F}(\alpha)}{\partial \alpha}\phi \right)\delta\alpha \right\rangle \tag{2.5.28}$$

As before, the direct effect $\left\langle \delta\Sigma_d, \phi \right\rangle$ on the RHS is easy to determine since it is a function of the parameters perturbations only. The indirect term $\left\langle \Gamma^*, \left(\frac{\partial \mathbf{L}(\alpha)}{\partial \alpha}\phi - \lambda \frac{\partial \mathbf{F}(\alpha)}{\partial \alpha}\phi \right)\delta\alpha \right\rangle$ requires a single solution of the adjoint model in Eq. (2.5.22). This term is evaluated as many times as there are perturbations. In practice, even with a large number of parameters perturbations, this cost is very small compared to the cost needed to solve Eq. (2.5.25) for the forward flux or Eq. (2.5.22) for the adjoint flux.

To estimate the first order of variations in the eigenvalue, first-order GPT uses:

$$\delta\lambda\big|_{1st} = \frac{\left\langle \phi^*, \left(\frac{\partial \mathbf{L}(\alpha)}{\partial \alpha}\phi - \lambda \frac{\partial \mathbf{F}(\alpha)}{\partial \alpha}\phi \right)\delta\alpha \right\rangle}{\left\langle \phi^*, \mathbf{F}(\alpha)\phi \right\rangle} \tag{2.5.29}$$

where the subscript '1*st*' indicates a first-order variational estimate, and ϕ^* is the fundamental solution calculated from the following unperturbed adjoint equation:

$$\mathbf{L}(\alpha)^{*}\phi^{*} = \lambda \mathbf{F}(\alpha)^{*}\phi^{*} \tag{2.5.30}$$

It is important to note that an exact variational estimate for the eigenvalue λ that is valid for any parameter perturbation can be obtained from:

$$\delta\lambda = \frac{\left\langle \phi^{*}, (\delta\mathbf{L} - \lambda\delta\mathbf{F})\phi' \right\rangle}{\left\langle \phi^{*}, (\mathbf{F}(\alpha) + \delta\mathbf{F})\phi' \right\rangle} \tag{2.5.31}$$

where ϕ' is the perturbed forward flux, $\delta\mathbf{L}$ and $\delta\mathbf{F}$ are perturbations to the operators $\mathbf{L}(\alpha)$ and $\mathbf{F}(\alpha)$, respectively. The drawback to this approach is that one must execute the forward model again to obtain the perturbed flux. Our objective is to avoid doing that and still approximate the exact variation in the eigenvalue and other responses to the user-defined precision.

Before concluding this section, we would like to note that the adjoint operator in Eq. (2.5.22) is singular which necessitates a special solution strategy to ensure that the solution (i.e., the generalized adjoint) is not contaminated by components from the null space of this operator. The traditional approach is to first identify the nullspace as the solution to Eq. (2.5.30), the fundamental adjoint solution, and as the solution of Eq. (2.5.22) is iteratively sought, the null space component is removed using a Gram-Schmidt orthogonalization approach (ArfKen 1985). In the rest of the discussion, whenever reference is made to solving the adjoint model *m* times, it is implied that one has already solved Eq. (2.5.30) once and employed the solution to remove the nullspace components when solving Eq. (2.5.22) *m* times.

2.6 Range-Finding Algorithm

Range finding algorithms (RFA) have been primarily developed in the linear algebra community and the machine learning community to determine an upper bound on the error resulting from constraining the range of a matrix to a subspace (Halko, Martinsson & Tropp 2011). Past research in the nuclear engineering community has also shown that the use of random matrix-vector products could be employed to find subspaces for the ranges of general rectangular matrices (Abdel-Khalik 2004). The algorithm employed in (Abdel-Khalik, Bang & Wang 2013) is summarized here for the sake of a complete discussion. Let $\mathbf{X} \in \mathbb{R}^{m \times n}$ be a general matrix operator whose elements cannot be accessed directly, however the following operation is possible for a given user-defined vector θ:

$$\omega = \mathbf{X}\theta \tag{2.6.1}$$

The objective is to find the effective range of the matrix $\mathbf{X}$ defined by a matrix $\mathbf{Q}$ such that:

$$\left\| \mathbf{X} - \mathbf{Q}\mathbf{Q}^T \mathbf{X} \right\| \le \varepsilon_{\text{user}} \tag{2.6.2}$$

where $\varepsilon_{\text{user}}$ is user-defined tolerance. The range of $\mathbf{Q}$ constitutes a subspace with size of r that capture most of the action $\mathbf{X}$, and we would like r to be as small as possible. It has been shown by (Halko, Martinsson & Tropp 2011), that the conditions in Eq. (2.6.2) could be met with a high probability $1 - \min\{m,n\} \times 10^{-s}$ by employing only $r+s$ matrix-vector products of the form in Eq. (2.6.1). In practice, s is a small integer, and the error estimator is reliable in a range of circumstances when we take $s = 10$. This may be achieved as follows:

1. Let s be a small integer;

2. Let d_0 represent the current estimate of the effective rank of the matrix $\mathbf{X}$;

3. Pick $d_0 + s$ random vectors: $\theta_1, \cdots, \theta_{d_0+s}$;

4. Calculate: $\omega_i = \mathbf{X}\theta_{i+d_0}$, $i = 1, \cdots, s$, $w_i = \mathbf{X}\theta_i$, $i = 1, \cdots, d_0$,

5. Pick d additional random vectors: $\xi_1, \cdots, \xi_d$;

6. Calculate: $w_{d_0+i} = \mathbf{X}\xi_i, i = 1, \cdots, d$;

7. Find an orthonormal set via SVD or Gram-Schmidt algorithm such that: $span\{w_1, \cdots, w_{d_0+d}\} = span\{q_1, \cdots, q_{d_0+d}\}$;

8. Let $\mathbf{Q} = \begin{bmatrix} q_1 & \cdots & q_{d_0+d} \end{bmatrix} \in \mathbb{R}^{m \times (d_0+d)}$;

9. Calculate: $z_i = \left(\mathbf{I} - \mathbf{Q}\mathbf{Q}^T\right)\omega_i, i = 1, \cdots, s$;

10. Let $d_0 = d_0 + d$;

11. If $\varepsilon_{user} < 10\sqrt{\frac{2}{\pi}} \max_{i=1,\cdots,s} \|z_i\|_2$, go back to step 5;

12. Let $r = d_0$;

This algorithm is based on the observation that when a matrix is multiplied by random vectors, the resulting vectors are expected to be independent with a very high probability. If the matrix has a low rank representation that satisfies the condition in Eq. (2.6.2), then one can find this subspace with at most r matrix vector product. Furthermore, this algorithm could be employed with minor modification to find the subspace for the variation in the solution of Eq. (2.5.4).

We first introduce the perturbed system with respect to the input parameters α for the Eq. (2.5.3):

$$\mathbf{A}(\alpha')\phi' = Q_{\text{ex}} \tag{2.6.3}$$

or in terms of numerical discretization

$$\mathbf{A}'\phi' = q_{\text{ex}} \tag{2.6.4}$$

Substituting Eq. (2.5.4) into Eq. (2.6.4), one can obtain the following equation:

$$\delta\phi = -\left(\mathbf{A}^{-1}\delta\mathbf{A}\right)\phi' \tag{2.6.5}$$

where $\delta\phi = \phi' - \phi$ and $\delta\mathbf{A} = \mathbf{A}' - \mathbf{A}$. It can be clearly seen from Eq. (2.6.5) that the $\delta\phi$ lies in the subspace $span\left\{\left(\mathbf{A}^{-1}\delta\mathbf{A}\right)\phi'\right\}_{\delta\alpha} \in \mathbb{C}$ generated by input parameters perturbations. Considering that $rank(\delta\mathbf{A}) = r_{\max}$, therefore, $rank\left(\mathbf{A}^{-1}\delta\mathbf{A}\right) = rank(\delta\mathbf{A}) = r_{\max}$, and the size of the explored subspace is less than or equal to $r_{\max}$. The main question remains as to how to determine the range of matrix operator $\left(\mathbf{A}^{-1}\delta\mathbf{A}\right)$. Note that this could be emulated by selecting input parameters with random perturbations in Eq. (2.6.5).

This completes the identification of the explored subspace. The assumption is that the variation in the solution of Eq. (2.5.4) will belong to a subspace with size of *r* such that the discrepancy between the exact solution and those constrained to the subspace is below the user-defined tolerance. This behavior is achieved as follows:

1. Given a mathematic model described as: $\mathbf{A}(\alpha)\phi = Q_{\text{ex}}$ or $\mathbf{A}\phi = q_{\text{ex}}$;

2. Read user-defined accuracy for the state variations, e.g., $\varepsilon_{\text{user}}$;

3. Let $\mathbf{Q}_0 = [\ ]$, the $n \times 0$ empty matrix , $i = 0$, and $\varepsilon_{\max} = 10\varepsilon_{\text{user}}$;

4. Let $i = i + 1$;

5. Randomly perturb input parameters within their user-defined ranges of perturbations;

6. Execute the given model and record the snapshots: $\delta\phi_i = \phi_i' - \phi \in \mathbb{R}^n$;

7. Find an orthonormal set via SVD or Gram-Schmidt algorithm such that: $span\{\delta\phi_1, \cdots, \delta\phi_i\} = span\{q_1, \cdots, q_i\}$ and $\langle q_i, q_j \rangle = \delta_{i,j}$, for $i, j = 1, \cdots, r$;

8. Append the vector q_i to form: $\mathbf{Q}_i = [\mathbf{Q}_{i-1} \quad q_i] \in \mathbb{R}^{n \times i}$;

9. Calculate $\beta_j = \langle q_j, \delta\phi_i \rangle$, for $j = 1, \cdots, i$, and Let $\beta = [\beta_1 \quad \cdots \quad \beta_i]$;

10. Calculate $z_i = \delta\phi_i - \mathbf{Q}\beta$, and let $\varepsilon_{\max} = \|z_i\|_2$;

11. If $\varepsilon_{\max} \geq \varepsilon_{\text{user}}$, go back to step 4;

12. Let $d_0 = i$;

13. Let s be a small integer;

14. Pick s random perturbed input parameters: $\alpha_1, \cdots, \alpha_s$;

15. Execute the given model and record the snapshots: $\delta\phi_k = \phi_k' - \phi \in \mathbb{R}^n, k = 1, \cdots, s$;

16. Calculate $M_{j,k} = \langle q_j, \delta\phi_k \rangle$, for $j = 1, \cdots, d_0; k = 1, \cdots, s$, and Let $[\mathbf{M}]_{j,k} = M_{j,k}$;

17. Calculate: $z_k = \delta\phi_k - \mathbf{Q}[\mathbf{M}]_{\bullet,k}, k = 1, \cdots, s$, where $[\mathbf{M}]_{\bullet,k}$ is the k^{th} column of **M;**

18. Let $\varepsilon_{\text{theory}} = 10\sqrt{\frac{2}{\pi}} \max_{k=1,\cdots,s} \|z_k\|_2$;

19. If $\varepsilon_{\text{user}} < \varepsilon_{\text{theory}}$, go back to step 5;

20. Let $r = d_0$;

The above algorithm, denoted hereinafter as the range-finding algorithm, is employed in this dissertation to identify with quantifiable accuracy a reduced basis space for the state variations, such that the following equations holds with probability at least $1 - n \times 10^{-s}$:

$$\left\| \delta\phi - \sum_{i=1}^{r} q_i \left\langle q_i, \delta\phi \right\rangle \right\| \leq \varepsilon_{\text{user}} \tag{2.6.6}$$

or in a more compact form:

$$\left\| \delta\phi - \mathbf{Q}\beta \right\| \leq \varepsilon_{\text{user}} \tag{2.6.7}$$

where $\beta \in \mathbb{R}^{r \times 1}$ and $\left[\beta\right]_i = \left\langle q_i, \delta\phi \right\rangle$, for $i = 1, \cdots, r$.

CHAPTER 3. E_PGPT METHODS

3.1 Overview

This dissertation employs the E_PGPT methods to evaluate the state-based responses variations in order to reduce the computational cost in nuclear reactor calculations. In previous studies, estimation of higher-order accuracy up to exact solutions for the flux variations (1) entailed the use of preconditioned iterative methods (Maldonado, Turinsky & Kropaczek 1995, Moore, Turinsky 1998, McKinley, Rahnema 2000, Maldonado, Turinsky 1995) or (2) demanded the availability of an extensive set of higher orders of eigen-modes of the unperturbed forward and adjoint system equations (Gandini 1978b), or (3) required the precomputation of massive adjoint calculations for each phase-space point (McKinley, Rahnema 2000, McKinley, Rahnema 2002).

The development presented in this dissertation is aimed essentially at enabling an efficient explicit or semi-explicit higher-order accurate treatment, based on the construction of the reduced basis space, of the flux shape variations caused by cross section perturbations, control rod insertions, material composition differentiations, and complete fuel assembly permutations at core level. The main difference between E_PGPT and existing GPT is in the formulation and interpretation of the adjoint models employed to calculate responses variations. GPT formulates an adjoint problem that is dependent on the response of interest. It tries to capture via the adjoint solution the relationship between the response of interest and the constraints on the state variations, e.g., Eq. (2.5.22). This allows one to calculate directly

the changes in response without calculating the state variations. The EPGPT however divorces the adjoint model from the given responses meaning that the adjoint model is solved independently of the given responses. This is done based on a set of pseudo responses which captures all possible state variations. Moreover, it has been observed by many scientific communities that although the dimensionality of the state space is very high in order to render high fidelity simulation, the state variability can be well approximated by a subspace, often of much smaller dimension than the state space (Chaturantabut, Sorensen 2010, Carlberg, Bou-Mosleh & Farhat 2011, Bashir et al. 2008, Bui-Thanh, Willcox & Ghattas 2008). Assume that all possible state variations belong to a subspace of size *r*. If *r* is much smaller than *n* (the size of the state space), one can recast GPT in terms of a set of *r* pseudo responses. In doing so, one recognizes that the remaining $n-r$ directions in the state phase space cannot change any response as the state does not vary along these directions.

Consequently, we employ different conventions to relate the reference and perturbed states to distinguish EPGPT and GPT approach. The convention to be used for EPGPT is illustrated by the following example:

$$\Delta\alpha = \alpha' - \alpha \tag{3.1.1}$$

$$\Delta\phi = \phi' - \phi \tag{3.1.2}$$

$$\Delta\mathbf{P} = \mathbf{P}(\alpha') - \mathbf{P}(\alpha) \tag{3.1.3}$$

$$\Delta\mathbf{H} = \mathbf{H}(\alpha') - \mathbf{H}(\alpha) \tag{3.1.4}$$

$$\Delta R = R(\alpha') - R(\alpha) \tag{3.1.5}$$

$$\Delta\lambda = \lambda' - \lambda \tag{3.1.6}$$

This convention will be maintained throughout this dissertation for E$_P$GPT. $\Delta\alpha$ and $\Delta\phi$ are known as the parameters perturbations and difference neutron flux, respectively. $\Delta\mathbf{P}$ and $\Delta\mathbf{H}$ are referred to as the perturbation operators. ΔR is the variation in the response of interest. $\Delta\lambda$ is the variation in the eigenvalue for neutron critical eigenvalue problems.

3.2 Preliminaries for E$_P$GPT

The general approach to identify the subspace for the state variations is provided in Section 2.6. In this section, we will discuss a little bit more about this reduced basis space. Eq. (2.6.5) may be re-written as:

$$\Delta\phi = -\left(\mathbf{Q}\mathbf{Q}^T + \mathbf{Q}^{\perp}\mathbf{Q}^{\perp T}\right)\left(\mathbf{A}^{-1}\Delta\mathbf{A}\right)\phi' \tag{3.2.1}$$

where $\mathbf{Q} \in \mathbb{R}^{n\times r}$ and $\mathbf{Q}^{\perp} \in \mathbb{R}^{n\times(n-r)}$ are orthonormal matrices such $\mathbf{Q}\mathbf{Q}^T + \mathbf{Q}^{\perp}\mathbf{Q}^{\perp T} = \mathbf{I}_{n\times n}$ is the identify matrix. In general, the matrices $\mathbf{Q}$ and $\mathbf{Q}^{\perp}$ are free to choose. As mentioned in the previous Chapter, the majority of state variations could be shown to belong to a reduced basis space. Thus, one can choose the columns of the matrix $\mathbf{Q}$ to span such subspace. Moreover, the columns of $\mathbf{Q}^{\perp}$ could be selected to span the small state variations, assumed smaller than some user-defined tolerance criterion. We will denote the subspace spanned by the columns of $\mathbf{Q}^{\perp}$ as the inactive subspace since it makes a minor contribution to the state variations. In contrary, we will denote the subspace spanned by the columns of $\mathbf{Q}$ as the active subspace. Therefore, the error introduced in the state estimation is given by:

$$\Delta\phi_{\text{error}} = -\left(\mathbf{I} - \mathbf{Q}\mathbf{Q}^T\right)\left(\mathbf{A}^{-1}\Delta\mathbf{A}\right)\phi' \tag{3.2.2}$$

Moreover, we utilize the range-finding algorithm to determine the matrix **Q** that will be employed in the derivation of EPGPT.

As assumed, we can also expand the state variations in the active subspace as shown in the following equations:

$$\begin{aligned}\Delta\phi &= \beta_1(\Delta\alpha)q_1 + \beta_2(\Delta\alpha)q_2 + \cdots + \beta_r(\Delta\alpha)q_r \\ &= \sum_{i=1}^{r}\beta_i(\Delta\alpha)q_i\end{aligned} \tag{3.2.3}$$

where $\langle q_i, q_j\rangle = \delta_{i,j}$ for $i, j = 1,\cdots,r$, and $\beta_i(\Delta\alpha) = \langle q_i, \Delta\phi\rangle$ for $i = 1,\cdots,r$; $\delta_{i,j}$ is the Kronecker symbol, and q_i , the i^{th} column of **Q**, represents an orthonormal basis vector function in the active subspace which is only dependent on the state variations; while the coefficient $\beta_i(\Delta\alpha)$ depends on the vector $\Delta\alpha$ only. Basically, there are two main different approaches to obtain the unknown coefficient $\beta_i(\Delta\alpha)$ in the literature. The first one is based on the Bubnov-Galerkin (B-G) scheme. Considering the coefficient $\beta_i(\Delta\alpha)$ is a function of input parameters perturbations, one need to exploit B-G scheme for each parameters perturbations. In particular, an alternative approach, i.e., adjoint-based GPT approach which can substantially reduce the computational cost incurred in obtaining state variations, has been successfully applied to nuclear reactor analysis since 1960s. In the following sections of this chapter, we will employ GPT to determine the unknown coefficient $\beta_i(\Delta\alpha)$. The ultimate goal is to show that any higher orders of variations could be expressed in terms of reduced basis.

In this dissertation, we define some pseudo responses as follows:

$$R_i \equiv \langle q_i, \phi \rangle, i = 1, 2, \cdots, r \tag{3.2.4}$$

From the definition of pseudo response, one can observe the following important relation

$$\beta_i(\Delta\alpha) = \Delta R_i = \langle q_i, \Delta\phi \rangle;\ i = 1, 2, \cdots, r \tag{3.2.5}$$

This means one can determine the unknown coefficient $\beta_i(\Delta\alpha)$ through evaluating the variations in the pseudo response R_i. If $\beta_i(\Delta\alpha)$ could be estimated efficiently with high accuracy, one can directly calculate similarly accurate estimates for the neutron flux, detector responses or reaction ratios variations.

3.3 EPGPT for Source-Driven Problem

For the source-driven problem, given by Eq. (2.5.6), one can write down the auxiliary functional for pseudo response R_i via employing a variational formalism:

$$K_i\left[\alpha, \phi, \Gamma_i^*\right] = R_i - \left\langle \Gamma_i^*, \left(\mathbf{P}\phi - q_{\text{ex}}\right) \right\rangle, i = 1, 2, \cdots, r \tag{3.3.1}$$

where Γ_i^* is the Lagrange multiplier associated with the constraint in Eq. (2.5.6). Exploiting the idea of the variational formalism that the functional K_i is stationary with respect to the variables ϕ, and Γ_i^*. This is done by equating the first-order derivatives of the auxiliary functional with respect to the variables ϕ, and Γ_i^* to zero as follows:

$$\frac{\partial K_i}{\partial \phi} = 0 \Rightarrow \mathbf{P}^* \Gamma_i^* = q_i \tag{3.3.2}$$

$$\frac{\partial K_i}{\partial \Gamma_i^*} = 0 \Rightarrow \mathbf{P}\phi = q_{\text{ex}} \tag{3.3.3}$$

Unlike GPT approach, EPGPT determines the exact variation in the functional K_i due to variations in α, and ϕ which is given by:

$$\begin{aligned}
\Delta K_i &= \Delta R_i - \left\langle \Gamma_i^*, \left((\mathbf{P}+\Delta\mathbf{P})(\phi+\Delta\phi) - (q_{\text{ex}}+\Delta q_{\text{ex}}) \right) \right\rangle \\
&= \left\langle q_i, \Delta\phi \right\rangle - \left\langle \Gamma_i^*, \left(\mathbf{P}\Delta\phi + \Delta\mathbf{P}\phi + \Delta\mathbf{P}\Delta\phi - \Delta q_{\text{ex}} \right) \right\rangle \\
&= \left\langle q_i, \Delta\phi \right\rangle - \left\langle \Gamma_i^*, \mathbf{P}\Delta\phi \right\rangle - \left\langle \Gamma_i^*, \left(\Delta\mathbf{P}\phi - \Delta q_{\text{ex}} \right) \right\rangle - \left\langle \Gamma_i^*, \Delta\mathbf{P}\Delta\phi \right\rangle \\
&= \left\langle q_i, \Delta\phi \right\rangle - \left\langle \mathbf{P}^*\Gamma_i^*, \Delta\phi \right\rangle - \left\langle \Gamma_i^*, \left(\Delta\mathbf{P}\phi - \Delta q_{\text{ex}} \right) \right\rangle - \left\langle \Gamma_i^*, \Delta\mathbf{P}\Delta\phi \right\rangle \\
&= \left\langle \left(q_i - \mathbf{P}^*\Gamma_i^* \right), \Delta\phi \right\rangle - \left\langle \Gamma_i^*, \left(\Delta\mathbf{P}\phi - \Delta q_{\text{ex}} \right) \right\rangle - \left\langle \Gamma_i^*, \Delta\mathbf{P}\Delta\phi \right\rangle
\end{aligned} \tag{3.3.4}$$

Substituting Eq. (3.3.2) into Eq. (3.3.4) and rearranging results in:

$$\Delta K_i = -\left\langle \Gamma_i^*, \left(\Delta\mathbf{P}\phi - \Delta q_{\text{ex}} \right) \right\rangle - \left\langle \Gamma_i^*, \Delta\mathbf{P}\Delta\phi \right\rangle, i = 1, 2, \cdots, r \tag{3.3.5}$$

We recall $\Delta K_i = \Delta R_i$, thus one can combine Eq. (3.2.5) and Eq. (3.3.5) to obtain:

$$\beta_i(\Delta\alpha) = -\left\langle \Gamma_i^*, \left(\Delta\mathbf{P}\phi - \Delta q_{\text{ex}} \right) \right\rangle - \left\langle \Gamma_i^*, \Delta\mathbf{P}\Delta\phi \right\rangle, i = 1, 2, \cdots, r \tag{3.3.6}$$

Note that the first term in the RHS of Eq. (3.3.6) is the linear approximation for $\beta_i(\Delta\alpha)$, while the second term in the RHS of Eq. (3.3.6) denotes the non-linear effects in $\beta_i(\Delta\alpha)$ with respect to the input parameters perturbations. If we neglect the second term in the RHS of Eq. (3.3.6), we can obtain the first-order approximation for the unknown coefficients $\beta_i(\Delta\alpha)$:

$$\beta_i(\Delta\alpha)\big|_{1st} = -\left\langle \Gamma_i^*, \left(\Delta\mathbf{P}\phi - \Delta q_{\text{ex}} \right) \right\rangle, i = 1, 2, \cdots, r \tag{3.3.7}$$

Therefore, one can evaluate the first-order approximation of Eq. (3.2.3) via only r adjoint solutions:

$$\Delta\phi\big|_{1st} = \sum_{i=1}^{r}\left(\beta_i(\Delta\alpha)\big|_{1st}\right)q_i = -\sum_{i=1}^{r}\left\langle\Gamma_i^*,(\Delta\mathbf{P}\phi-\Delta q_{\text{ex}})\right\rangle q_i \tag{3.3.8}$$

This is denoted hereinafter as the **first-order EPGPT for source-driven problem**.

In many situations, one needs to consider the non-linear effects in the neutron flux corresponding to the large perturbations in the input parameters. For example, control rod insertion, adjustment of moderator densities and burnable poison rod densities. How can we evaluate the non-linear effects in the neutron flux without re-solving the forward system? We address this question by introducing the higher-order EPGPT.

We first rewrite the Eq. (3.3.6) into a more compact vector form:

$$\beta = \beta_{\text{lin}} + \beta_{\text{non-lin}} \tag{3.3.9}$$

where

$$\beta = \left[\beta_1(\Delta\alpha) \quad \cdots \quad \beta_r(\Delta\alpha)\right]^T$$

$$\begin{aligned}\beta_{\text{lin}} &= -\left[\left\langle\Gamma_1^*,(\Delta\mathbf{P}\phi-\Delta q_{\text{ex}})\right\rangle \quad \cdots \quad \left\langle\Gamma_r^*,(\Delta\mathbf{P}\phi-\Delta q_{\text{ex}})\right\rangle\right]^T \\ &= \left[\beta_1(\Delta\alpha)\big|_{1st} \quad \cdots \quad \beta_r(\Delta\alpha)\big|_{1st}\right]^T\end{aligned}$$

$$\beta_{\text{non-lin}} = -\left[\left\langle\Gamma_1^*,\Delta\mathbf{P}\Delta\phi\right\rangle \quad \cdots \quad \left\langle\Gamma_r^*,\Delta\mathbf{P}\Delta\phi\right\rangle\right]^T$$

The term $\Delta\mathbf{P}\Delta\phi$ involves the second and higher orders of variations. Recalling $\Delta\phi = \sum_{j=1}^{r}\beta_j(\Delta\alpha)q_j$, one can obtain

$$
\begin{aligned}
\beta_{\text{non-lin}} &= -\left[\left\langle \Gamma_1^*, \Delta\mathbf{P}\Delta\phi \right\rangle \quad \cdots \quad \left\langle \Gamma_r^*, \Delta\mathbf{P}\Delta\phi \right\rangle\right]^T \\
&= -\left[\left\langle \Gamma_1^*, \Delta\mathbf{P}\left(\sum_{j=1}^{r}\beta_j(\Delta\alpha)q_j\right)\right\rangle \quad \cdots \quad \left\langle \Gamma_r^*, \Delta\mathbf{P}\left(\sum_{j=1}^{r}\beta_j(\Delta\alpha)q_j\right)\right\rangle\right]^T \\
&= -\left[\sum_{j=1}^{r}\beta_j(\Delta\alpha)\left\langle \Gamma_1^*, \Delta\mathbf{P}q_j \right\rangle \quad \cdots \quad \sum_{j=1}^{r}\beta_j(\Delta\alpha)\left\langle \Gamma_r^*, \Delta\mathbf{P}q_j \right\rangle\right]^T \\
&= \begin{bmatrix} \left\langle \Gamma_1^*, \Delta\mathbf{P}q_1 \right\rangle & \cdots & \left\langle \Gamma_1^*, \Delta\mathbf{P}q_r \right\rangle \\ \vdots & \ddots & \vdots \\ \left\langle \Gamma_r^*, \Delta\mathbf{P}q_1 \right\rangle & \cdots & \left\langle \Gamma_r^*, \Delta\mathbf{P}q_r \right\rangle \end{bmatrix}\begin{bmatrix} \beta_1(\Delta\alpha) \\ \vdots \\ \beta_r(\Delta\alpha) \end{bmatrix} \\
&= \mathbf{C}\beta
\end{aligned}
\tag{3.3.10}
$$

where $\mathbf{C} \in \mathbb{R}^{r\times r}$, denoted hereinafter as the parameter perturbation-induced matrix, is defined as

$$
\mathbf{C} \equiv \begin{bmatrix} \left\langle \Gamma_1^*, \Delta\mathbf{P}q_1 \right\rangle & \cdots & \left\langle \Gamma_1^*, \Delta\mathbf{P}q_r \right\rangle \\ \vdots & \ddots & \vdots \\ \left\langle \Gamma_r^*, \Delta\mathbf{P}q_1 \right\rangle & \cdots & \left\langle \Gamma_r^*, \Delta\mathbf{P}q_r \right\rangle \end{bmatrix}
$$

Substituting Eq. (3.3.10) into Eq. (3.3.9) results in

$$
\beta = \beta_{\text{lin}} + \mathbf{C}\beta \tag{3.3.11}
$$

Solving Eq. (3.3.11) for β, one can obtain

$$
\beta = \left(\mathbf{I}_{r\times r} - \mathbf{C}\right)^{-1}\beta_{\text{lin}} \tag{3.3.12}
$$

where $\mathbf{I}_{r\times r} \in \mathbb{R}^{r\times r}$ is a $r\times r$ identity matrix. Eq. (3.3.12) implies that one can calculate the exact coefficients using r forward and r generalized adjoint evaluations. Note that the computational cost of Eq. (3.3.12) mainly depends on the evaluation of $\mathbf{C}$ and β_{lin}.

Therefore, the exact variation in the neutron flux of Eq. (3.2.3) can be approximated using the following equations within user-defined tolerance:

$$\Delta\phi = \sum_{i=1}^{r} \beta_i (\Delta\alpha) q_i = \mathbf{Q}\beta = \mathbf{Q}\left(\mathbf{I}_{r\times r} - \mathbf{C}\right)^{-1} \beta_{\text{lin}} \tag{3.3.13}$$

This completes the derivation of the **higher-order E_PGPT for source-driven problem**.

The E_PGPT for source-driven systems can be summarized as follows:

Algorithm: E_PGPT for Source-Driven Systems

Step 1: Given a mathematical model described by: $\mathbf{P}(\alpha)\phi = q_{\text{ex}}(\alpha)$;

Step 2: Execute the given mathematical model and record the reference flux ϕ;

Step 3: Read user-defined accuracy for the neutron flux variations $\varepsilon_{\text{user}}$;

Step 4: Let $\mathbf{Q}_0 = [\ ]$, the $n\times 0$ empty matrix; $i = 0$, and $\varepsilon_{\max} = 10\varepsilon_{\text{user}}$;

Step 5: DO WHILE $\varepsilon_{\max} \geq \varepsilon_{\text{user}}$;

Step 6: Let $i = i + 1$

Step 7: Randomly perturb all input parameters as follows: $\alpha' = \alpha + \Delta\alpha$;

Step 8: Execute the forward model and record the perturbed flux ϕ_i;

Step 9: Calculate the flux variation: $\Delta\phi_i = \phi_i - \phi$;

Step 10: Find an orthonormal set $\{q_j\}_{j=1}^{i}$ via the Gram-Schmidt algorithm such that:

$$span\{\Delta\phi_1, \cdots, \Delta\phi_i\} = span\{q_1, \cdots, q_i\}, \text{ where } \langle q_i, q_j \rangle = \delta_{i,j}, \text{ for } j = 1, \cdots, i;$$

Step 11: Update the matrix $\mathbf{Q}_i = [\mathbf{Q}_{i-1} \quad q_i]$;

Step 12: Calculate $\beta_j = \langle q_j, \Delta\phi_i \rangle$, for $j = 1, \cdots, i$, and Let $\beta = [\beta_1 \quad \cdots \quad \beta_i]$;

Step 13: Calculate the orthogonal projection of $\Delta\phi_i$ onto the active subspace $\mathbb{C}$: $\mathbf{Q}\beta$;

Step 14: Calculate the projection residual: $z_i = \Delta\phi_i - \mathbf{Q}\beta$, and let $\varepsilon_{\max} = \|z_i\|_2$;

Step 15: END WHILE;

Step 16: Execute forward system *s* more times, and calculate: $\varepsilon_{\text{theory}} = 10\sqrt{\frac{2}{\pi}} \max_{k=1,\cdots,s} \|z_k\|_2$;

Step 17: If $\varepsilon_{\text{user}} < \varepsilon_{\text{theory}}$, then $\varepsilon_{\max} = \varepsilon_{\text{theory}}$ and go back to step 5;

Step 18: Let $r = i$;

Step 19: Calculate the adjoint solutions for the adjoint systems: $\mathbf{P}^*\Gamma_i^* = q_i$, $i = 1, \ldots, r$;

Step 20: Calculate 1st-order evaluation of β: $[\beta_{\text{lin}}]_i = -\left\langle \Gamma_i^*, (\Delta\mathbf{P}\phi - \Delta q_{\text{ex}}) \right\rangle$, $i = 1, \ldots, r$;

Step 21: Calculate 1st-order approximation for neutron flux variations: $\Delta\phi|_{1st} = \mathbf{Q}\beta_{\text{lin}}$;

Step 22: Calculate the matrix **C**: $[\mathbf{C}]_{i,j} \equiv \left\langle \Gamma_i^*, \Delta\mathbf{P}q_j \right\rangle$, $i, j = 1, \ldots, r$;

Step 23: Calculate higher-order evaluation of β: $\beta = (\mathbf{I}_{r\times r} - \mathbf{C})^{-1}\beta_{\text{lin}}$;

Step 24: Calculate higher-order approximation for neutron flux variations:
$\Delta\phi = \mathbf{Q}(\mathbf{I}_{r\times r} - \mathbf{C})^{-1}\beta_{\text{lin}}$;

Note that the bulk of the computational burden in this algorithm is in constructing the active subspace (Step 8) and solving the adjoint systems with respect to the pseudo responses (Step 19) where both the forward model and adjoint model are executed *r* times. In order to calculate the upper error bound for EPGPT, we need to solve the forward model *s* more times. The rest of the computational burden involves only linear algebra operations which are computationally cheap when compared to the cost of executing the forward and/or adjoint

model. For example, the operation in Step 20 involves the evaluation of the inner product of the form: $\langle \Gamma_i^*, \Delta \mathbf{P} \phi \rangle$. This operation is similar to the $\langle \phi^*, \Delta \mathbf{P} \phi \rangle$ operation required by first-order GPT approach, but now is executed r times with ϕ^* replaced by Γ_i^*. Similarly, we need to execute the operation $\langle \Gamma_i^*, \Delta \mathbf{P} q_j \rangle$ in Step 22 r^2 times with ϕ^* replaced by Γ_i^* and ϕ replaced by q_i to calculate parameter perturbation-induced matrix **C**. It is clear that we can readily evaluate the response variations by employing the approximated neutron flux from Step 21 or Step 24. In fact, the EPGPT can be divided into two phases. The first phase is a ***pre-computation phase*** meaning that it is done only once, i.e., Step 1 to Step 19. The second phase is a ***response evaluation phase*** that evaluates for a given response and a given parameters perturbation the exact-to-precision variation in the response, i.e., Step 20 to Step 24. All necessary forward model and adjoint model executions are carried out in the pre-computation phase. For a given response, the response evaluation phase calculates the exact variation in the response using only inner products operations, which are computationally inexpensive compared to the execution cost of forward and adjoint models.

3.4 EPGPT for Critical Eigenvalue Problem

The most common application of perturbation theory is in predicting the variation in the critical eigenvalue corresponding to a small perturbation made to the reactor. In addition, perturbation theory has also been employed to estimate the uncertainty of the multiplication factor due to uncertainties in cross section data.

In this section, we will extend the EPGPT to the critical eigenvalue problems (i.e., Eq. (2.5.16) and Eq. (2.5.17)). We first introduce a set of auxiliary functionals for the pseudo responses R_i via variational formalism:

$$K_i\left[\alpha,\phi,\lambda,N_i^*,\Gamma_i^*\right]=R_i-N_i^*\left(\langle h,\phi\rangle-N\right)-\left\langle\Gamma_i^*,\left(\mathbf{L}\phi-\lambda\mathbf{F}\phi\right)\right\rangle,\ \text{for } i=1,\ldots,r \quad (3.4.1)$$

where R_i is defined by Eq. (3.2.4), N_i^* and Γ_i^* are the Lagrange multipliers associated with the constraints in Eq. (2.5.17) and Eq. (2.5.16), respectively. Exploiting the idea of the variational formalism that the functional K_i is stationary with respect to the variables ϕ, λ, N_i^*, and Γ_i^*. This is done by equating the first-order derivatives of the auxiliary functional with respect to the variables ϕ, λ, N_i^*, and Γ_i^* to zero as follows:

$$\frac{\partial K_i}{\partial\phi}=0\Rightarrow\mathbf{L}^*\Gamma_i^*-\lambda\mathbf{F}^*\Gamma_i^*=q_i-N_i^*h,\ \text{for } i=1,\cdots,r \quad (3.4.2)$$

$$\frac{\partial K_i}{\partial\lambda}=0\Rightarrow\left\langle\Gamma_i^*,\mathbf{F}\phi\right\rangle=0,\ \text{for } i=1,\cdots,r \quad (3.4.3)$$

$$\frac{\partial K_i}{\partial N_i^*}=0\Rightarrow\langle h,\phi\rangle=N \quad (3.4.4)$$

$$\frac{\partial K_i}{\partial\Gamma_i^*}=0\Rightarrow\mathbf{L}\phi-\lambda\mathbf{F}\phi=0 \quad (3.4.5)$$

The N_i^* is determined by requiring the RHS of Eq. (3.4.2) to be orthogonal to the forward flux:

$$\left\langle\left(q_i-N_i^*h\right),\phi\right\rangle=0\Rightarrow N_i^*=\frac{\langle q_i,\phi\rangle}{\langle h,\phi\rangle},\ \text{for } i=1,\cdots,r \quad (3.4.6)$$

Before continuing the detailed derivation for EPGPT, we will first define two different operators representing the critical eigenvalue neutron transport equation to shorten the derivation.

$$\mathbf{P} \equiv \mathbf{L} - \lambda \mathbf{F} \tag{3.4.7}$$

and

$$\Delta\mathbf{P} \equiv \Delta\mathbf{L} - \lambda\Delta\mathbf{F} - \Delta\lambda\mathbf{F} - \Delta\lambda\Delta\mathbf{F} \tag{3.4.8}$$

We now can express Eqs. (3.4.1), (3.4.2) and (3.4.5) as

$$K_i\left[\alpha,\phi,\lambda,N_i^*,\Gamma_i^*\right] = R_i - N_i^*\left(\langle h,\phi\rangle - N\right) - \left\langle \Gamma_i^*, \mathbf{P}\phi\right\rangle, \text{ for } i=1,\ldots,r \tag{3.4.9}$$

$$\mathbf{P}^*\Gamma_i^* = q_i - N_i^* h, \text{ for } i=1,\cdots,r \tag{3.4.10}$$

$$\mathbf{P}\phi = 0 \tag{3.4.11}$$

Similarly, unlike GPT, EPGPT determines the exact variation in the functional K_i due to variations in α, ϕ, and λ which is given by:

$$\begin{aligned}
\Delta K_i &= \Delta R_i - N_i^*\langle h,\Delta\phi\rangle - \left\langle \Gamma_i^*, \left(\mathbf{P}\Delta\phi + \Delta\mathbf{P}\phi + \Delta\mathbf{P}\Delta\phi\right)\right\rangle \\
&= \langle q_i,\Delta\phi\rangle - \left\langle N_i^* h,\Delta\phi\right\rangle - \left\langle \Gamma_i^*, \mathbf{P}\Delta\phi\right\rangle - \left\langle \Gamma_i^*, \Delta\mathbf{P}\phi\right\rangle - \left\langle \Gamma_i^*, \Delta\mathbf{P}\Delta\phi\right\rangle \\
&= \left\langle \left(q_i - N_i^* h\right),\Delta\phi\right\rangle - \left\langle \mathbf{P}^*\Gamma_i^*,\Delta\phi\right\rangle - \left\langle \Gamma_i^*, \Delta\mathbf{P}\phi\right\rangle - \left\langle \Gamma_i^*, \Delta\mathbf{P}\Delta\phi\right\rangle \\
&= \left\langle \left(q_i - N_i^* h - \mathbf{P}^*\Gamma_i^*\right),\Delta\phi\right\rangle - \left\langle \Gamma_i^*, \Delta\mathbf{P}\phi\right\rangle - \left\langle \Gamma_i^*, \Delta\mathbf{P}\Delta\phi\right\rangle
\end{aligned} \tag{3.4.12}$$

Substituting Eq. (3.4.10) into Eq. (3.4.12) results in:

$$\Delta K_i = -\left\langle \Gamma_i^*, \Delta\mathbf{P}\phi\right\rangle - \left\langle \Gamma_i^*, \Delta\mathbf{P}\Delta\phi\right\rangle, \text{ for } i=1,2,\cdots,r \tag{3.4.13}$$

Recall that $\Delta R_i = \Delta K_i$ and $\beta_i(\Delta\alpha) = \Delta R_i$, we can then evaluate $\beta_i(\Delta\alpha)$ using the following relation:

$$\beta_i(\Delta\alpha) = -\left\langle \Gamma_i^*, \Delta\mathbf{P}\phi \right\rangle - \left\langle \Gamma_i^*, \Delta\mathbf{P}\Delta\phi \right\rangle, \text{ for } i = 1,2,\cdots,r \tag{3.4.14}$$

Note that the first term in the RHS of Eq. (3.4.14) is the linear approximation for $\beta_i(\Delta\alpha)$, while the second term in the RHS of Eq. (3.4.14) denotes the non-linear effects in $\beta_i(\Delta\alpha)$ with respect to the input parameters perturbations. If we neglect the second term in the RHS of Eq. (3.4.14), we can obtain the first-order approximation for the unknown coefficients $\beta_i(\Delta\alpha)$:

$$\beta_i(\Delta\alpha)\big|_{1st} = -\left\langle \Gamma_i^*, \Delta\mathbf{P}\phi \right\rangle, i = 1,2,\cdots,r \tag{3.4.15}$$

Therefore, one can evaluate the first-order approximation of Eq. (3.2.3) via only r adjoint solutions:

$$\Delta\phi\big|_{1st} = \sum_{i=1}^{r} \left(\beta_i(\Delta\alpha)\big|_{1st} \right) q_i = -\sum_{i=1}^{r} \left\langle \Gamma_i^*, \Delta\mathbf{P}\phi \right\rangle q_i \tag{3.4.16}$$

This is denoted hereinafter as the **first-order EPGPT for critical eigenvalue problem**.

Similar to the source-driven problem, we can employ the parameter perturbation-induced matrix **C** to determine the non-linear effects for the neutron flux variations. First, we will rewrite the Eq. (3.4.14) into a more compact vector form:

$$\beta = \beta_{\text{lin}} + \beta_{\text{non-lin}} \tag{3.4.17}$$

where

$$\beta = \left[\beta_1(\Delta\alpha) \quad \cdots \quad \beta_r(\Delta\alpha) \right]^T$$

$$\beta_{\text{lin}} = -\left[\left\langle \Gamma_1^*, \Delta\mathbf{P}\phi \right\rangle \quad \cdots \quad \left\langle \Gamma_r^*, \Delta\mathbf{P}\phi \right\rangle\right]^T$$
$$= \left[\beta_1(\Delta\alpha)\big|_{1st} \quad \cdots \quad \beta_r(\Delta\alpha)\big|_{1st}\right]^T$$

$$\beta_{\text{non-lin}} = -\left[\left\langle \Gamma_1^*, \Delta\mathbf{P}\Delta\phi \right\rangle \quad \cdots \quad \left\langle \Gamma_r^*, \Delta\mathbf{P}\Delta\phi \right\rangle\right]^T$$

Recall that $\Delta\phi = \sum_{j=1}^{r} \beta_j(\Delta\alpha) q_j$, thus

$$\begin{aligned}
\beta_{\text{non-lin}} &= -\left[\left\langle \Gamma_1^*, \Delta\mathbf{P}\Delta\phi \right\rangle \quad \cdots \quad \left\langle \Gamma_r^*, \Delta\mathbf{P}\Delta\phi \right\rangle\right]^T \\
&= -\left[\left\langle \Gamma_1^*, \Delta\mathbf{P}\left(\sum_{j=1}^{r} \beta_j(\Delta\alpha) q_j\right)\right\rangle \quad \cdots \quad \left\langle \Gamma_r^*, \Delta\mathbf{P}\left(\sum_{j=1}^{r} \beta_j(\Delta\alpha) q_j\right)\right\rangle\right]^T \\
&= -\left[\sum_{j=1}^{r} \beta_j(\Delta\alpha)\left\langle \Gamma_1^*, \Delta\mathbf{P}q_j \right\rangle \quad \cdots \quad \sum_{j=1}^{r} \beta_j(\Delta\alpha)\left\langle \Gamma_r^*, \Delta\mathbf{P}q_j \right\rangle\right]^T \\
&= \begin{bmatrix} \left\langle \Gamma_1^*, \Delta\mathbf{P}q_1 \right\rangle & \cdots & \left\langle \Gamma_1^*, \Delta\mathbf{P}q_r \right\rangle \\ \vdots & \ddots & \vdots \\ \left\langle \Gamma_r^*, \Delta\mathbf{P}q_1 \right\rangle & \cdots & \left\langle \Gamma_r^*, \Delta\mathbf{P}q_r \right\rangle \end{bmatrix} \begin{bmatrix} \beta_1(\Delta\alpha) \\ \vdots \\ \beta_r(\Delta\alpha) \end{bmatrix} \\
&= \mathbf{C}\beta
\end{aligned} \tag{3.4.18}$$

where the parameter-induced matrix $\mathbf{C} \in \mathbb{R}^{r\times r}$ is defined as

$$\mathbf{C} \equiv \begin{bmatrix} \left\langle \Gamma_1^*, \Delta\mathbf{P}q_1 \right\rangle & \cdots & \left\langle \Gamma_1^*, \Delta\mathbf{P}q_r \right\rangle \\ \vdots & \ddots & \vdots \\ \left\langle \Gamma_r^*, \Delta\mathbf{P}q_1 \right\rangle & \cdots & \left\langle \Gamma_r^*, \Delta\mathbf{P}q_r \right\rangle \end{bmatrix}$$

Substituting Eq. (3.4.18) into Eq. (3.4.17) results in

$$\beta = \beta_{\text{lin}} + \mathbf{C}\beta \tag{3.4.19}$$

Solving Eq. (3.4.19) for β, one can obtain

$$\beta = (\mathbf{I}_{r\times r} - \mathbf{C})^{-1} \beta_{\text{lin}} \tag{3.4.20}$$

where $\mathbf{I}_{r\times r} \in \mathbb{R}^{r\times r}$ is an identity matrix. Therefore, the exact variation in the neutron flux of Eq. (3.2.3) can be approximated using the following equation within user-defined tolerance:

$$\Delta\phi = \sum_{i=1}^{r} \beta_i(\Delta\alpha) q_i = \mathbf{Q}\beta = \mathbf{Q}\left(\mathbf{I}_{r\times r} - \mathbf{C}\right)^{-1} \beta_{\text{lin}} \tag{3.4.21}$$

This is denoted hereinafter as the **higher-order E$_P$GPT for critical eigenvalue problem**.

Note that, the deceptively simple operator notations lead to the identity expression for the neutron flux variations in both Eq. (3.4.21) for critical eigenvalue problem and Eq. (3.3.13) obtained from source-driven problem. However, there's a significant difference between this two equations. The neutron flux variations in critical eigenvalue problems depend on the variation in eigenvalue since $\Delta\mathbf{P}$ is dependent on $\Delta\lambda$ in Eq. (3.4.8). In the previous derivation, we presume that the exact variation $\Delta\lambda$ in the eigenvalue is known, thus the problem degenerates to a source-driven problem. The question raised here is how to evaluate the exact variation $\Delta\lambda$ without re-solving the forward equations for a given active subspace. We will answer this question in the rest of this section and we will demonstrate our approach with several numerical cases in Chapter 6.

Recalling Eq. (2.5.31), one can rewrite the exact eigenvalue variation as:

$$\Delta\lambda = \frac{\left\langle \phi^*, \left(\Delta\mathbf{L} - \lambda\Delta\mathbf{F}\right)\phi \right\rangle + \left\langle \phi^*, \Delta\mathbf{P}\Delta\phi \right\rangle}{\left\langle \phi^*, \mathbf{F}\phi \right\rangle + \left\langle \phi^*, \Delta\mathbf{F}\phi \right\rangle} \tag{3.4.22}$$

where $\Delta\mathbf{P}$ is defined in Eq. (3.4.8). Since $\Delta\mathbf{P}\Delta\phi$ depends on $\Delta\lambda$, we invoke a Rayleigh quotient like iterative approach to solve for $\Delta\lambda$:

(a) Given $\Delta\lambda_k$, the k^{th} iterate for $\Delta\lambda$;

(b) Calculate: $\Delta\mathbf{P}_k = \Delta\mathbf{L} - \lambda\Delta\mathbf{F} - \Delta\lambda_k\mathbf{F} - \Delta\lambda_k\Delta\mathbf{F}$;

(c) Calculate: β_{lin} and $\mathbf{C}$;

(d) Calculate: $\Delta\phi_k = \mathbf{Q}\left(\mathbf{I}_{r\times r} - \mathbf{C}\right)^{-1}\beta_{\text{lin}}$

(e) Calculate: $\Delta\mathbf{P}_k\Delta\phi_k$

(f) Calculate the next iterate: $\Delta\lambda_{k+1} = \dfrac{\left\langle\phi^*, (\Delta\mathbf{L} - \lambda\Delta\mathbf{F})\phi\right\rangle + \left\langle\phi^*, \Delta\mathbf{P}_k\Delta\phi\right\rangle}{\left\langle\phi^*, \mathbf{F}\phi\right\rangle + \left\langle\phi^*, \Delta\mathbf{F}\phi\right\rangle}$

(g) Continue until stopping criteria satisfied.

In practice, the iterative approach for eigenvalue variation is summarized as follows:

Iterative Algorithm for the Variations in the Eigenvalues

From pre-computation phase, one can obtain $\{q_i\}_{i=1}^{r}$ and $\{\Gamma_i^*\}_{i=1}^{r}$;
Given $\Delta\lambda_0$=0, $\Delta\lambda_1 = 10^{-5}$, and tolerance η,
Calculate $A = \left\langle\phi^*, (\Delta\mathbf{L} - \lambda\Delta\mathbf{F})\phi\right\rangle, B = \left\langle\phi^*, \mathbf{F}\phi\right\rangle + \left\langle\phi^*, \Delta\mathbf{F}\phi\right\rangle$;
Let $i = 1$ and $j = 1$;
If $i \le r$; then
  Calculate $[\mathrm{c}_1]_i = \left\langle\phi^*, (\Delta\mathbf{L} - \lambda\Delta\mathbf{F})q_i\right\rangle$ and $[c_2]_i = \left\langle\phi^*, (\mathbf{F} + \Delta\mathbf{F})q_i\right\rangle$;
  Calculate $[d_1]_i = \left\langle\Gamma_i^*, (\Delta\mathbf{L} - \lambda\Delta\mathbf{F})\phi\right\rangle$ and $[d_2]_i = \left\langle\Gamma_i^*, \Delta\mathbf{F}\phi\right\rangle$;
  $i = i + 1$;
  If $j \le r$; then
    Calculate $[\mathbf{C}_1]_{i,j} = -\left\langle\Gamma_i^*, (\Delta\mathbf{L} - \lambda\Delta\mathbf{F})q_j\right\rangle$ and $[\mathbf{C}_2]_{i,j} = -\left\langle\Gamma_i^*, (\mathbf{F} + \Delta\mathbf{F})q_j\right\rangle$;
    $j = j + 1$
  End if
End if

Let $k = 1$;
Do While $\left|\Delta\lambda_k - \Delta\lambda_{k-1}\right| > \eta$
Calculate the $r \times r$ parameter perturbation-induced matrix: $\mathbf{C} = \mathbf{C}_1 - \Delta\lambda_k \mathbf{C}_2$
Calculate $C_k = -\left(c_1 - \Delta\lambda_k c_2\right)^T \left(\mathbf{I}_{r\times r} - \mathbf{C}\right)^{-1} \left(d_1 - \Delta\lambda_k d_2\right)$
Calculate the next iterate: $\Delta\lambda_{k+1} = \dfrac{A + C_k}{B}$
$k = k + 1$
End While

The algorithm of EPGPT for critical eigenvalue systems is similar to the algorithm adopted for the source-driven systems. For the critical eigenvalue systems, we need to add the Raleigh quotient like iterative approach for the estimation of eigenvalue into the algorithm only.

CHAPTER 4. EVALUATION OF USER-DEFINED RESPONSE VARIATIONS

4.1 Overview

This chapter describes how to recast the two typical responses encountered, defined in Eq. (2.5.1) and Eq. (2.5.2), in nuclear reactor calculations in terms of the r pseudo responses determined from the previous chapter. Before embarking on the practical responses variations evaluations, we first recall the expression β:

$$\beta = \left(\mathbf{I}_{r\times r} - \mathbf{C}\right)^{-1} \beta_{\text{lin}} \tag{4.1.1}$$

where

$$\beta_{\text{lin}} = \begin{cases} -\left[\left\langle \Gamma_1^*, \left(\Delta\mathbf{P}\phi - \Delta q_{\text{ex}}\right)\right\rangle \quad \cdots \quad \left\langle \Gamma_r^*, \left(\Delta\mathbf{P}\phi - \Delta q_{\text{ex}}\right)\right\rangle\right]^T & \text{Source-Driven} \\ -\left[\left\langle \Gamma_1^*, \Delta\mathbf{P}\phi\right\rangle \quad \cdots \quad \left\langle \Gamma_r^*, \Delta\mathbf{P}\phi\right\rangle\right]^T & \text{Eigenvalue} \end{cases}$$

and

$$\mathbf{C} \equiv \begin{bmatrix} \left\langle \Gamma_1^*, \Delta\mathbf{P}q_1\right\rangle & \cdots & \left\langle \Gamma_1^*, \Delta\mathbf{P}q_r\right\rangle \\ \vdots & \ddots & \vdots \\ \left\langle \Gamma_r^*, \Delta\mathbf{P}q_1\right\rangle & \cdots & \left\langle \Gamma_r^*, \Delta\mathbf{P}q_r\right\rangle \end{bmatrix}$$

The significant difference between the source-driven problem and eigenvalue problem lies on the determination of $\Delta\mathbf{P}$. Note that $\Delta\mathbf{P}$ for source-driven problem depends only on the parameters perturbations which is easily determined, whereas $\Delta\mathbf{P}$ for eigenvalue problem depends on both parameters perturbations and eigenvalue variations. One should adopt particular approaches, i.e., Raleigh quotient like iterative approach adopted in Chapter 3, to evaluate the variations in the eigenvalue. Furthermore, β in Eq. (4.1.1) can be pre-

determined by employing $r+s$ forward calculations and r generalized adjoint calculations. In the next section, we will show that we can succinctly describe the variations in the responses by employing the pre-determined β.

4.2 Reaction Rate Calculation

The definition of reaction rate is given by Eq. (2.5.1), and the variation in the response is given by:

$$\Delta R = \langle \Delta\Sigma_d, \phi \rangle + \langle \Sigma_d, \Delta\phi \rangle + \langle \Delta\Sigma_d, \Delta\phi \rangle \tag{4.2.1}$$

As mentioned earlier, the direct term $\langle \Delta\Sigma_d, \phi \rangle$ is the easiest to calculate since it does not depend on the state variations. The second and third terms can be related to the active subspace by expanding both Σ_d and $\Delta\Sigma_d$ as follows:

$$\Sigma_d = \sum_{i=1}^{r} S_i q_i + \Sigma_d{}^{\perp} \text{ and } \Delta\Sigma_d = \sum_{i=1}^{r} \Delta S_i q_i + \Delta\Sigma_d{}^{\perp}$$

where $S_i = \langle \Sigma_d, q_i \rangle$, $\Delta S_i = \langle \Delta\Sigma_d, q_i \rangle$, $\Sigma_d{}^{\perp} \in \mathbb{C}^{\perp}$, and $\Delta\Sigma_d{}^{\perp} \in \mathbb{C}^{\perp}$. Now substituting in Eq. (4.2.1):

$$\begin{aligned} \Delta R &= \langle \Delta\Sigma_d, \phi \rangle + \langle \Sigma_d, \Delta\phi \rangle + \langle \Delta\Sigma_d, \Delta\phi \rangle \\ &= \langle \Delta\Sigma_d, \phi \rangle + \sum_{i=1}^{r} (S_i + \Delta S_i) \langle q_i, \Delta\phi \rangle + \langle (\Sigma_d{}^{\perp} + \Delta\Sigma_d{}^{\perp}), \Delta\phi \rangle \end{aligned} \tag{4.2.2}$$

Note that this is an exact expression for the variation in the response. Recalling that the state varies along the active subspace $\mathbb{C}$ only, one may ignore the last term on the RHS thereby reducing Eq. (4.2.2) to:

$$\begin{aligned}\Delta R_{\mathrm{E_pGPT}} &= \left\langle \Delta\Sigma_d, \phi \right\rangle + \sum_{i=1}^{r} \left(S_i + \Delta S_i \right) \left\langle q_i, \Delta\phi \right\rangle \\ &= \left\langle \Delta\Sigma_d, \phi \right\rangle + w^T \beta\end{aligned} \tag{4.2.3}$$

where $w = \left[S_1 + \Delta S_1, \quad S_2 + \Delta S_2, \quad \ldots \quad , S_r + \Delta S_r \right]^T$.

4.3 Flux Ratios Calculation

Recall the definition of flux ratios that is given by Eq. (2.5.2):

$$R = \frac{\left\langle \Sigma_1, \phi \right\rangle}{\left\langle \Sigma_2, \phi \right\rangle} \tag{4.3.1}$$

To calculate the exact variation in this response, one could repeat the above procedure for both the numerator and denominator, treating them as two different responses. Therefore, the response variations can be determined by:

$$\Delta R_{\mathrm{EpGPT}} = \frac{\left\langle \Delta\Sigma_1, \phi \right\rangle + w_1^T \beta}{\left\langle \Delta\Sigma_2, \phi \right\rangle + w_2^T \beta} \tag{4.3.2}$$

where

$$w_1 = \left[\left\langle \left(\Sigma_1 + \Delta\Sigma_1 \right), q_1 \right\rangle \quad \cdots \quad \left\langle \left(\Sigma_1 + \Delta\Sigma_1 \right), q_r \right\rangle \right]^T$$

$$w_2 = \left[\left\langle \left(\Sigma_2 + \Delta\Sigma_2 \right), q_1 \right\rangle \quad \cdots \quad \left\langle \left(\Sigma_2 + \Delta\Sigma_2 \right), q_r \right\rangle \right]^T$$

4.4 Error Analysis for Response Variations

In this section, we invoke the reaction rate as the response to calculate the error bound on the response variations. Recalling that EPGPT presumes $\Delta\phi = \sum_{i=1}^{r} \beta_i q_i = \mathbf{Q}\beta$, thus Eq. (4.2.1) could be approximated by:

$$\Delta R_{\mathrm{E_PGPT}} = \langle \Delta\Sigma_d, \phi \rangle + \langle \Sigma_d, \mathbf{Q}\beta \rangle + \langle \Delta\Sigma_d, \mathbf{Q}\beta \rangle \tag{4.4.1}$$

We can then evaluate

$$\Delta R - \Delta R_{\mathrm{E_PGPT}} = \langle \Sigma_d, (\Delta\phi - \mathbf{Q}\beta) \rangle + \langle \Delta\Sigma_d, (\Delta\phi - \mathbf{Q}\beta) \rangle \tag{4.4.2}$$

Employing the Cauchy-Schwarz inequality, the error in the response due to EPGPT approximation may be constrained by:

$$\left| \Delta R - \Delta R_{\mathrm{E_PGPT}} \right| \le \left\| \Sigma_d + \Delta\Sigma_d \right\|_2 \left\| \Delta\phi - \mathbf{Q}\beta \right\|_2 \le \left\| \Sigma_d + \Delta\Sigma_d \right\|_2 \varepsilon_{\mathrm{user}} \tag{4.4.3}$$

We recall that $\left\| \Delta\phi - \mathbf{Q}\beta \right\|_2 \le \varepsilon_{\mathrm{user}}$. This expression has two important implications:

a) for any response of the form: $R = \langle \Sigma_d^{\perp}, \phi \rangle$ where $\Sigma_d^{\perp} \in \mathbb{C}^{\perp}$ and $\Delta\Sigma_d^{\perp} \in \mathbb{C}^{\perp}$, the corresponding response variation as predicted by EPGPT will be zero with the error upper-bounded by $\varepsilon_{\mathrm{user}} \left\| \Sigma_d^{\perp} + \Delta\Sigma_d^{\perp} \right\|_2$;

b) for any response of the form : $R = \langle \Sigma_d, \phi \rangle$ where $\Sigma_d \in \mathbb{C}$, and $\Delta\Sigma_d \in \mathbb{C}$, the corresponding response variation will depend on only *r* degrees of freedom (denoting the active responses) which describe the possible ways in which the state can vary for all possible parameters perturbations.

CHAPTER 5. AN ANALYTIC EXAMPLE

The purpose of this chapter is to demonstrate EPGPT by solving a simple analytic example. Many of the properties discussed in Chapter 3 can be illustrated in this manner. The system considered for demonstration EPGPT is a two-group neutron balance problem with infinite homogenous medium. For this case, the transport operators are 2 by 2 matrices such that one can easily obtain the analytic solution. The parameters for the first group are arbitrarily assigned as $\Sigma_{t,1}=5$, $\Sigma_{c,1}=3$, $\Sigma_{f,1}=1$, $\Sigma_{s,1\to1}=0$, $\Sigma_{s,1\to2}=1$, $\overline{\nu}_1=4$, and $\chi_1=0.75$ where the symbols have their usual definitions. Similarly, the parameters for the second group are assigned as $\Sigma_{t,2}=2$, $\Sigma_{c,2}=1$, $\Sigma_{f,2}=1$, $\Sigma_{s,2\to1}=0$, $\Sigma_{s,2\to2}=0$, $\overline{\nu}_2=2$, and $\chi_2=0.25$. Notice that for each group the absorption $\left(\Sigma_c\phi+\Sigma_f\phi\right)$ equals the neutron production $\nu\Sigma_f\phi$; therefore, the system is critical and the neutron transport operator can be obtained:

$$\mathbf{L}=\begin{bmatrix}\Sigma_{t,1}-\Sigma_{s,1\to1} & -\Sigma_{s,2\to1}\\ -\Sigma_{s,1\to2} & \Sigma_{t,2}-\Sigma_{s,2\to2}\end{bmatrix}=\begin{bmatrix}5 & 0\\ -1 & 2\end{bmatrix}$$

and

$$\mathbf{F}=\begin{bmatrix}\chi_1\nu_1\Sigma_{f,1} & \chi_1\nu_2\Sigma_{f,2}\\ \chi_2\nu_1\Sigma_{f,1} & \chi_2\nu_2\Sigma_{f,2}\end{bmatrix}=\begin{bmatrix}3 & 1.5\\ 1 & 0.5\end{bmatrix}$$

Moreover, $\mathbf{L}^*=\mathbf{L}^T$, and $\mathbf{F}^*=\mathbf{F}^T$, the "T" superscript indicates algebraic transpose. The characteristic equation for this problem is:

$$\det\left(\mathbf{L}-\lambda\mathbf{F}\right)=\begin{vmatrix}5-3\lambda & -1.5\lambda\\ -1-\lambda & 2-0.5\lambda\end{vmatrix}=0 \tag{5.1.1}$$

The fundamental forward solution is: $\lambda=1$ and $\phi=\left[3/7 \quad 4/7\right]^T$. While the fundamental adjoint solution is: $\lambda=1$; and $\phi^*=\left[0.5 \quad 0.5\right]^T$. Note that all fluxes are normalized to one for simplicity. The perturbation equation for $\Delta\lambda$ is illustrated by considering the perturbation given by:

$$\Delta\mathbf{L}=\begin{bmatrix}\Delta\Sigma_{c,1} & 0\\ 0 & 0\end{bmatrix}$$

This perturbation represents a change in the capture cross section for the first group. The first-order estimation for the variation in λ via GPT is:

$$\Delta\lambda_{1st}=\frac{\left\langle\phi^*,\Delta\mathbf{L}\phi\right\rangle}{\left\langle\phi^*,\mathbf{F}\phi\right\rangle}=\frac{3}{20}\Delta\Sigma_{c,1} \tag{5.1.2}$$

The characteristic equation for the perturbed system can be solved to obtain the following exact result for the variation in λ resulting from the perturbation $\Delta\Sigma_{c,1}$:

$$\Delta\lambda_{\text{Exact}}=\frac{3\Delta\Sigma_{c,1}}{20+\Delta\Sigma_{c,1}} \tag{5.1.3}$$

Considering the flux is normalized, only one basis vector is needed for EPGPT calculation since there is only one degree of freedom in the neutron flux variations. This basis vector is obtained by the range-finding algorithm:

$$\mathbf{q}_1=\left[1/\sqrt{2} \quad -1/\sqrt{2}\right]^T$$

The comparison of numerical results obtained using Eqs. (3.4.22), (5.1.2), and (5.1.3) is shown in **Table 5-1,** and the reduction errors of neutron flux are presented in **Table 5-2**.

Table 5-1. Exact and Approximate Errors for $\Delta\lambda$

$\Delta\Sigma_{c,1}/\Sigma_{c,1}$	$\Delta\lambda_{\text{Exact}}$ **(pcm)**	ε_1^* **(pcm)**	ε_2^* **(pcm)**
0.01	449.33	-0.67	0.00
-0.01	-450.68	-0.68	0.00
0.05	2233.25	-16.75	0.00
-0.05	-2267.00	-17.00	0.00
0.10	4433.50	-66.50	0.00
-0.10	-4568.53	-68.53	0.00
0.25	10843.37	-406.63	0.00
-0.25	-11688.31	-438.31	0.00
0.50	20930.23	-1569.77	0.00
-0.50	-24324.32	-1824.32	0.00

*: $\varepsilon_1 = \Delta\lambda_{\text{Exact}} - \Delta\lambda_{1st}$; $\varepsilon_2 = \Delta\lambda_{\text{Exact}} - \Delta\lambda_{\text{E}_\text{p}\text{GPT}}$

Table 5-2. Errors in Neutron Flux

$\frac{\Delta\Sigma_{c,1}}{\Sigma_{c,1}}$	rel.rms*
0.01	1.43E-16
-0.01	2.63E-16
0.05	1.54E-16
-0.05	1.78E-16
0.10	1.67E-16
-0.10	1.97E-16
0.25	3.56E-16
-0.25	9.82E-17
0.50	1.44E-16
-0.50	1.64E-16

*: rel.rms= $\left\|\phi_{\text{Exact}} - \phi_{\text{E}_\text{p}\text{GPT}}\right\|_2 / \left\|\phi_{\text{Reference}}\right\|_2$;

The first group capture cross section is randomly perturbed by 10%. The results calculated by E_PGPT and first-order GPT are compared to those computed by solving the exact perturbed forward equation, as presented in **Figure 5-1** for 100 different cases. The variational error shown in **Figure 5-1** is defined as:

$$\textbf{Variational Error}: \ \Delta k_{\text{exact}} - \Delta k_{\text{approx}}$$

where Δ implies a variation from the reference calculation, Δk_{exact} and Δk_{approx} denote the exact variation in k-eigenvalue estimated by direct forward perturbation and the variation estimated by E_PGPT or first-order GPT.

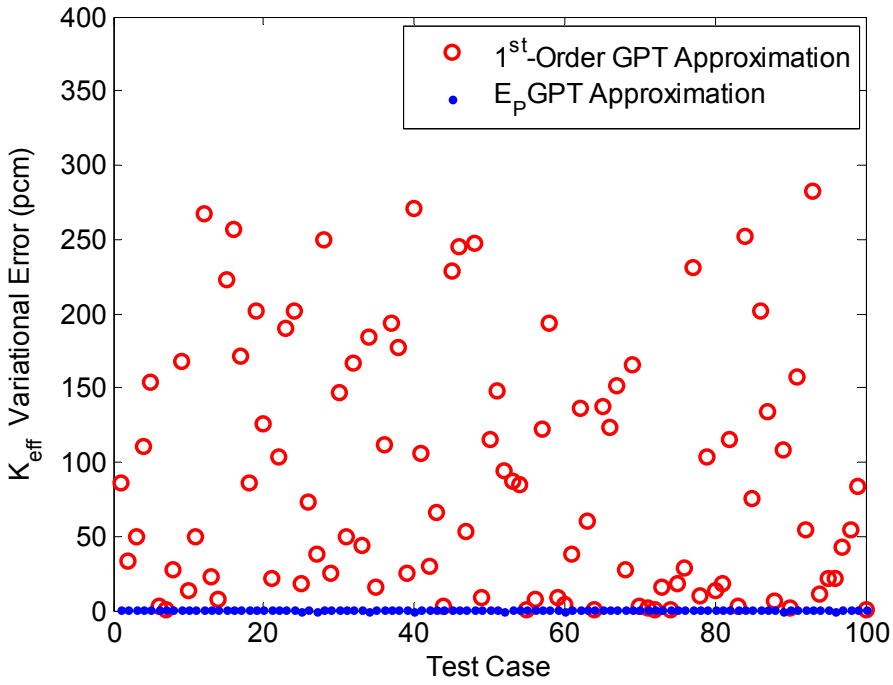

Figure 5-1. Comparison of Estimation Accuracy (100 cases)

CHAPTER 6. NUMERICAL RESULTS FOR E_PGPT

6.1 Examination of Active Subspace

Two cases are studied to show the size of the active subspace is small compared to the number of input parameters (i.e., cross sections, number densities), and flux phase space. These cases are based on a realistic BWR model. Figure 6-1 depicts the lattice model analyzed; it is a benchmark of a stand-alone single assembly mini-core model designed by the OECD/NEA to assess the assumptions in current LWR standard lattice physics scheme (Ivanov et al. 2007). Main calculations are completed using SCALE 6.1. The neutron angular flux is obtained by the NEWT module in SCALE 6.1. NEWT (**N**ew **E**SC-based **W**eighting **T**ransport Code) is a multigroup discrete-ordinates radiation transport computer code that allows 2-D neutron transport calculations using complex geometric models. The data library v5-44 (or 44GROUPNDF5) is employed. In this model, S-6 quadrature, P-1 scattering (P-2 in the moderator), spatial stopping criteria of $\varepsilon = 10^{-7}$, and an eigenvalue stopping criteria of $\varepsilon = 10^{-7}$ are used. There're total 4624 computational cells for this lattice model. Thus, the dimension of scalar flux space is $4624 \times 44 = 203456$. Additionally, total of 9 different fuel rods containing 29 different isotopes are adopted for this model.

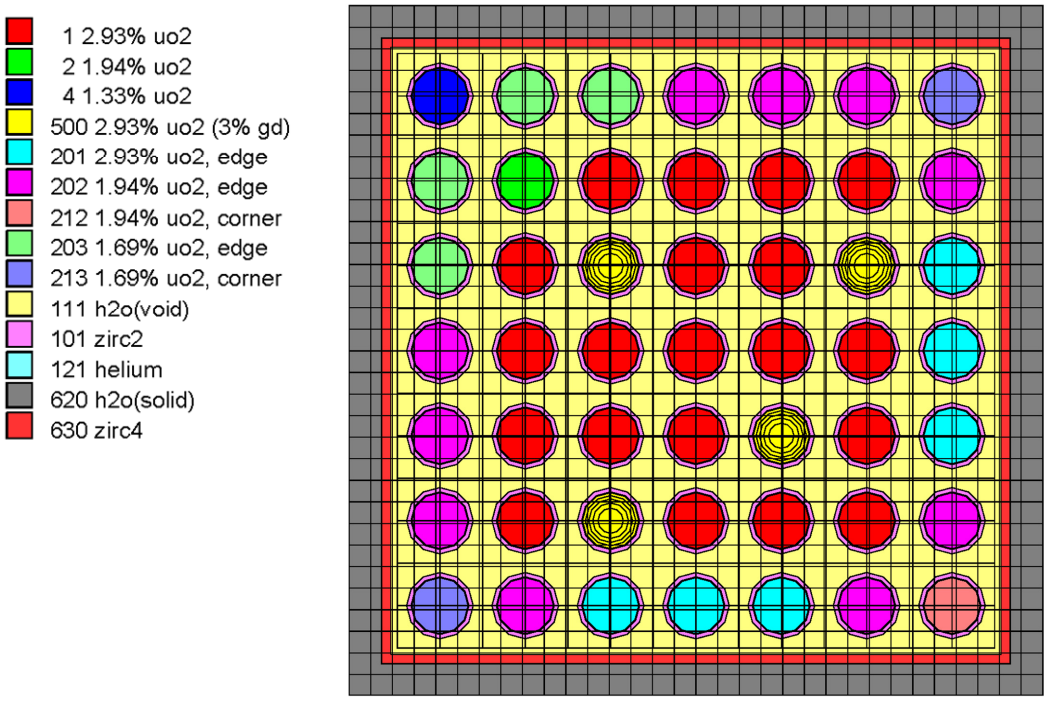

Figure 6-1. A 7×7 BWR Benchmark Lattice Model

To check robustness of the active subspace, we employ the range-finding algorithm to obtain the active subspace. In the first case, we calculate the flux variations with respect to the microscopic cross sections perturbations. All independent microscopic cross sections (i.e., inelastic scattering, effective (n, 2n), fission, capture, ν, χ) perturbations are randomly selected from a uniform distribution with 10% standard derivation relative to their reference values. The dimension of the perturbed parameters space is 7656 (i.e., 29 isotopes, 44 energy groups, and 6 reaction types). In total, 361 forward calculations are executed by NEWT, i.e., 1 reference calculation, 350 perturbed calculations, and 10 extra perturbed calculations used to evaluate the residuals of flux variations. Figure 6-2 shows the singular value spectrum of 350 flux variations. The components associated with singular values smaller than 10^{-5} could

be easily contaminated by numerical errors, i.e. single precision for multigroup cross sections and the stopping criteria used for the lattice calculations.

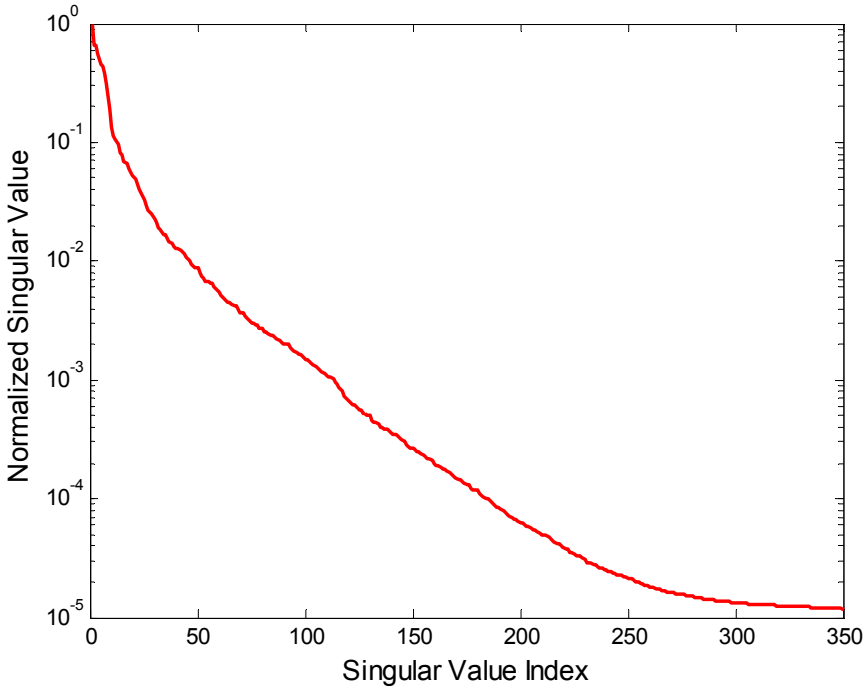

Figure 6-2. Singular Value Spectrum of 350 Flux Variations

For a given perturbed configuration, the flux variations that cannot be explained by the subspace with size $r = 350$ are plotted in Figure 6-3 against the perturbed flux. The flux values are ordered in an increasing order to check whether there are any correlations rendered by the reduction process. This experiment is repeated for 10 different random model executions (i.e., T1-T10), to check whether the flux variations are well described by the active subspace. The *abs.rms* of the flux variations that cannot be explained by the active subspace are compared in Figure 6-4. The *abs.rms* metric is defined to be:

$$abs.rms = \frac{1}{\sqrt{n}} \left\| \Delta\phi_{\text{exact}} - \Delta\phi_{\text{approx}} \right\|_2 \tag{6.1.1}$$

where the Δ implies a variation from the reference calculation. The *abs.rms* calculates the discrepancy between the exact variation estimated by direct forward perturbation, $\Delta\phi_{\text{exact}}$, and the variation estimated by projection method, $\Delta\phi_{\text{approx}}$.

In Figure 6-4, different sizes of the active subspace are employed to show that as the active subspace size is increased, one is able to enhance to meet tighter numerical tolerances. It also shows that the active subspace equally predicts flux variations for all possible input parameters perturbations. Also notice the saturation trend in Figure 6-4 which is expected since at one point, one cannot reduce the errors beyond the numerical tolerance employed in forward calculations. This phenomena asserts that the exact (within the precision of forward calculations) estimates of the flux variations could be employed using an active subspace of small size, in this case $r = 250$. This is a very small number when compared to the number of cross sections representing the input parameters to lattice calculations, the dimension of the flux field required to get accurate estimates, and the number of few-group cross sections evaluated at different points in lattice life and at different thermal hydraulics conditions.

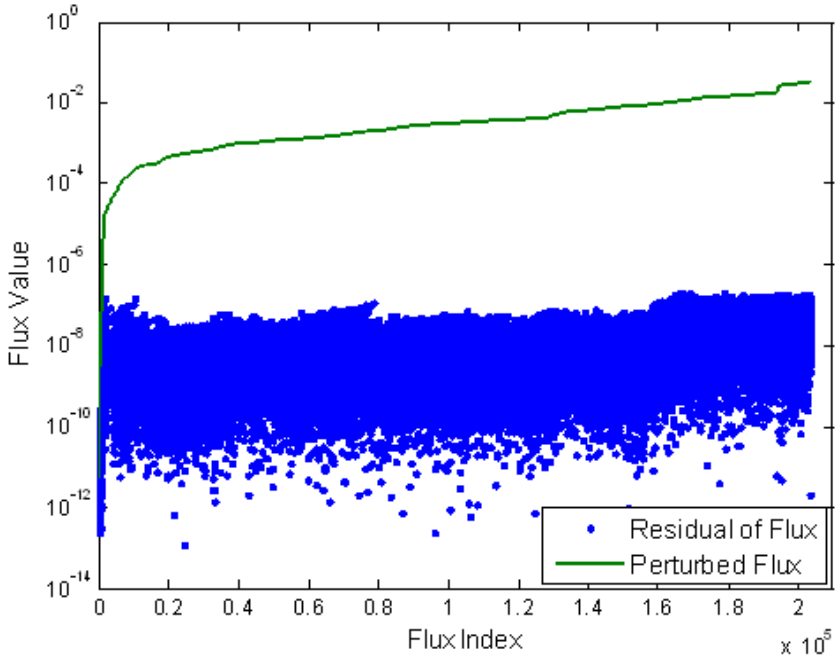

Figure 6-3. Flux Variations outside the Active Subspace

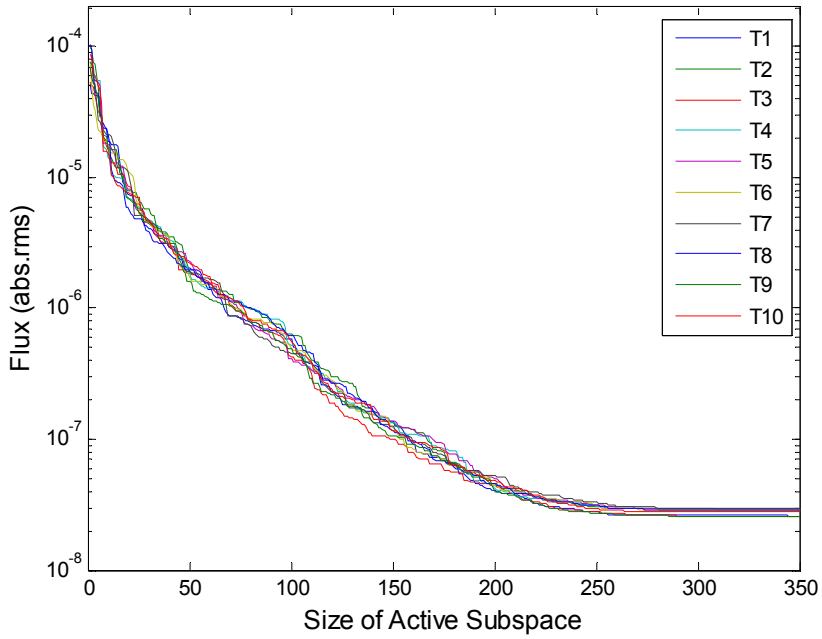

Figure 6-4. Flux Tolerance vs. Size of Active Subspace

In the second case, we employ the same lattice model to examine the active subspace for the depletion problem. We employ the TRITON module in SCALE 6.1 to do the depletion calculations. One calculates the flux variations with respect to the number densities perturbations at different depletion stages, which means the fuel burnup represents in this case the perturbation of the nuclear system. One has considered the lattice operating with a constant lattice-average power of 22.25MW/MTHM, during a 395-day burnup period. The burnup period was divided into 11 time steps. For each time step, one calculates the number densities of depletion nuclides existing in the depletion chains along the burnup period. There are 32 depletion isotopes, 11 time steps, and 9 different mixture types in this lattice model, thus the dimension of total input space is 3168. We randomly select the depletion period within 395 days, and interpolate the number density of each nuclide using the pre-calculated number density of 11 depletion time steps. Then, the NEWT module will be executed with the interpolated number densities as input to calculate the scale flux values. The reference flux is obtained at the initial depletion step. Figure 6-5 shows the singular value spectrum of 290 flux variations. In Figure 6-6, different sizes of the active subspace are employed to show that as the active subspace size is increased, one is able to enhance to meet tighter numerical tolerances. Again, it shows that the active subspace equally predicts flux variations for all possible input parameters perturbations. Also notice that the saturation trend in Figure 6-6 which is expected since at one point, one cannot reduce the errors beyond the numerical tolerance employed in forward calculations. This phenomena asserts that the exact (within

the precision of forward calculations) estimates of the flux variations could be employed using an active subspace of small dimension, in this case $r = 200$.

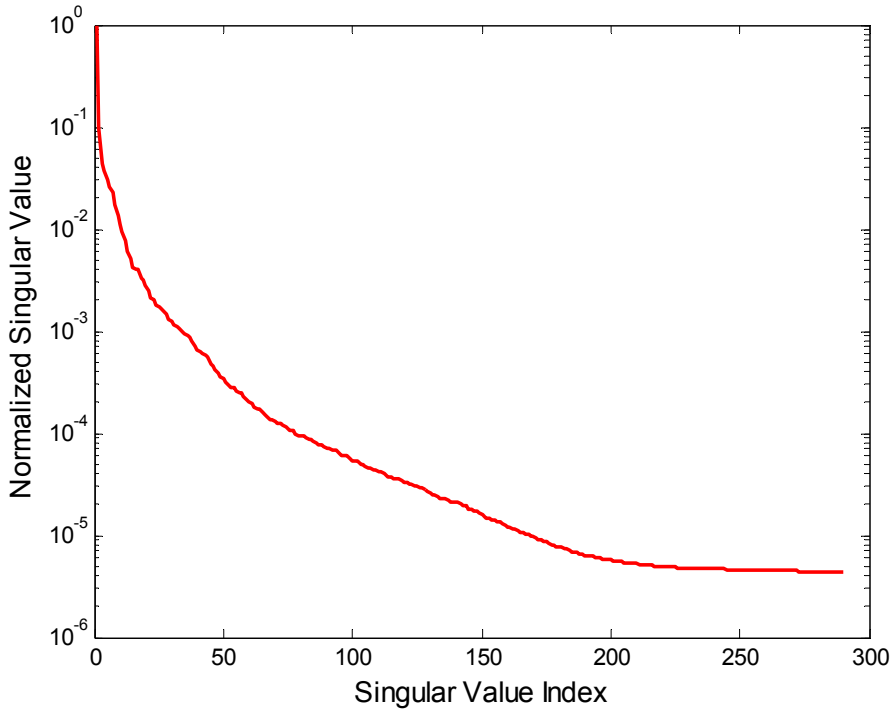

Figure 6-5. Singular Value Spectrum of 290 Flux Variations

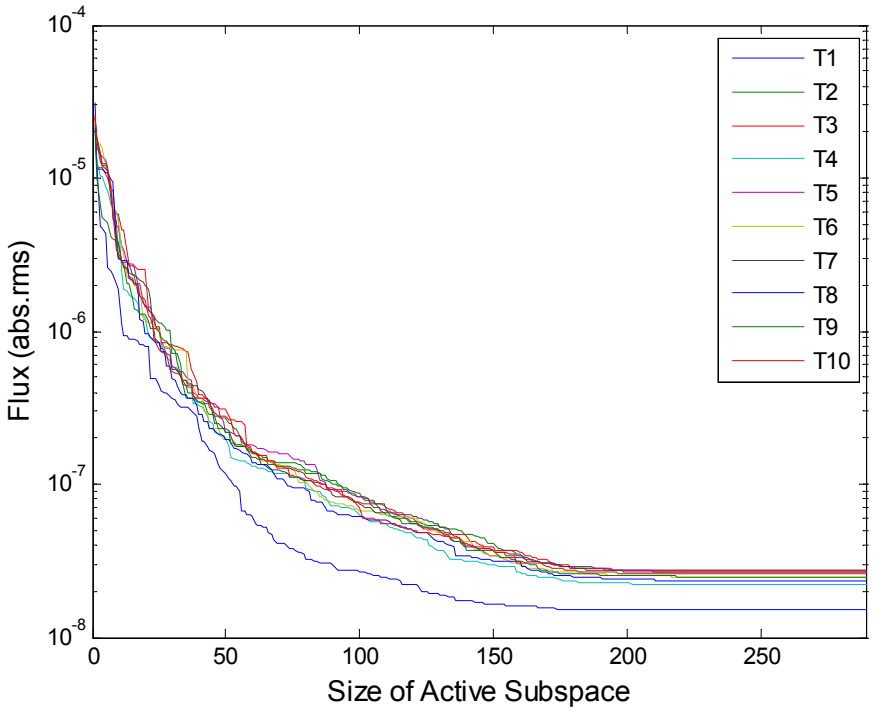

Figure 6-6. Flux Tolerance vs. Size of Active Subspace

6.2 Error Metrics for EPGPT Numerical Analysis

In order to demonstrate that the EPGPT could be employed to calculate the neutron flux variations, we can envision computing two extra quantities:

$$\text{Flux variation: } rms = \frac{1}{\sqrt{n}} \frac{\left\| \Delta\phi_{\text{exact}} - \Delta\phi_{\text{approx}} \right\|_2}{\mathrm{E}(\phi)} \tag{6.2.1}$$

$$\text{Flux Variation: } abs.rel = \left| \frac{\left[\Delta\phi_{\text{exact}} \right]_i - \left[\Delta\phi_{\text{approx}} \right]_i}{\mathrm{E}(\phi)} \right| \tag{6.2.2}$$

where the neutron flux $\phi \in \mathbb{R}^n$ and Δ implies a variation from the reference calculation. The *rms* calculates the discrepancy between the exact variation estimated by direct forward

perturbation, $\Delta\phi_{\text{exact}}$, and the variation estimated by EPGPT or first-order GPT, $\Delta\phi_{\text{approx}}$. All *rms* errors are normalized based on the reference average flux value, i.e., $\mathrm{E}(\phi)$. Similarly, the *abs.rel* calculates the relative discrepancy between each element in the exact variation estimated by direct forward perturbation, $\Delta\phi_{\text{exact}}$, and each element in the variation estimated by EPGPT or first-order GPT, $\Delta\phi_{\text{approx}}$.

In neutron critical eigenvalue calculations, we usually encounter the effective multiplication factor k_{eff} (or k-eigenvalue) which is the reciprocal of the λ-eigenvalue. We will define the following metric to measure the accuracy of variations in k_{eff}:

$$k-\text{Eigenvalue variation: } abs.rel = \frac{\left|\Delta k_{\text{exact}} - \Delta k_{\text{approx}}\right|}{k_0} \tag{6.2.3}$$

where k_0 denotes the k-eigenvalue at the reference case, and the Δ implies a variation from the reference calculation as before. The exact variation, i.e., Δk_{exact}, in the k-eigenvalue is estimated by directly solving the forward perturbed equation; while the variation estimated by EPGPT or first-order GPT is denoted as Δk_{approx}.

6.3 EPGPT Results for Diffusion Source-Driven Problem

This case study is based on a one dimensional one speed diffusion model with reflective boundary conditions. This model consists of four different unit cells, and each unit cell is provided with homogenized cross sections. The setup is shown in Figure 6-7, the cross

sections and input parameters are defined in Table 6-1, and the flux shape is shown in Figure 6-8. In this model, the flux has 40 dimensions representing 40 spatial locations, i.e., $\phi \in \mathbb{R}^{40}$.

Table 6-1. Model Specification *

Region	Domain (cm)	Σ_t	Σ_s	Σ_f	v_f	μ_0	Q	h_i
1	[0,1]	3	1	0.5	1.5	0	1	0.1
2	[1,2]	10	8	0	0	0	0	0.1
3	[2,3]	3	1	1.025	2	0	0	0.1
4	[3,4]	10	1	0	0	0	0	0.1

*Diffusion coefficient is defined as $D = \frac{1}{3(\Sigma_t - \mu_0 \Sigma_s)}$; h_i is the mesh interval for region *i*.

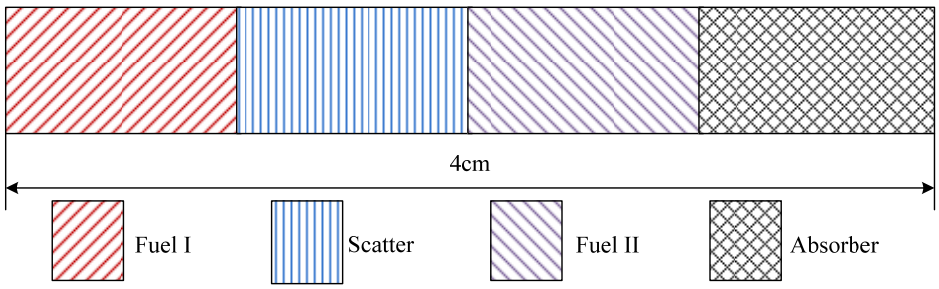

Figure 6-7. Model Layout

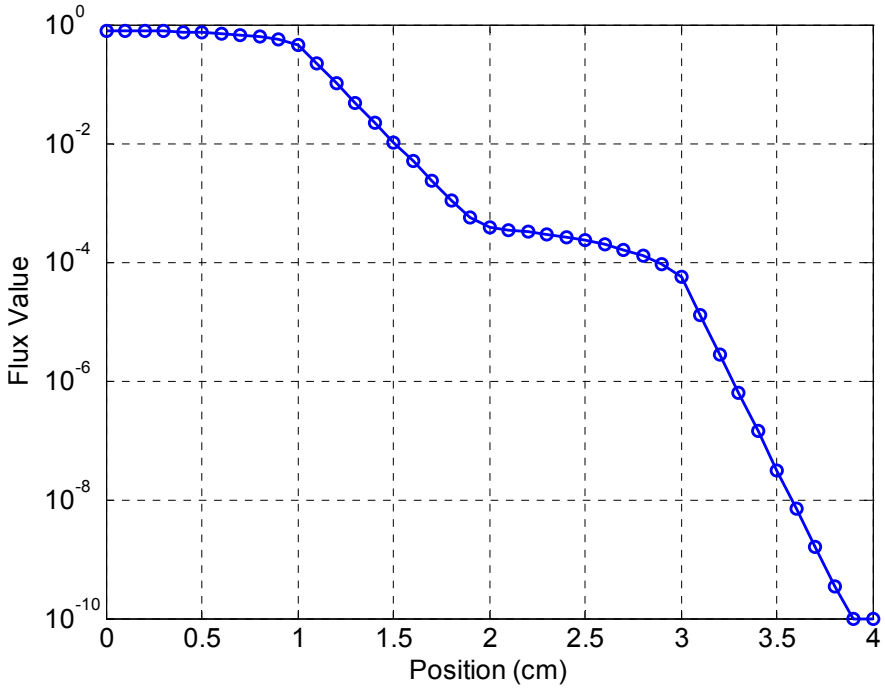

Figure 6-8. Forward Flux Shape

The E_PGPT algorithm is executed and is tested for a perturbed model such that all cross sections perturbations were randomly selected from uniform distributions within 15% relative to their reference values. The exact perturbed responses are calculated using direct forward perturbation which requires a full forward model execution. To study the performance of E_PGPT for different sizes of the active subspace, the *rms* metric defined in Eq. (6.2.1) are employed. For this case study, $n = 40$. Figure 6-9 shows *rms* errors of neutron flux against the size of the active subspace. For reference, the *rms* error calculated by first-order GPT is shown on the same graph as a horizontal line.

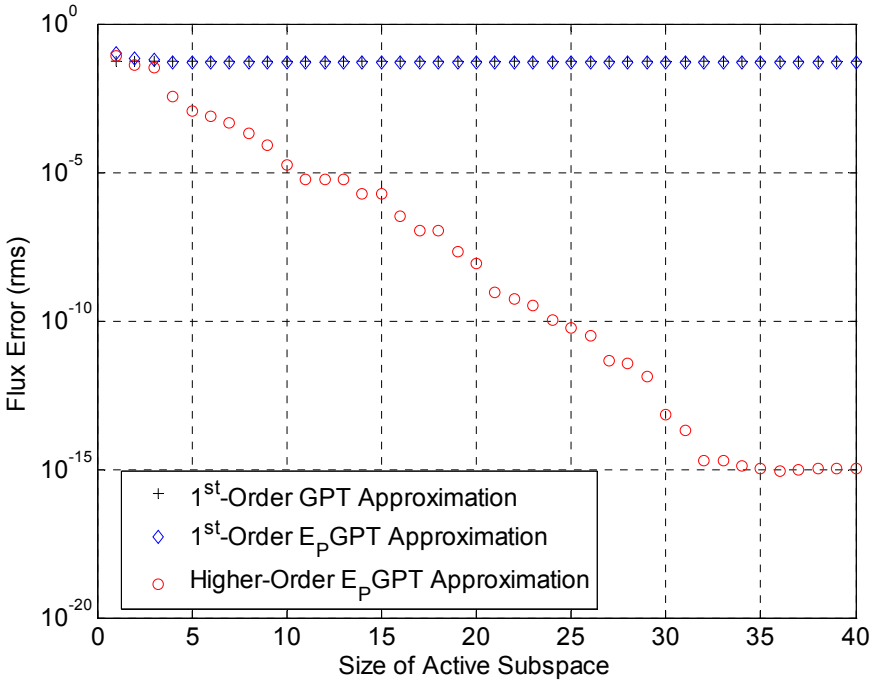

Figure 6-9. Analysis of E_PGPT Errors versus *r*

Analysis of Figure 6-9 indicates that first-order GPT errors are comparable to E_PGPT when the active subspace is too small to properly capture all possible responses variations. As the size of the subspace is increased, it starts to capture larger portions of responses variations, and the associated errors are reduced accordingly. In these calculations, the associated machine precision is of the order of 10^{-16}. Note that the accuracy of E_PGPT approaches machine precision as the size of the active subspace is increased. From a practical considerations however, one does not need to reach machine precision since the accuracy of the flux calculations is limited by many other factors, e.g., numerical errors, input parameters uncertainties, and model form errors. Therefore in practice, a much higher, i.e., relaxed, error

tolerance would be acceptable, e.g., 10^{-5} or perhaps even more relaxed depending on the application.

Next, Figure 6-10 compares the errors plotted in Figure 6-9 to the maximum theoretical error predicted by the E_PGPT range-finding algorithm. Note that the maximum error is consistently higher than the exact error calculated by direct forward perturbations.

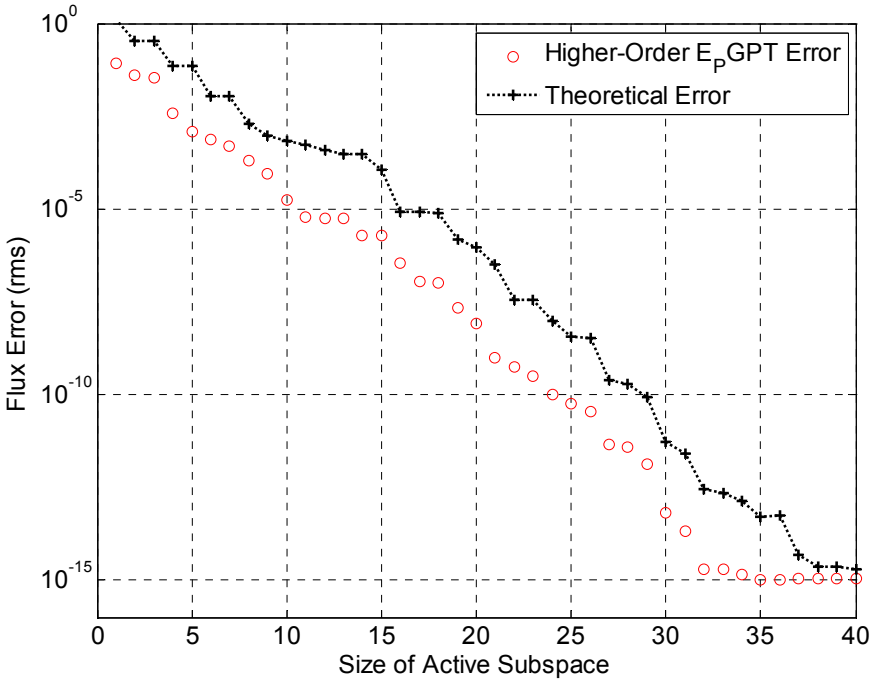

Figure 6-10. EPGPT Theoretical and Exact Responses Variations

To understand the impact of mesh refinement on the size of the active subspace, the previous results in Figure 6-9 and Figure 6-10 are repeated but now using a model with 80 dimensions for the flux space. This is achieved via mesh refinement. For the sake of

comparison, let us pick a user-defined error tolerance, say $rms_{\mathrm{E_pGPT}} = \frac{1}{10} rms_{\mathrm{1^{st}GPT}}$. From Figure 6-9 and Figure 6-11 the corresponding sizes of the active subspace to meet this error tolerance are 4 and 5, respectively. This result implies that despite the increase in the dimension of the flux phase space, the size of the active subspace required to maintain the same tolerance remains essentially the same. This is an important result as it shows the potential of E_PGPT to combat the explosion in dimension of the flux space which is often sought via mesh refinement to achieve high accuracy predictions.

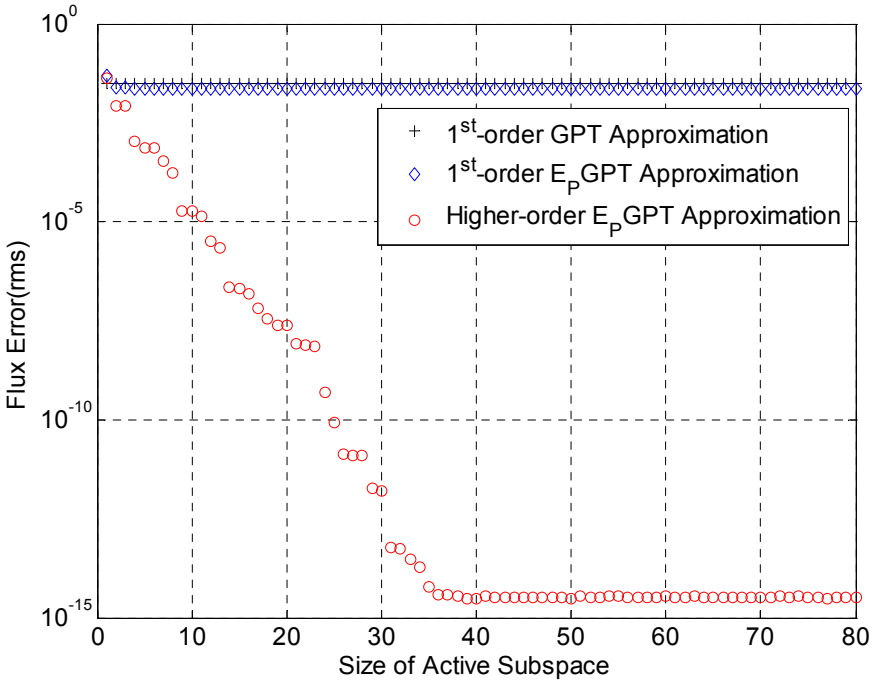

Figure 6-11. Analysis of EPGPT Errors versus *r* (w/ Refined Mesh)

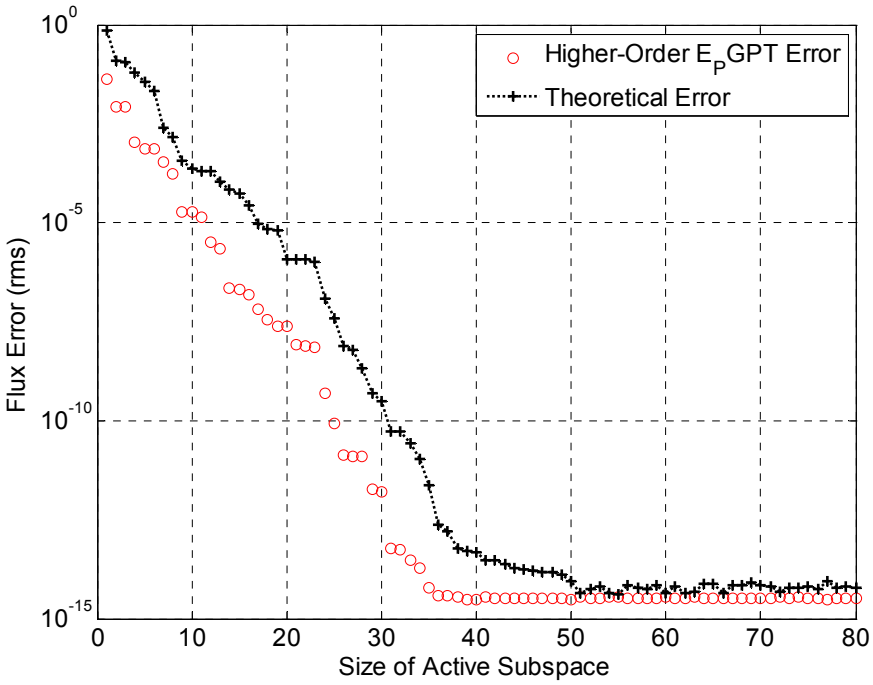

Figure 6-12. E_PGPT Theoretical and Exact Responses Variations

To provide some comparison of the performance of this method to other higher-order GPT methods, we adopt the method proposed by Rahnema for boundary conditions perturbations to apply to cross sections perturbations (see Appendix B). The applicability of this method to eigenvalue models has been demonstrated elsewhere, see Refs. (McKinley, Rahnema 2000, McKinley, Rahnema 2002). In Rahnema's development, a single adjoint model evaluation is needed at each point in the flux phase space; this implies 40 adjoint model evaluations that must be pre-computed. These adjoints are then employed to calculate the response variations using an iterative scheme. Figure 6-13 shows these results. As expected the errors are very small and comparable to the errors produced by the proposed E_PGPT.

It is important to remark here that this comparison is only employed as a sanity check. This follows as several other higher-order methods have already been established in the literature and rigorously proven to converge to the correct solution. So, there is little value in comparing different higher-order methods to one another since the exact variations could be calculated using direct forward perturbations. The important value of the comparison however is the reduction in the computational overhead required to reach the solution which is the main objective of this dissertation. As discussed earlier, the Rahnema's approach requires an adjoint model evaluation for each point in the phase space. The EPGPT philosophy is however different, it determines the number of adjoint model evaluations needed to reach a user-defined error tolerance. Both approaches are expected to produce the same results if one calculates an adjoint function for each point in the phase space. However, the EPGPT provides more flexibility for practical engineering calculations, where one cannot afford to calculate that many adjoint model evaluations on a routine basis. In reality, for typical models, the flux phase space is too big to store the adjoint functions much less evaluate them. Moreover, real-world calculations do not require machine precision estimate of the responses variations. The EPGPT takes advantage of that by reducing the number of adjoint model evaluations. More importantly, it provides an upper bound on the error for the responses variations, a feature that is not currently provided by other higher-order variational methods.

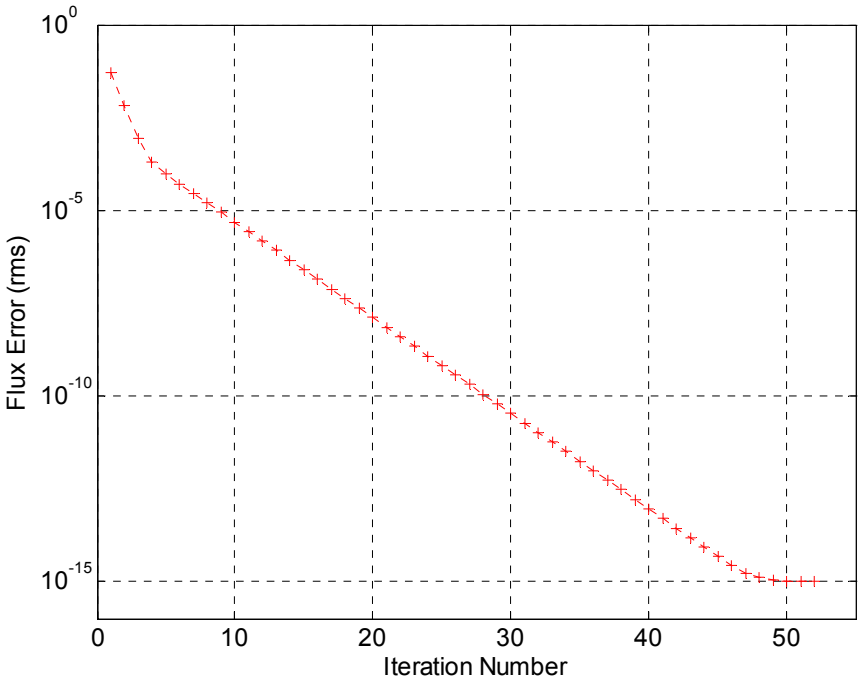

Figure 6-13. Rahnema-Based Higher-Order GPT Method

6.4 EPGPT Results for Diffusion Eigenvalue Problems

Case Study I: A one-dimensional two-group heterogeneous diffusion model representing two fuel assemblies with reflective boundary conditions is employed to test EPGPT (Anistratov 2005). Each lattice involves 8 uniform unit cells. The state is described by the two-group flux solution. The input parameters are represented by the two-group cross sections. The model schematic is shown in Figure 6-14 and the associated specifications are listed in Table 6-2. In this model, the flux has 256 dimensions representing 128 spatial nodes with equal spatial intervals and 2 energy groups per node. The responses are the flux values evaluated everywhere in the space-energy phase space, i.e., $\phi \in \mathbb{R}^{256}$. The first 128 values of

ϕ denote the fast group flux, the last 128 values of ϕ denote the thermal group flux. The reference flux distribution is shown in Figure 6-15.

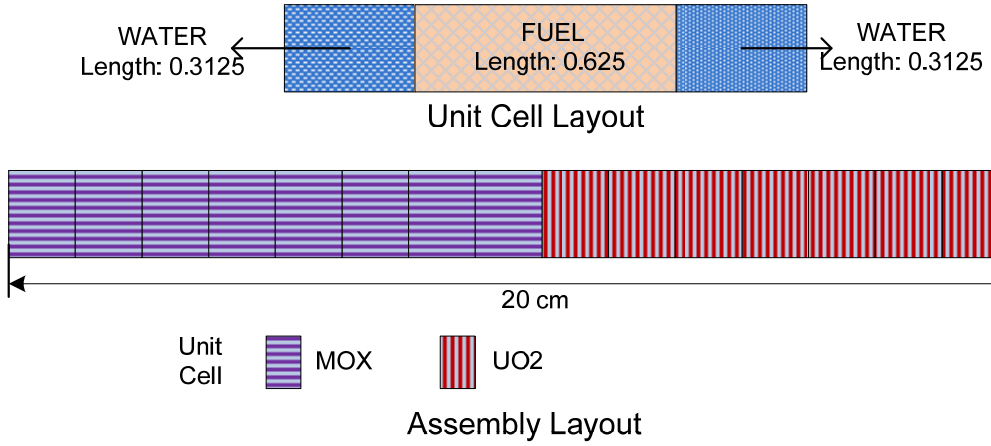

Figure 6-14. Model Layout

Table 6-2. Cross Section Data *

Materials	Input Parameters							
	Σ_t^1	$\Sigma_{s,0}^{1\to1}$	$\Sigma_{s,0}^{1\to2}$	χ^1	Σ_t^2	$\Sigma_{s,0}^{2\to2}$	Σ_f^2	ν_f^2
MOX	0.2	0.185	0.015	1	1.2	0.9	0.3	1.5
UO2	0.2	0.185	0.015	1	1.0	0.9	0.1	1.5
Water	0.2	0.17	0.03	0	1.1	1.1	0	0

* $\Sigma_f^1, \nu_f^1, \overline{\mu}_0^1, \Sigma_{s,0}^{2\to1}, \chi^2, \overline{\mu}_0^2$ are all zeros, and diffusion coefficient is defined as $D^g = \frac{1}{3\Sigma_{tr}^{\ g}}$, where $\Sigma_{tr}^{\ g} = \Sigma_t^{\ g} - \overline{\mu}_0^{\ g}\Sigma_s^{\ g}$ and g is the energy group index .

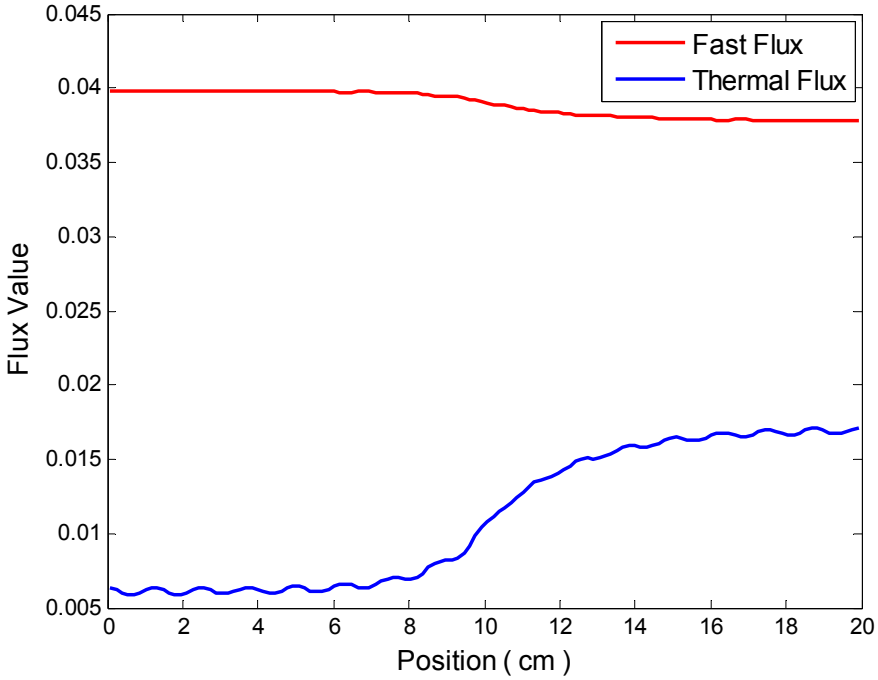

Figure 6-15. Reference Flux Solution

The EPGPT algorithm is executed, and is tested for a perturbed model such that cross sections perturbations, i.e., scattering, fission and v, were randomly selected from uniform distributions with 10% standard deviation relative to their reference values. The exact perturbed neutron flux is calculated using direct forward perturbation which requires a full forward model execution. Figure 6-16 compares the exact flux variations to those estimated by EPGPT employing an active subspace of size $r = 20$ employing *abs.rel* metric defined in Eq. (6.2.2); for reference the first-order GPT variations are also compared on the same figure. Figure 6-16 shows that the results calculated by EPGPT are two orders of magnitude more accurate than the first-order GPT approach.

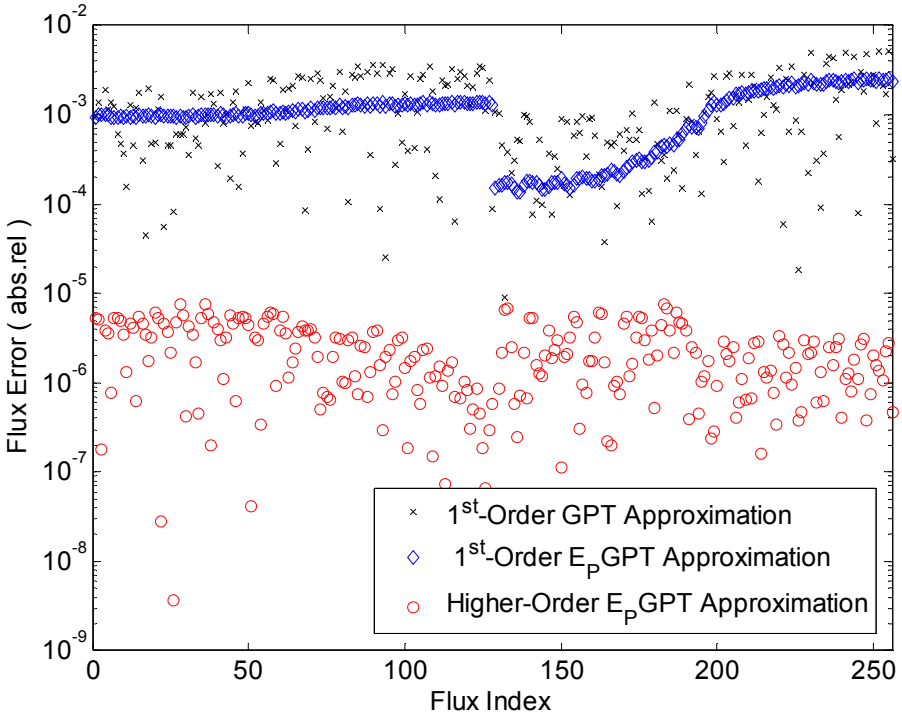

Figure 6-16. Performance of E_PGPT with $r = 20$

To study the performance of E_PGPT for different sizes of the active subspace, the *rms* metric is employed. Figure 6-17 condenses the errors of Figure 6-16 for all responses into one *rms* metric that is plotted against the size of the active subspace. The *rms* metric is defined in Eq. (6.2.1) and $n = 256$ for this case. For reference, the *rms* error calculated by first-order GPT is shown on the same graph as a horizontal line. The x-axis in this figure runs from 1 to 256 over all space-energy indices for the flux. The values are ordered such that the first 64 values are the fast flux in the MOX lattice followed by 64 values for the fast flux in the UO2 lattice followed by the thermal flux values.

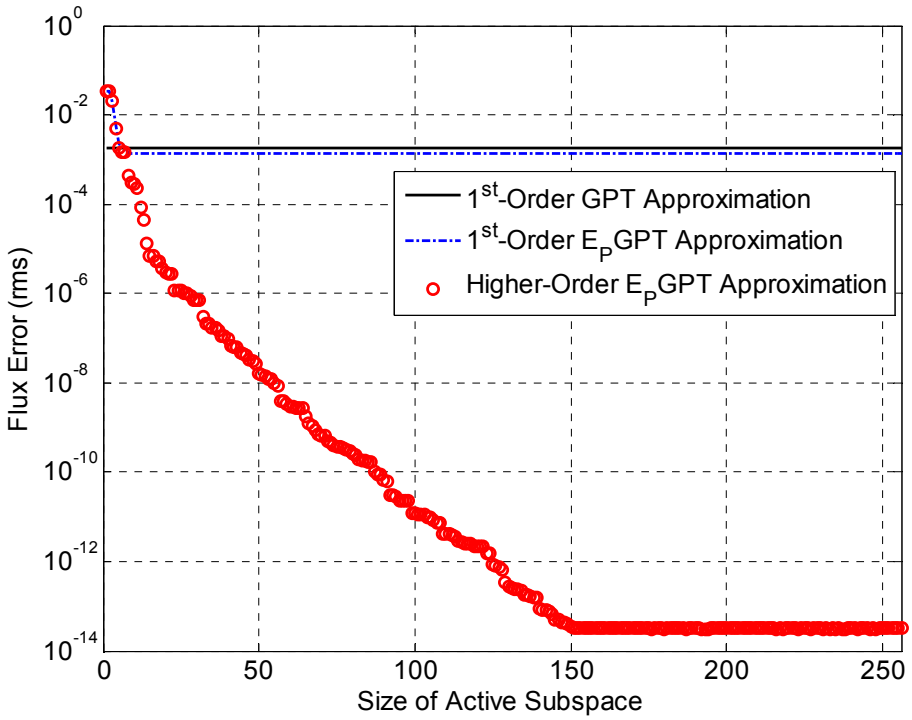

Figure 6-17. Analysis of E_PGPT Errors versus *r*

Analysis of Figure 6-17 indicates that first-order GPT errors are comparable to E_PGPT when the active subspace is too small to properly capture all possible responses variations. As the size of the subspace is increased, it starts to capture a larger component of responses variations, and the associated errors are reduced accordingly. Note that the accuracy of E_PGPT approaches machine precision as the size of the active subspace is increased. Next, Figure 6-18 compares the errors plotted in Figure 6-17 to the maximum theoretical error predicted by the E_PGPT range-finding algorithm. Note that the maximum error is consistently higher than the exact error calculated by direct forward perturbations until the *rms* errors for responses are converged.

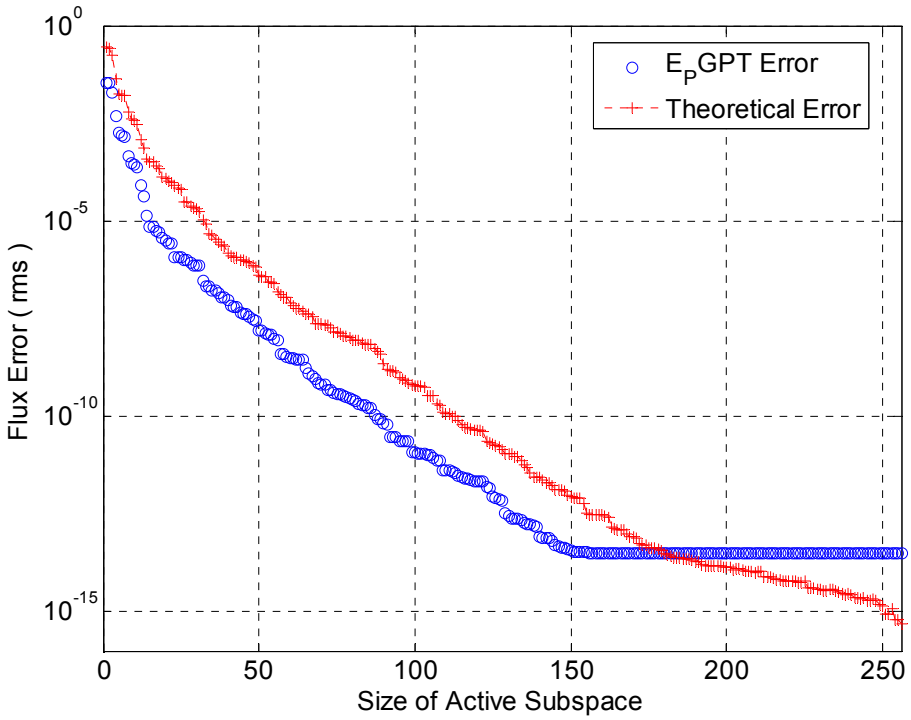

Figure 6-18. E_PGPT Theoretical versus Exact Variational Errors

As discussed before, the accuracy of estimated responses is dependent on the accuracy of the calculated eigenvalues. The eigenvalues' calculation will converge very fast, but the error in the eigenvalues will be propagated to the responses' calculation, as showed in Figure 6-18, when we continue to increase the size of subspace after 150, we get no improvement for the flux calculation. Table 6-3 displays the results of the iterative procedure employed to update the eigenvalue with r = 10. The reference eigenvalue is $\lambda_0 = 0.667$, and the perturbation results in a 0.0313 change, i.e., approximately 4.7% change from the reference value. The errors in the estimated variations in Table 6-3 is defined by:

$$abs.error(\lambda) = \left(\lambda_{\text{exact}} - \lambda_{\text{approx}}\right) \times 10^{5}$$

where λ_{exact} is calculated exactly using the perturbed forward model. The first-order GPT predicts approximately 90.8% of that change. The EPGPT results show that very accurate estimates are quickly obtained with again a relatively small size of the active subspace.

Table 6-3. Eigenvalue Variational Estimate ($r = 10$)

Iterations	EPGPT ($abs.error(\lambda)$)	1st-Order GPT ($abs.error(\lambda)$)
1	2.24E+01	2.86E+02
2	-1.75E+00	-
3	1.37E-01	-
4	-1.07E-02	-
5	8.33E-04	-
6	-6.72E-05	-
7	3.15E-06	-
8	-2.35E-06	-
9	-1.92E-06	-
10	-1.95E-06	-
11	-1.95E-06	-

To check the adequacy of EPGPT for severe flux variations, the methodology is employed to estimate flux variations resulting from the insertion of a control rod. The control rod is simulated by significantly increasing the absorption cross section in the middle of the MOX lattice. The corresponding relative changes in the fluxes with respect to the expected reference flux values are shown in Figure 6-19. Notice that the group fluxes change by up to 75% from their reference values. Figure 6-20 and Figure 6-21 show these results in a similar manner to Figure 6-17 and Figure 6-18, respectively. Table 6-4 repeats the results of Table 6-3 but now with the control rod inserted.

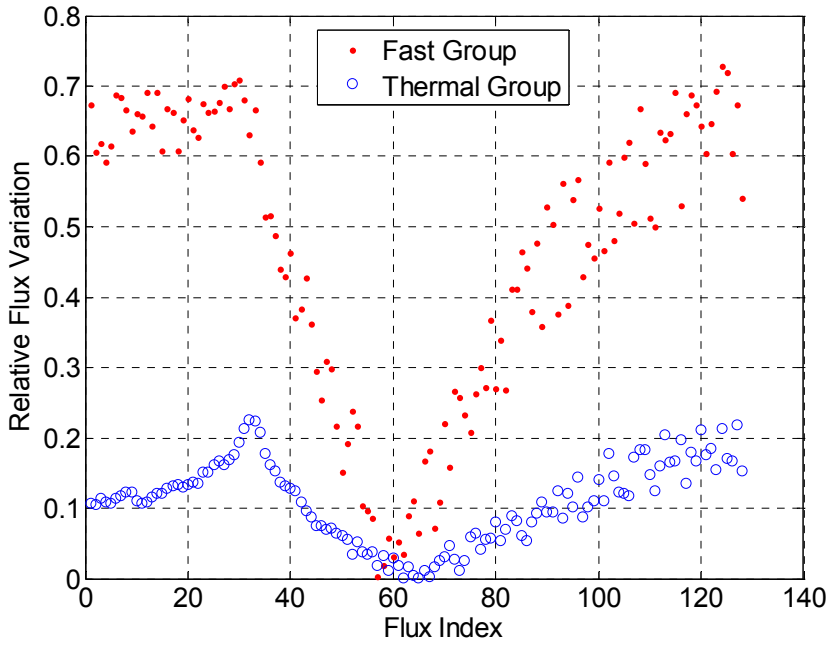

Figure 6-19. Exact Flux Variations (w/ CR Insertion)

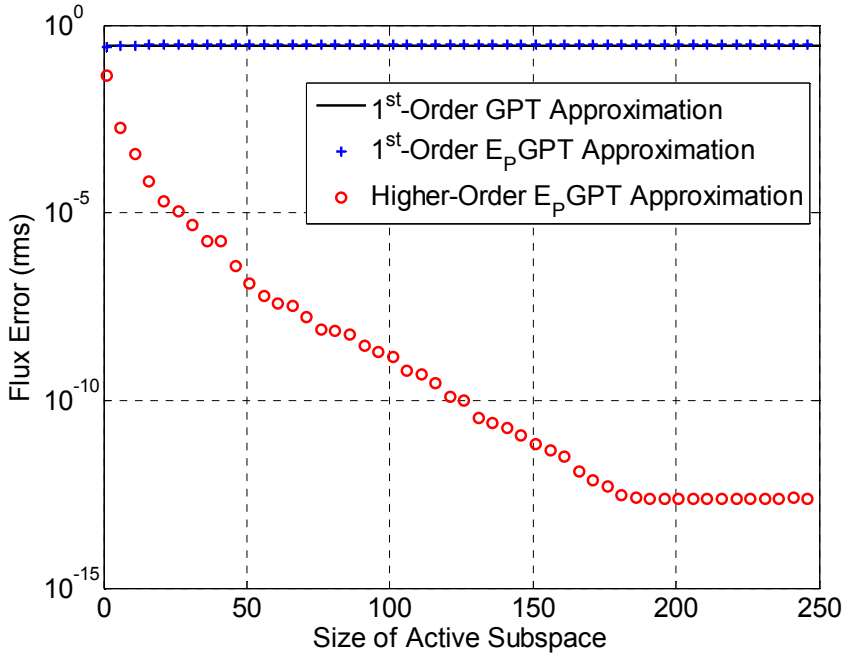

Figure 6-20. Analysis of E_PGPT Errors versus *r* (w/ CR Insertion)

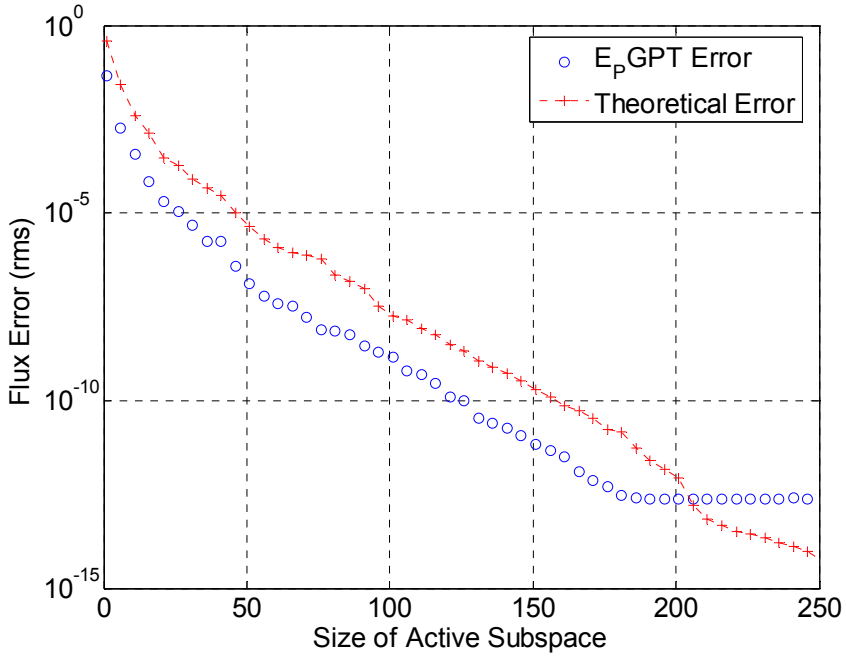

Figure 6-21. E_PGPT Theoretical vs. Exact Variational Errors (w/ CR Insertion)

Table 6-4. Eigenvalue Variational Estimate ($r = 20$ w/ CR Insertion)

Iterations	E_PGPT ($abs.error(\lambda)$)	1st-Order GPT ($abs.error(\lambda)$)
1	-1.31E+03	-4.11E+04
2	-1.49E+01	-
3	-1.07E+00	-
4	-9.35E-01	-
5	-9.34E-01	-
6	-9.34E-01	-

With E_PGPT, the size of the error is reduced significantly with a very small active subspace. Moreover, despite the huge change in the eigenvalue (approximately a 43% change from the reference value of 0.667), the E_PGPT iterative procedure is able to converge on the

exact variation with few iterations. Also, as shown before, the flux errors decrease with increasing the size of the active subspace.

Case Study II: A seven-group neutron diffusion model in 1-D slab geometry with two fuel assemblies (Anistratov 2005) is employed for this case study. There're total 224 cell-averaged flux values for each group. The seven-group flux is denoted as:

$$\phi \in \mathbb{R}^{1568\times 1},\ \text{and}\left[\phi\right]_{i+(g-1)\times 224} = \phi_{i,g},\ \text{for } i = 1,\cdots,224; g = 1,\cdots,7 \qquad (6.4.1)$$

where $\phi_{i,g}$ indicates the i^{th} cell-averaged flux for group g. The input parameters are represented by the seven-group cross sections. The model scheme is shown in Figure 6-22. The cross sections are given in (Lewis et al. 2001). Neutron transport cross sections are considered as the total cross sections, this is because $\Sigma_{tr}{}^{g}$ is equal to $\Sigma_{a}{}^{g} + \Sigma_{c}{}^{g} + \Sigma_{s}{}^{g}$ for each energy group as provided in (Lewis et al. 2001). As before, the diffusion coefficient is calculated as $D^{g} = \dfrac{1}{3\left(\Sigma_{t}{}^{g} - \overline{\mu}_{0}{}^{g}\Sigma_{s}{}^{g}\right)}$.

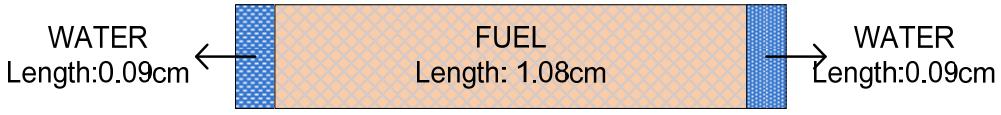

Figure 6-22a. Unit Cell Design

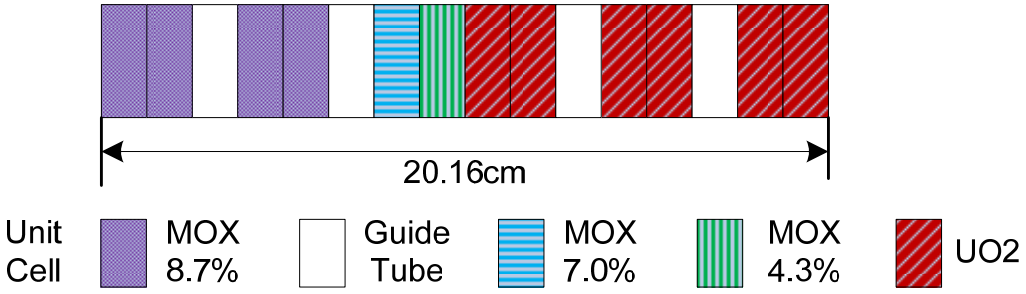

Figure 6-22b. Unit Cell Layout

Figure 6-22. Model Layout

The EPGPT is employed to test for this model such that all cross sections are randomly selected from uniform distribution within 10% relative to their nominal values. Exact neutron flux solution is obtained by resolving the forward diffusion equation. Figure 6-23 compares the real errors in the flux (*rms*) calculated by the EPGPT to the theoretical error predicted by range-finding algorithm. The *rms* metric is defined in Eq. (6.2.1) and n = 1568 for this case. Note that the theoretical error is consistently higher than the exact error calculated by directly solving forward equation. Figure 6-24 shows the accuracy of EPGPT against the size of the active subspace; for reference, the flux variation error calculated by first-order GPT is shown on the same graph as a horizontal line. Note that one needs to solve the generalized adjoint equation 1568 times in order to obtain the first-order approximation as shown in Figure 6-24.

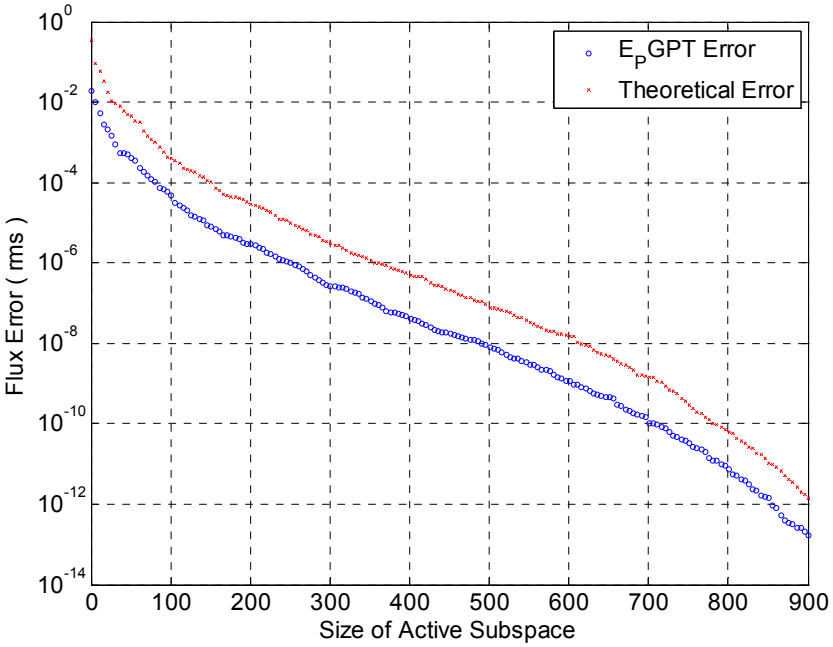

Figure 6-23. Theoretical vs. Exact Variational Errors

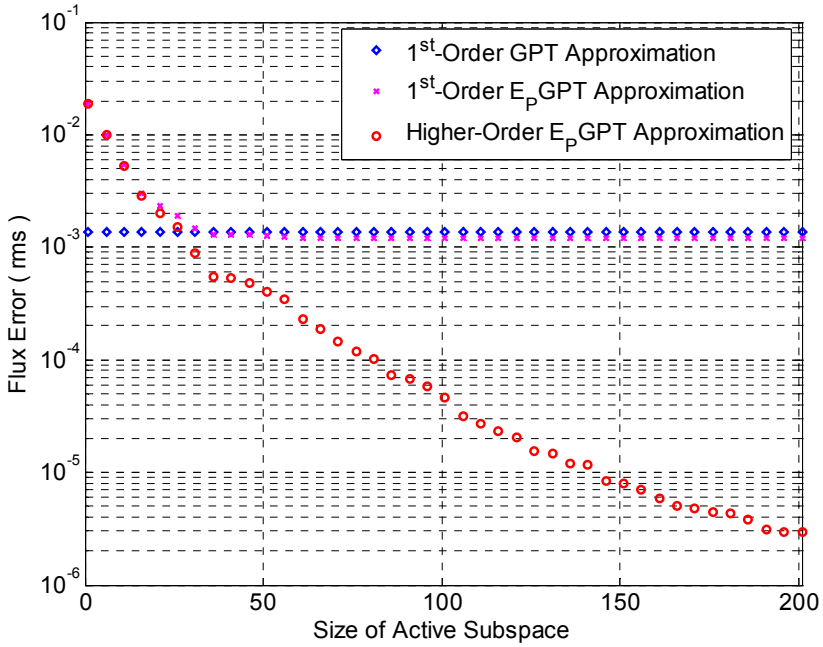

Figure 6-24. Analysis of E_PGPT Errors vs. *r*

Next, Figure 6-25 shows the flux discrepancy between the exact flux variation and the flux variation estimated by E_PGPT or first-order GPT; for reference, the exact flux variation is shown on the same graph. The x-axis in Figure 6-25 runs from 1 to 1568 over all space-energy indices for the flux, and the errors in Figure 6-25 is defined in Eq. (6.2.2). Note that the results calculated by first-order E_PGPT with only 80 basis vectors are comparable to the results estimated by first-order GPT, which means that one only need to solve the generalized adjoint equation 80 times, instead of 1568 times, in order to obtain the same accuracy as first-order GPT. Moreover, one can obtain much accurate results with higher order E_PGPT.

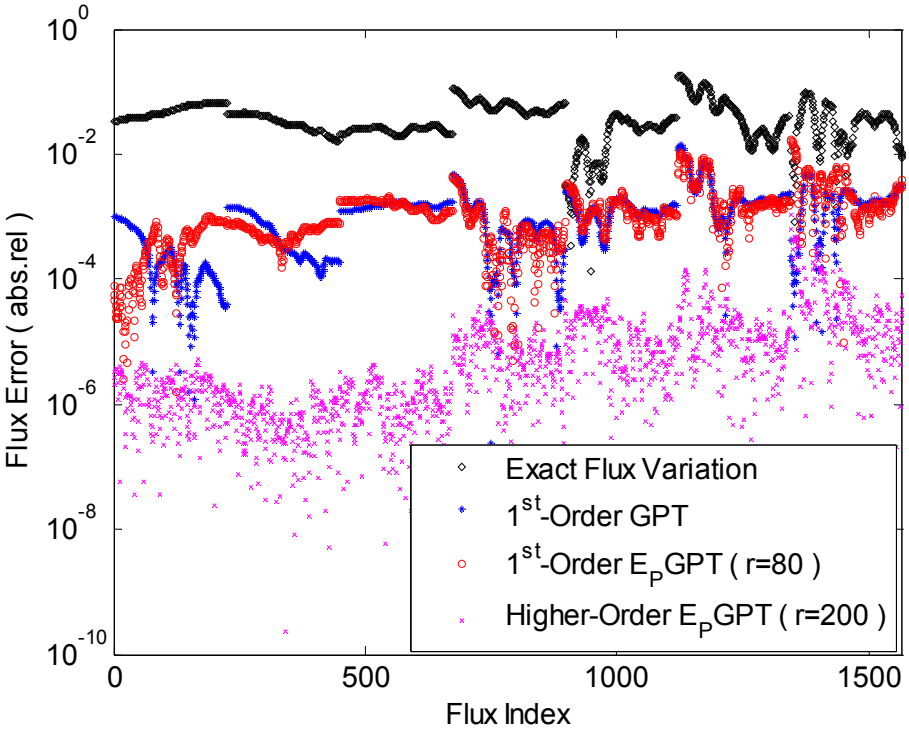

Figure 6-25. Comparison of Estimation Accuracy

6.5 E_PGPT for Neutron Transport Calculations

The main computational calculations in this section are completed using SCALE 6.1. It is a comprehensive modeling and simulation suite for nuclear safety analysis and design to perform reactor physics, criticality safety, radiation shielding and so on (RSICC 2011). To implement the E_PGPT, several modules of SCALE 6.1 are employed and some of them are modified for the purpose of the experiments, e.g. BONAMI/CENTRM, NEWT, SAMS, TSUNAMI-2D, etc. In particular, The BONAMI/CENTRM modules are self-shielding codes that can be used to generate self-shielded multi-group cross sections for subsequent criticality calculations (e.g., NEWT). NEWT is a multigroup discrete-ordinates radiation transport computer code that allows 2-D neutron transport calculations using complex geometric models. SAMS (Sensitivity Analysis Module for Scale) utilizes data from NEWT forward and NEWT adjoint neutron transport calculations to compute sensitivity coefficients for the system multiplication factor (k_{eff}) and reaction rate ratios. Additionally, we employ TSUNAMI-2D sequence in TRITON – a control module in SCALE for transport, depletion and sensitivity and uncertainty analysis – to perform automated, problem-dependent cross section processing in BONAMI/CENTRM, calculation of 2D forward and adjoint transport solutions in NEWT, calculation of sensitivity coefficients in SAMS. Currently, NEWT is not applicable to solve GPT equations with linear responses, e.g., reaction rates, and SAMS doesn't perform variation calculations in k_{eff} and neutron flux. These two modules have been modified in order to perform E_PGPT calculations. Three different models have been adopted to exercise the modification in SCALE and E_PGPT calculations.

CASE I: A simplified lattice model with seven uniform pin-cells is employed. Table 6-5 provides the design characteristics and Figure 6-26 depicts the model analyzed. This model is modified from input file of NEWT sample 2 (Jessee, Dehart 2011). In this model, reflective boundary conditions are applied on all outer boundaries, and the cross section library v5-44 (or 44GROUPNDF5) is employed. The control module TSUNAMI-2D is utilized to perform the reference calculation, i.e., calculations of fundamental forward and adjoint neutron flux. NEWT forward is employed to generate the active subspace with respect to perturbed microscopic multigroup cross sections. Modified NEWT generalized adjoint (or GPT) is utilized to calculate the generalized adjoint solutions with respect to pseudo responses. Modified SAMS will perform first-order GPT calculation by employing fundamental forward and adjoint solution and E_PGPT calculations utilizing the active subspace and generalized adjoint solutions. All subsequent calculations are conducted by using MATLAB 2011a, e.g., eigenvalue iteration approach, flux variation reconstruction. In short, this sequence is denoted as TSUNAMI-2D (reference) – NEWT forward (identify active subspace) – Modified NEWT GPT (adjoint solutions) – Modified SAMS (E_PGPT) – Post-processing.

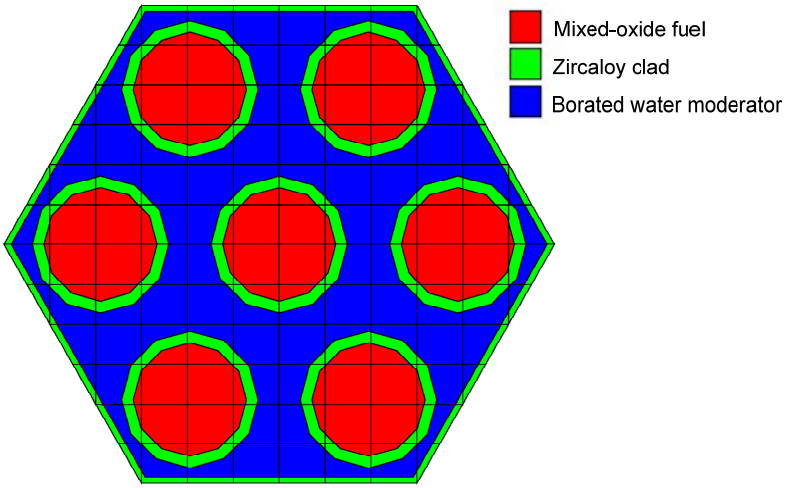

Figure 6-26. Model Layout with Grid Structure

Table 6-5. Lattice Design for Case I

Parameters	**Data**
Fuel Lattice	
Lattice	7 uniform pin-cells
Number of fuel rod	7
Fuel rod	
Type fuel pellet	MOX
Initial fuel composition (atom/(cm.barn))	
U-235	5.5300E-05
U-234	2.6436E-07
U-238	2.1786E-02
Pu-238	3.6128E-05
Pu-241	1.3557E-04
Pu-242	1.0233E-04
Pu-240	3.7403E-04
Pu-239	7.8717E-04
Rod pitch (cm)	1.22
Rod outer diameter (cm)	0.91
Rod inner diameter (cm)	0.755
Clad material	Zircaloy-4
Clad temperature (K)	620

In this model, S-6 quadrature, P-1 scattering (P-2 in the moderator), spatial and eigenvalue stopping criteria of 1.0E-9 are used for the NEWT forward calculation. The eigenvalue at the reference condition for this case is given by $k_{eff} = 1.040982$. For the adjoint and generalized adjoint calculations, the spatial and eigenvalue stopping criteria of 1.0E-5 are employed. There're total 332 computational cells for this lattice model. Thus, the dimension of neutron angular flux space is $332 \times 44 \times 24 = 350592$, i.e., $\phi \in \mathbb{R}^{350592}$. Additionally, total of 7 uniform fuel rods containing 13 different isotopes are adopted for this model. The microscopic multigroup cross sections – fission, radiation capture, ν – of all isotopes are randomly perturbed by $\pm 30\%$. The dimension of the perturbed parameters space is $\alpha \in \mathbb{R}^{1276}$. In Figure 6-27, the singular value spectrum of 150 flux variations is presented. One can observe that the spectrum of the singular values is decaying rapidly. Note that after 100^{th} singular value, the magnitudes of them are below 10E-4 which is very small. Moreover, considering the precision of cross section values, i.e., single precision, and the stopping criteria used for LWR lattice calculations, i.e., typically 10E-4, the components associated to those small singular values can be neglected.

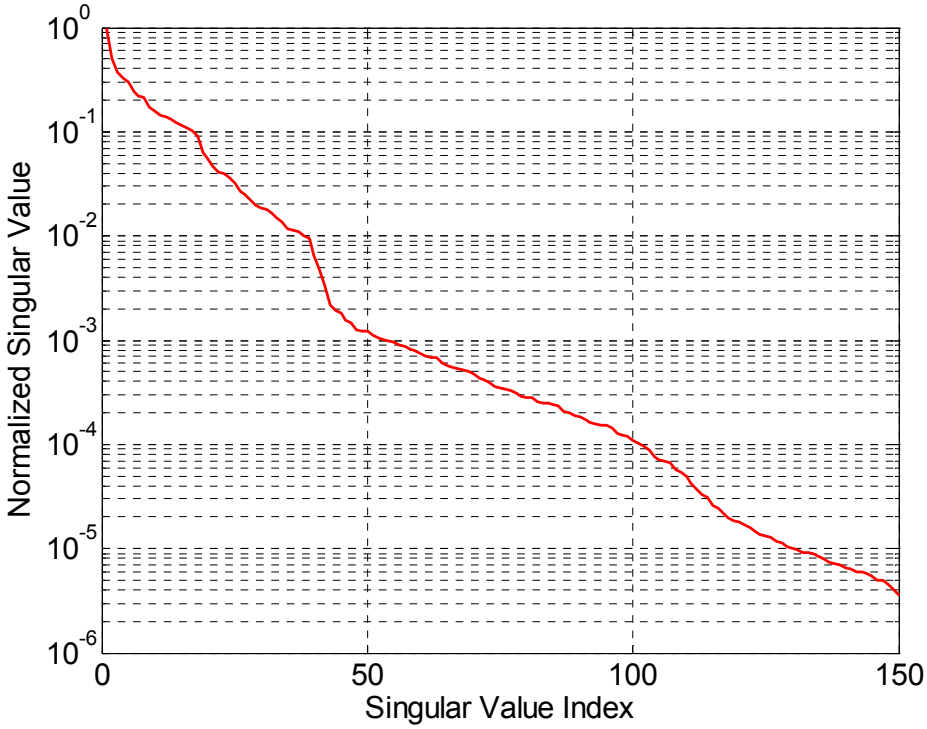

Figure 6-27. Singular Value Spectrum

The EPGPT is executed and is tested for a perturbed case with respect to randomly perturbed microscopic multigroup cross sections. The exact values of the perturbed neutron angular flux are calculated using direct forward calculation which requires a full NEWT forward execution. To study the performance of EPGPT for different sizes of the active subspace, the *rms* metric defined in Eq. (6.2.1) are employed. Figure 6-28 shows *rms* errors of neutron angular flux against the different sizes of the active subspace.

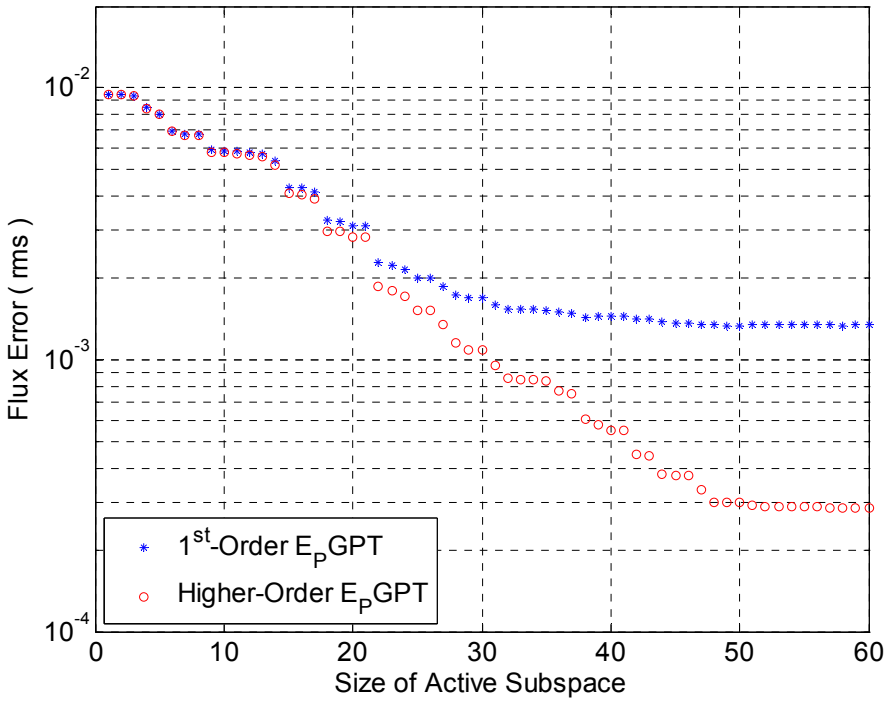

Figure 6-28. Analysis of E_PGPT Errors versus *r*

Analysis of Figure 6-28 indicates that first-order E_PGPT errors are comparable to E_PGPT when the active subspace is too small to properly capture all possible flux variations. As the size of the active subspace is increased, it starts to capture larger portions of flux variations, and the associated errors are reduced accordingly. Note that we will gain no more improvement on the estimated neutron flux after the size of active subspace reaches 50. This is because the estimated neutron flux is contaminated by numerical errors, e.g. adjoint solutions of NEWT GPT calculations. Therefore, the effective size of the active subspace for this case is $r = 50$. Figure 6-29 shows eigenvalue error against the size of the active subspace. For reference, the eigenvalue error calculated by first-order GPT is shown on the same graph

as a horizontal line. The perturbed eigenvalue is $k_{eff}' = 1.108159$, and the exact variation in the eigenvalue is $\Delta k_{\text{exact}} = 6717.7\text{pcm}$. The error in Figure 6-29 is defined as:

$$\left|\Delta k_{\text{exact}} - \Delta k_{\text{approx}}\right| \times 10^5 \tag{6.5.1}$$

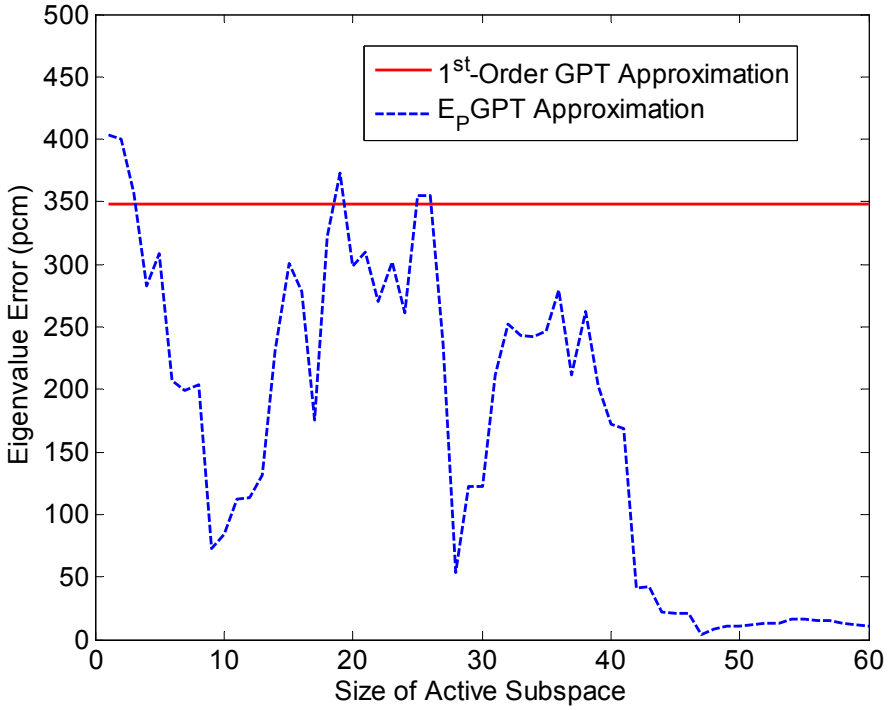

Figure 6-29. Eigenvalue Tolerance versus *r*

From Figure 6-29, one can observe two important properties of the proposed Rayleigh quotient like iterative approach for eigenvalue variation. First, the eigenvalue variation calculated by the proposed approach is comparable to first order of eigenvalue variation when the size of the active subspace is small. This is because one only need to update the

higher orders of variations for the proposed approach, since the first order of variation is pre-calculated. Another important observation is that the estimated eigenvalue variation approaches the exact value after certain number of basis vectors (for this case, r = 40). The reason is that the larger portions of flux variations lie in the active subspace spanned by the r = 40 basis vectors. Furthermore, Figure 6-29 implies that if we estimate the flux variations with enough basis vectors, we can also obtain very accurate eigenvalue.

In order to examine the accuracy of EPGPT for user-defined response, we define the following response for each energy group

$$R(E) = \int_V dV \int_0^\infty dE' \int_{4\pi} d\Omega \delta(E' - E) \phi(r, E', \Omega) = \phi(E) \tag{6.5.2}$$

or approximated using numerical method:

$$R_g = \sum_{i=1}^{NOM} V_i \sum_{mm=1}^{NOA} \phi_{i,g,mm} w_{mm}, \text{ for } g = 1, \cdots, NOG \tag{6.5.3}$$

where *NOM*, *NOG*, and *NOA* denote the total number of spatial meshes, the total number of energy groups, and the total number of directions, respectively; V_i denotes the volume for the i^{th} cell, and w_{mm} denotes the weight for the mm^{th} direction. For this test case, *NOG* is equal 44, thus we will evaluate 44 different responses using EPGPT. For comparison, the exact variations in these responses are calculated by NEWT forward. Figure 6-30 shows the 44 responses values at the reference condition against the neutron lethargy u. The neutron lethargy u is defined as follows:

$$u = \ln\left(\frac{E_0}{E}\right)$$

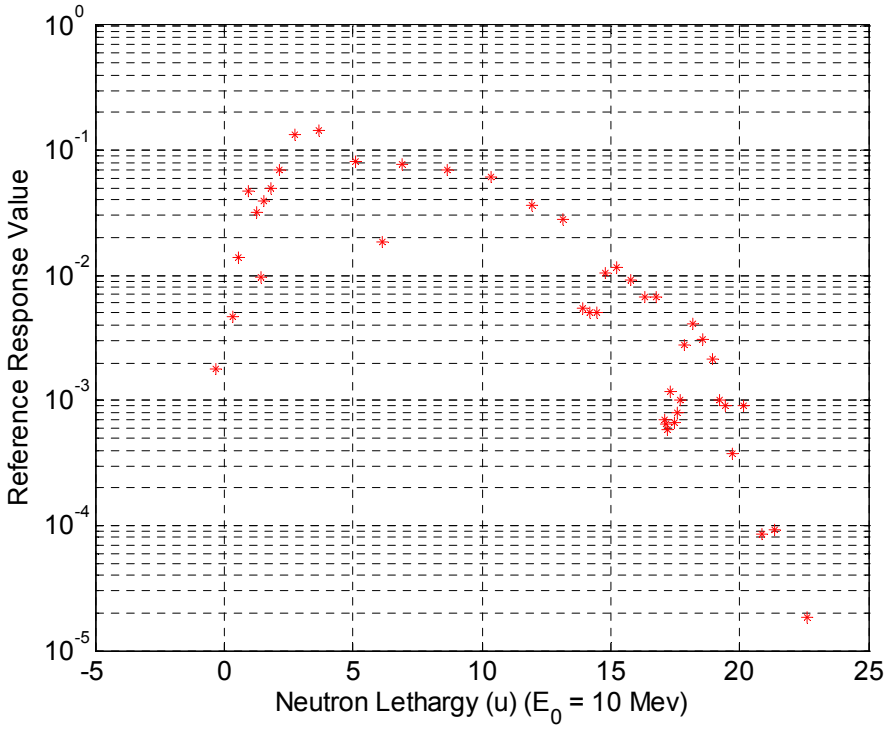

Figure 6-30. Reference Response Values

Figure 6-31 compares the responses variations estimated by the EPGPT to the direct forward calculation, and Figure 6-32 compares the relative responses variations estimated by the EPGPT to the direct forward calculation. Figure 6-33 shows discrepancies between the exact responses variations and the estimated responses variations by EPGPT for all 44 responses. The discrepancy shown in Figure 6-33 is defined as

$$\frac{\Delta R_{\text{exact,g}} - \Delta R_{\text{E}_\text{P}\text{GPT,g}}}{R_{\text{reference,g}}} \tag{6.5.4}$$

where Δ denotes a variation from the reference calculations. For comparison, the exact relative responses variations are also shown in Figure 6-33.

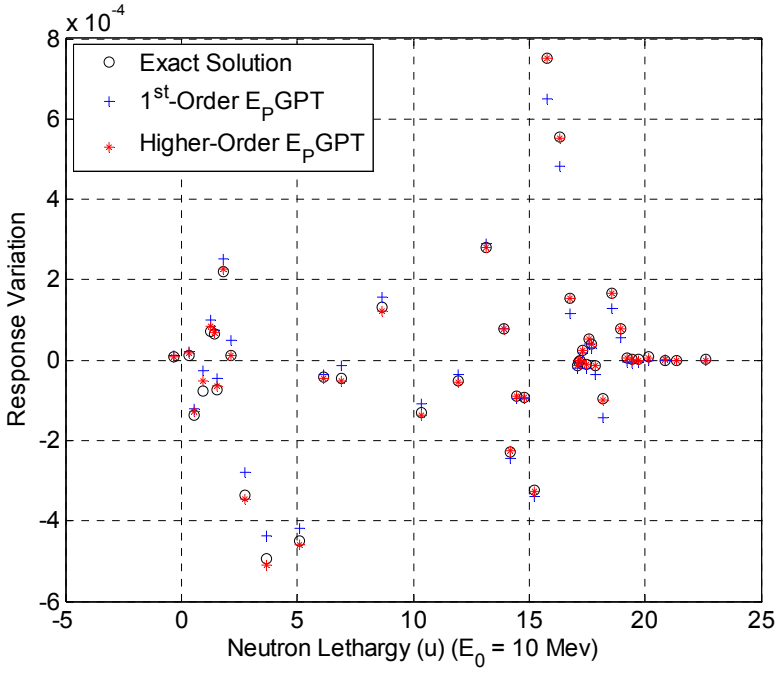

Figure 6-31. Estimation of Response Variations (*r* = 60)

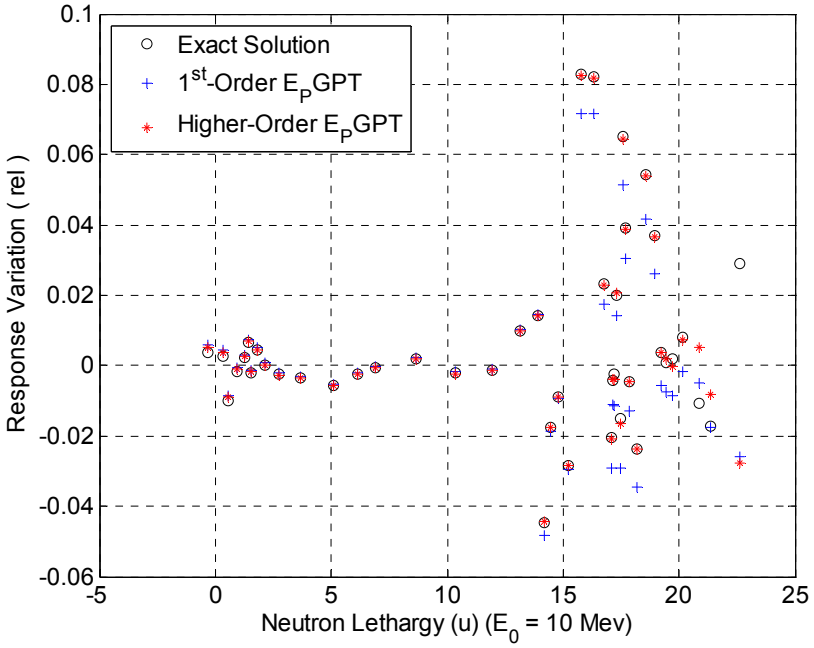

Figure 6-32. Estimation of Response Variations (Relative and *r* = 60)

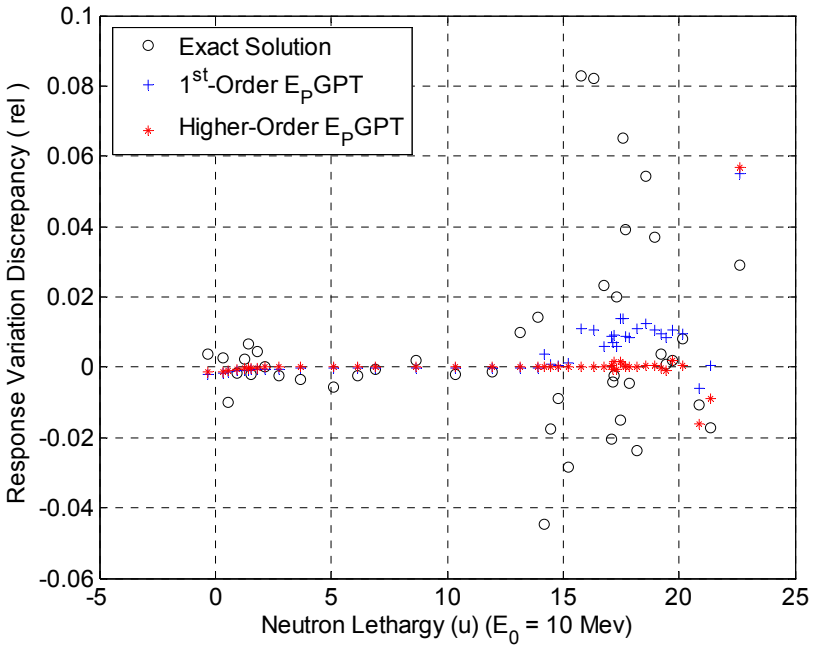

Figure 6-33. Comparison of Response Estimation Accuracy (r = 60)

From Figure 6-31, Figure 6-32 and Figure 6-33, one can observe that the estimated responses variations by higher-order EPGPT have a good agreement with the exact responses variations. Additionally, when the responses values are small, the variations in the response can be easily contaminated by the numerical errors, as can be observed in the neuron thermal range from Figure 6-30 and Figure 6-33.

Moreover, the estimation accuracy is examined by using 27 test samples (i.e., t = 27). As can be seen in Figure 6-34, the higher-order EPGPT using 60 basis vectors can evaluate the k-eigenvalue (or k_{eff}) variation more accurately than the first-order GPT approximation by an order level. Figure 6-35 shows the neutron flux *rms* error defined in Eq. (6.2.1) for all 27 test samples.

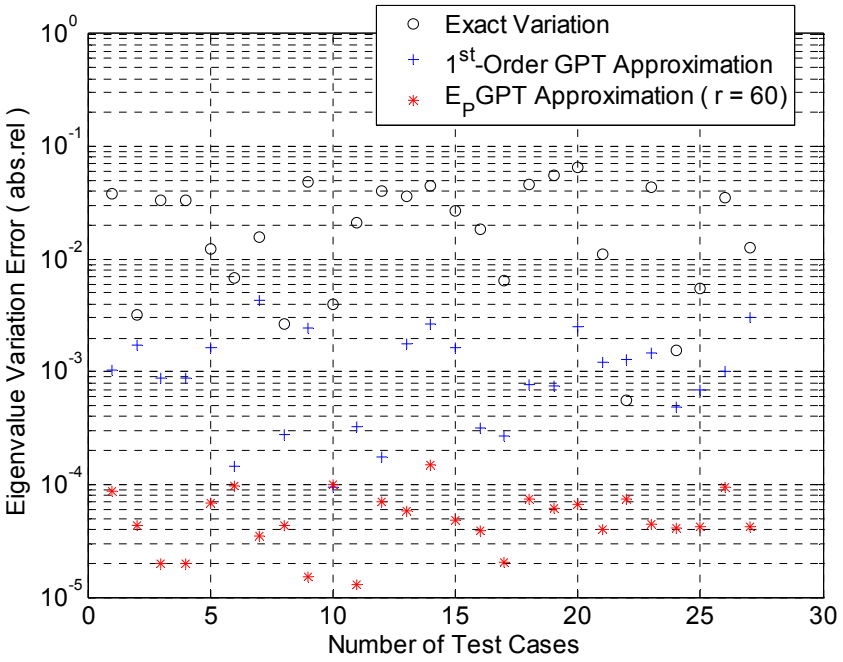

Figure 6-34. Comparison of Estimation Accuracy for Eigenvalue Variation (t = 27)

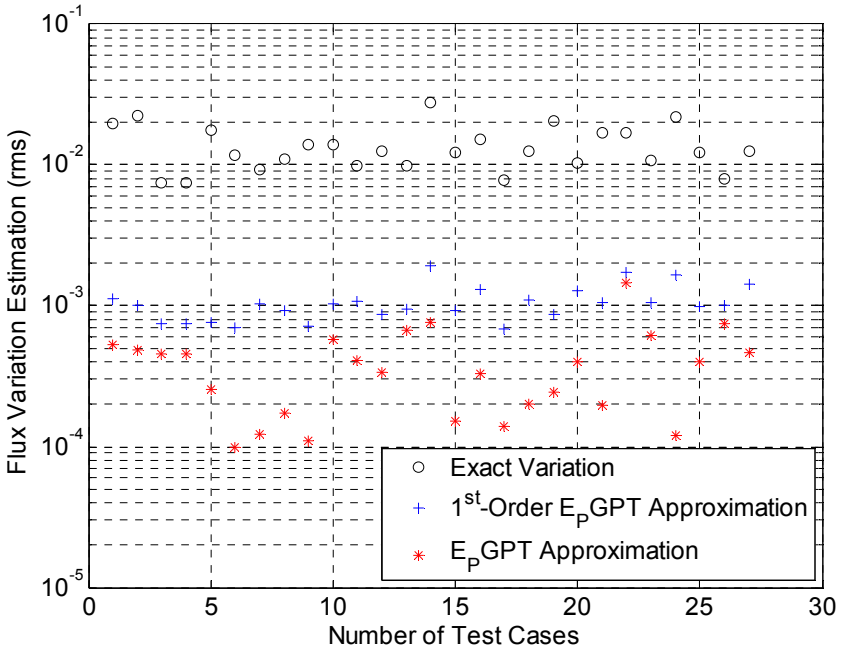

Figure 6-35. Analysis E_PGPT Errors for Angular Flux (t = 27)

CASE II: This case study is based on the Westinghouse fuel lattice with a 15×15 pin cells employed in H. B. Robinson Unit 2 PWR model (Radulescu, Gauld & Ilas 2010). The modeling detail is provided in Figure 6-36 for H. B. Robinson Lattice BO-5 showing the location of burnable poison rods (BPRs), e.g., borosilicate glass absorber rods, and neighboring fuel rod N-9. Table 6-6 provides the design characteristics of lattice BO-5 and Table 6-7 describes the chemical composition and density of the burnable poison rod. The model is developed using a one-quarter lattice representation, taking advantage of the lattice symmetry. A reflective boundary condition was applied to the outer boundary of this configuration. Similar to case I, we employ the TSUNAMI-2D (reference) – NEWT forward (identify active subspace) – Modified NEWT GPT (adjoint solutions) – Modified SAMS (E_PGPT) – Post-processing sequence to calculate the flux/response variations. The original input file of NEWT sample 4 provided by (Jessee, Dehart 2011) is modified for E_PGPT study. In this model, the v5-44 cross section library is employed; S-4 quadrature, P-1 scattering (P-2 in the moderator), spatial and eigenvalue stopping criteria of 1.0E-8 are used for NEWT forward calculation. The eigenvalue at the reference condition for this case is given by $k_{eff} = 1.036746$. For the adjoint and generalized adjoint calculations, spatial and eigenvalue stopping criteria of 5.0E-6 are employed. There're total 3462 computational cells for this lattice model. Thus, the dimension of neutron angular flux space is $3462 \times 44 \times 12 = 1827936$, i.e., $\phi \in \mathbb{R}^{1827936}$. Additionally, 3 different types of rods are employed, and 24 different isotopes are adopted for this model. The microscopic multigroup

cross sections – fission, radiation capture, ν – of all isotopes are randomly perturbed by $\pm 30\%$. The size of the perturbed parameters space is $\alpha \in \mathbb{R}^{1408}$.

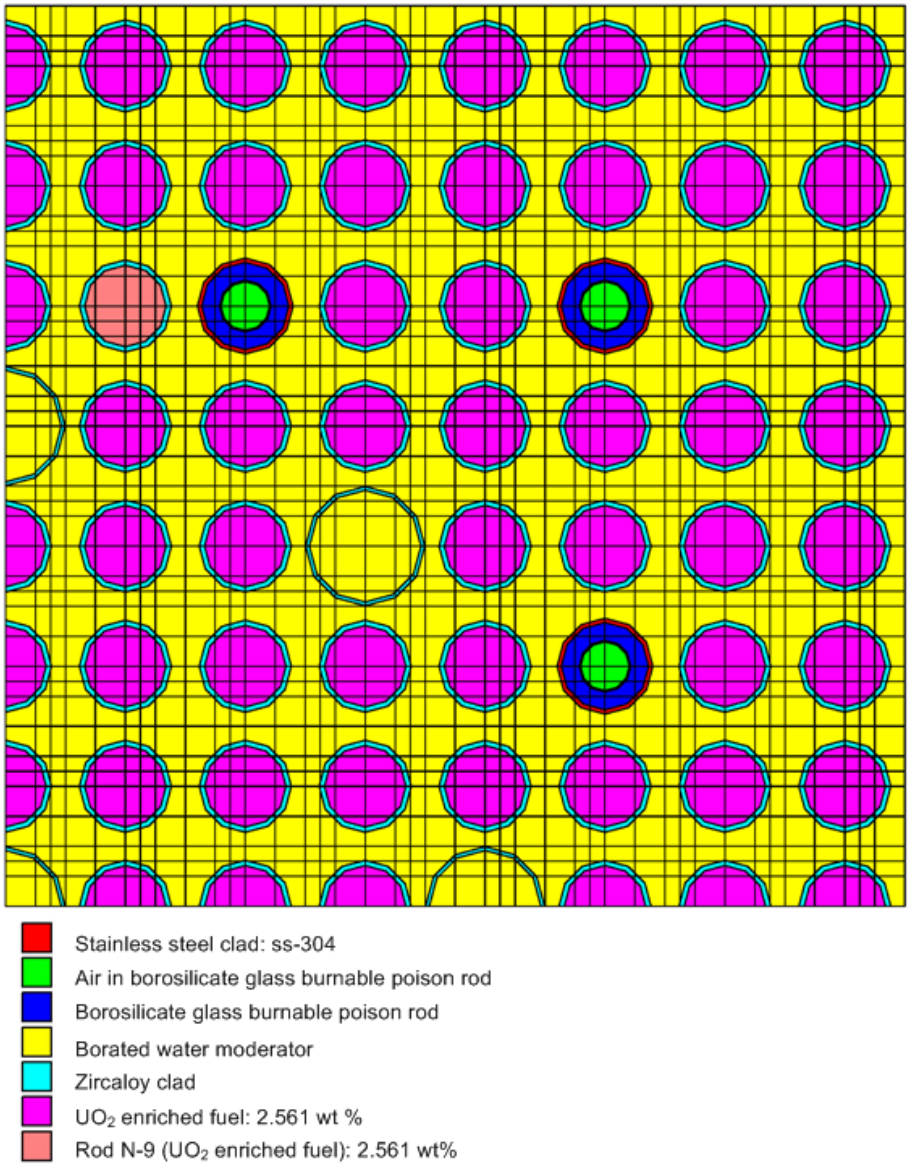

Figure 6-36. Model Layout and Grid Structure

Table 6-6. Lattice Design for H. B. Robinson

Parameters	**Data**
Reactor core	
Design	Westinghouse, PWR 15×15
Lattice pitch (cm)	21.50364
Reactivity control	Soluble boron, BPR, and control rod
Fuel Lattice BO-5	
Lattice	15×15
Number of fuel rod	204
Uranium weight (kg)	443.7
Number of guide tubes	21
Fuel rod	
Type fuel pellet	UO_2
Pellet stack density (g/cm^3)	9.55
Initial fuel composition (wt% in U total)	
U-235	2.561
U-234	0.023
U-236	0.013
U-238	97.403
Rod pitch (cm)	1.43
Rod outer diameter (cm)	1.0719
Rod inner diameter (cm)	0.9484
Pellet diameter (cm)	0.9294
Clad material	Zircaloy-4
Clad temperature (*K*)	595
Guide tube	
Material	Zircaloy-4
Inner radius (cm)	0.6502
Outer radius (cm)	0.6934
Burnable poison rod (BPR)	
Air outer diameter (cm)	0.5677
SS304 outer diameter (cm)	0.6007
Borosilicate glass outer diameter (cm)	1.0173
SS304 outer diameter (cm)	1.1151

Table 6-7. Atom Densities for BPR

Description	Material	Weight Percent	Atom Density (atoms/cm·barn)
BPR	o-16	53.53	4.1979E-02
	b-10	0.696	1.7941E-04
	b-11	3.186	3.6046E-03
	na-23	2.82	1.5369E-03
	al-27	1.758	8.1645E-04
	si	37.63	1.6791E-02
	k	0.33	1.0577E-04

In Figure 6-37, the singular value spectrum of 120 flux variations is presented. One can observe that the spectrum of the singular values is decaying rapidly. Note that after 120th singular value, the magnitudes of them are below 10E-4 which is typically used as the stopping criteria for LWR lattice calculations.

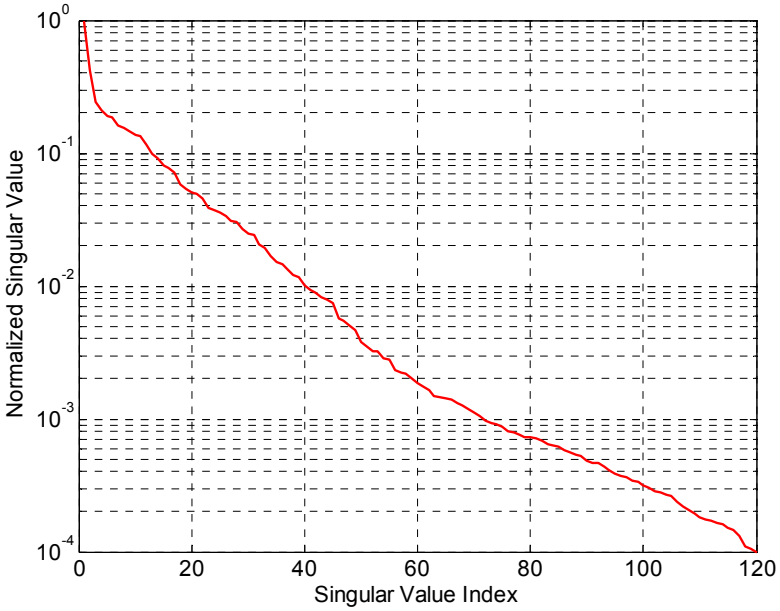

Figure 6-37. Singular Value Spectrum

The E_PGPT is executed and is tested for a perturbed case with respect to random microscopic multigroup cross sections perturbations. The exact values of perturbed neutron angular flux are calculated using direct forward calculation which requires a full NEWT forward execution. To study the performance of E_PGPT for different sizes of the active subspace, the *rms* metric defined in Eq. (6.2.1) are employed. Figure 6-38 shows *rms* errors of neutron angular flux against different sizes of the active subspace.

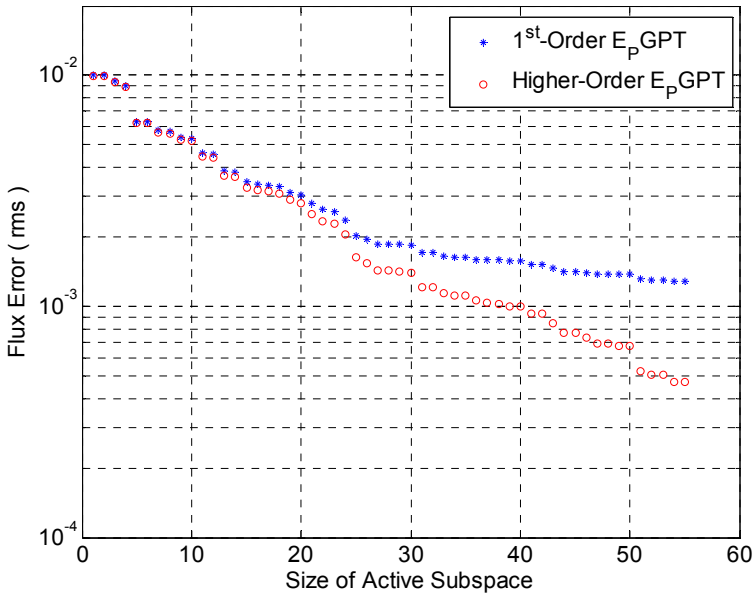

Figure 6-38. Analysis of E_PGPT Errors versus *r*

As before, similar characteristics can be observed from Figure 6-38. The first-order E_PGPT errors are comparable to E_PGPT when the active subspace is too small to properly capture all possible flux variations. As the size of the subspace is increased, it starts to capture larger portions of flux variations, and the associated errors are reduced accordingly.

Figure 6-39 shows eigenvalue error, defined in Eq. (6.5.1), against the size of the active subspace. For reference, the eigenvalue error calculated by first-order GPT is shown on the same graph as a horizontal line. The perturbed eigenvalue is $k_{eff}' = 0.981414$, and the exact variation in the eigenvalue is $\Delta k_{\text{exact}} = -5533.2\text{pcm}$.

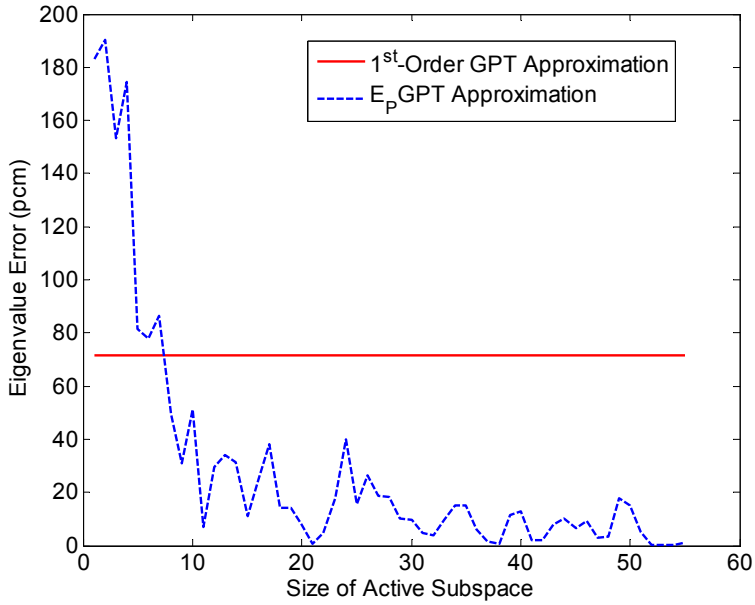

Figure 6-39. Eigenvalue Tolerance versus *r*

And furthermore, we will calculate the responses variations using the EPGPT, where the responses are defined in Eq. (6.5.3), and the discrepancies are defined in Eq. (6.5.4). For this case study, *NOG* is equal 44, thus we will evaluate 44 different responses using EPGPT. For comparison, the exact variations in these responses are calculated by NEWT forward. Figure 6-40 shows the 44 responses values at the reference condition against the neutron lethargy.

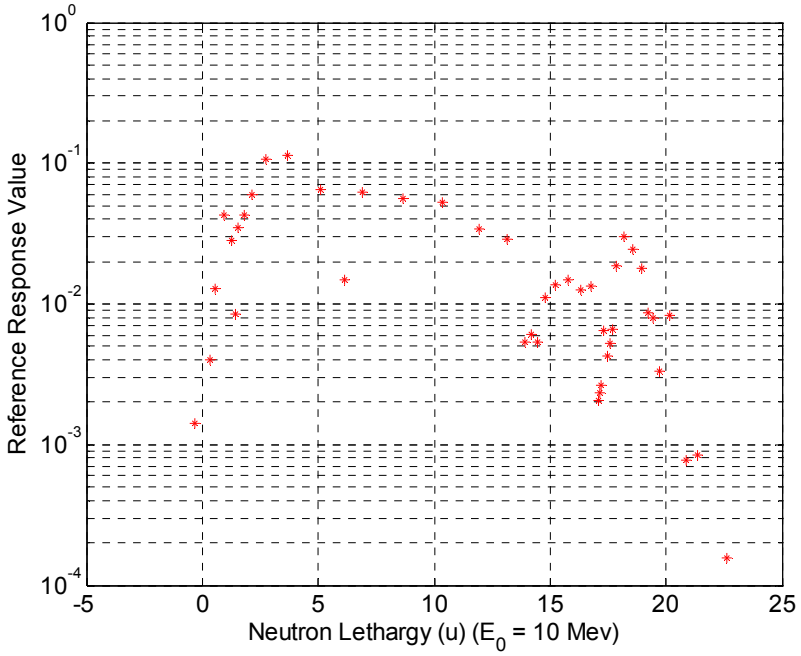

Figure 6-40. Reference Response Values

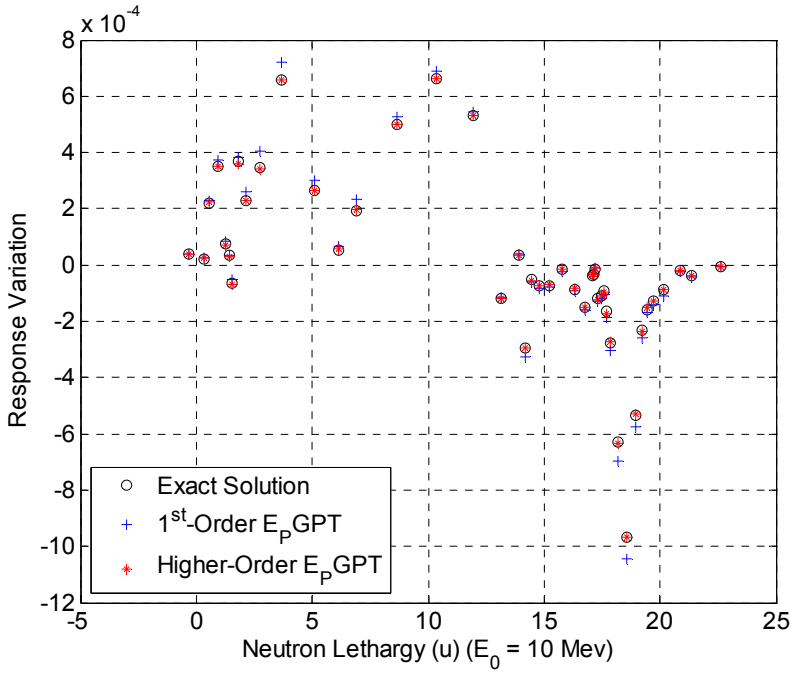

Figure 6-41. Estimation of Response Variations (*r* = 55)

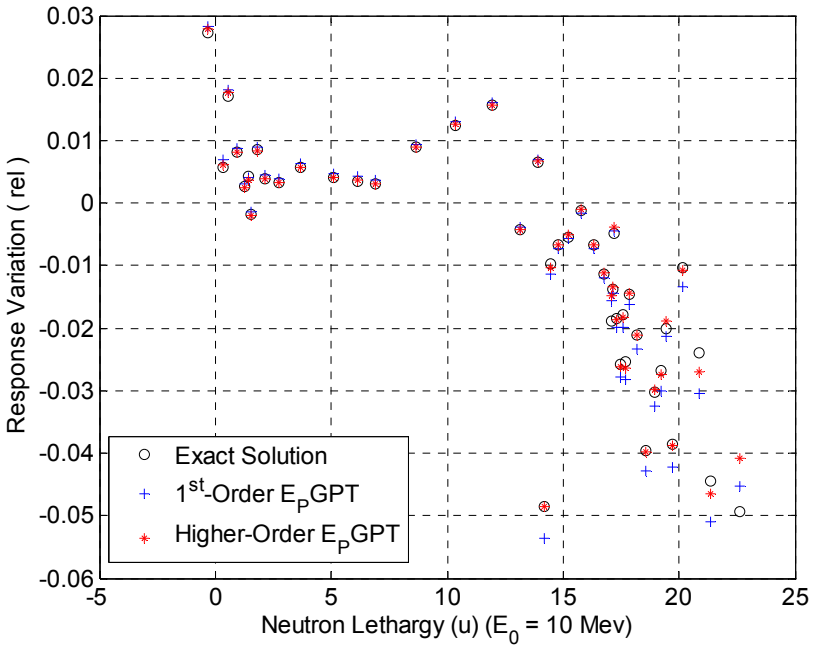

Figure 6-42. Estimation of Response Variations (Relative and *r* = 55)

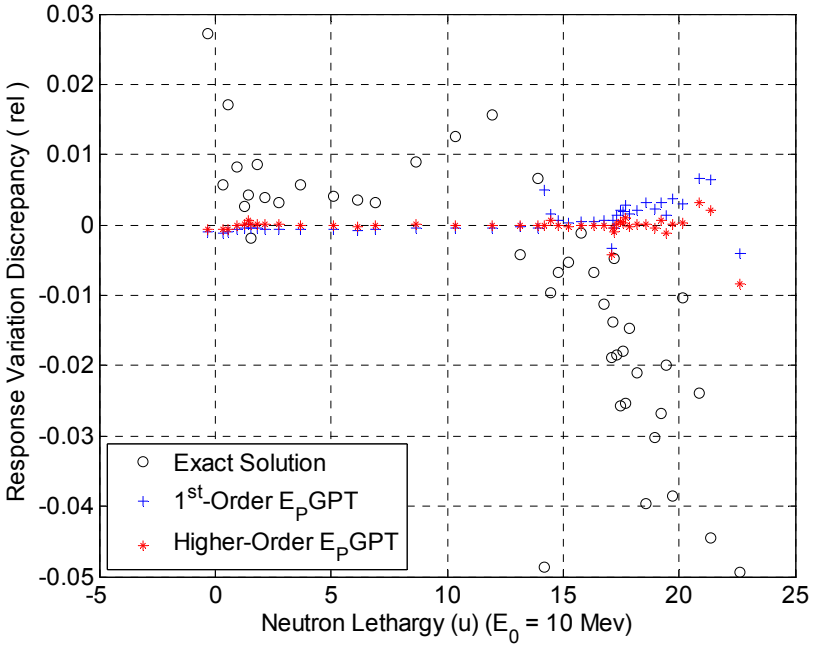

Figure 6-43. Comparison of Response Estimation Accuracy (*r* = 55)

The results presented in Figure 6-41, Figure 6-42 and Figure 6-43 show that higher-order E_PGPT consistently provides accurate estimations for user-defined responses, whereas first-order approximation cannot give sufficiently accurate results.

Moreover, the estimation accuracy is examined by using 30 test samples (i.e., $t = 30$). As can be seen in Figure 6-44, the higher-order E_PGPT using 55 basis vectors can evaluate the *k*-eigenvalue (or k_{eff}) variation more accurately than the first-order GPT approximation. Roughly speaking, the maximum exact variation in the eigenvalue is around 10% (or 10,000pcm), the maximum discrepancy between first-order and exact variation is around 0.4% of reference eigenvalue (or 400pcm), whereas the maximum discrepancy between higher-order E_PGPT and exact variation is around 0.02% (or 20pcm). In addition, Figure 6-45 shows the neutron flux *rms* error defined in Eq. (6.2.1) for all 30 test samples.

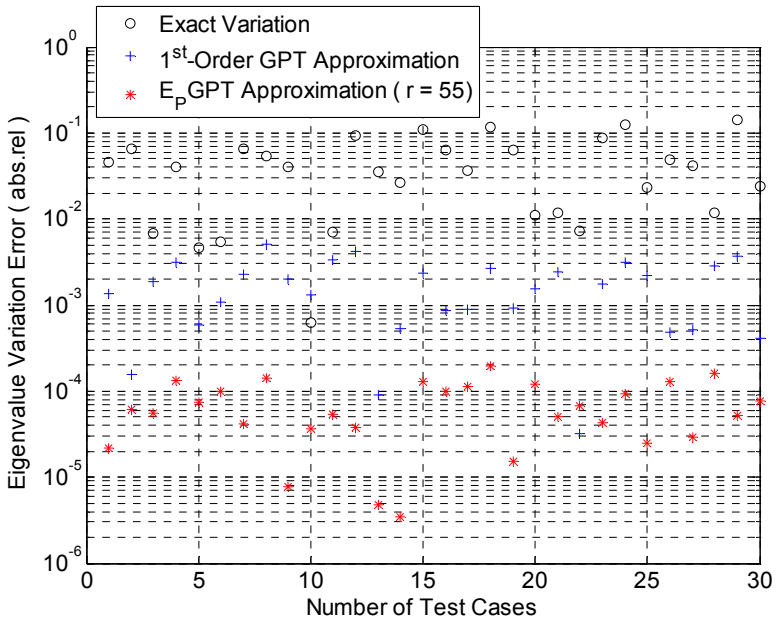

Figure 6-44. Comparison of Estimation Accuracy for Eigenvalue Variation ($t = 30$)

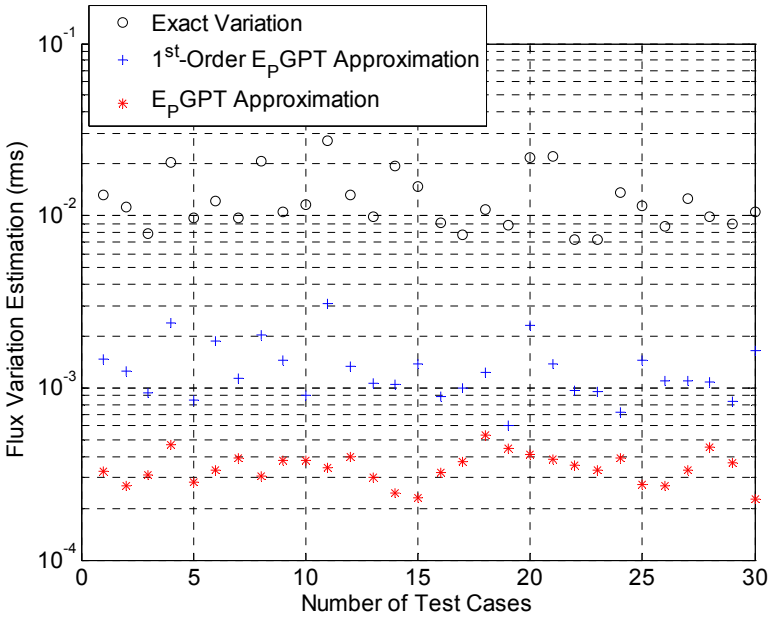

Figure 6-45. Analysis E_PGPT Errors for Angular Flux (t = 30)

CASE II (BPRs Insertion): In previous case studies, one can observe that there're no significant changes in the neutron flux by comparing the numerical results calculated by the first-order and higher-order E_PGPT. Therefore, first-order E_PGPT can be used to predict the flux/response variations when the cross sections perturbations are small. This property makes first-order E_PGPT suitable for sensitivity analysis and uncertainty quantification. In this case study, we will introduce the BPRs insertion into the lattice model as shown in Figure 6-36. This is achieved by increasing the poison material densities significantly. Initial chemical composition and density of BPRs are provided in Table 6-7. The ranges of variations in the densities of BPRs are shown in Table 6-8. For each perturbed case, all materials atom densities in BPRs are perturbed as follows:

$$n_p = n_0 + \Delta n_{\max} \bullet \zeta \tag{6.5.5}$$

where vector n_p describes the perturbed atom densities, n_0 and $\Delta n_{\max}$ denote the initial atom densities and maximum variations in the initial atom densities, respectively; ζ is a random value from the uniform distribution on the interval (0,1). Furthermore, the temperature variations in the fuel rod and moderator is achieved by randomly perturbing the microscopic cross sections – fission, radiation capture, ν – by $\pm 10\%$. The dimension of the perturbed parameters space is $\alpha \in \mathbb{R}^{1107}$.

As before, the sequence TSUNAMI-2D (reference) – NEWT forward (identify active subspace) – Modified NEWT GPT (adjoint solutions) – Modified SAMS (E_PGPT) – Post-processing is employed here to calculate the flux/response variations. In Figure 6-46, the singular value spectrum of 100 flux variations is presented.

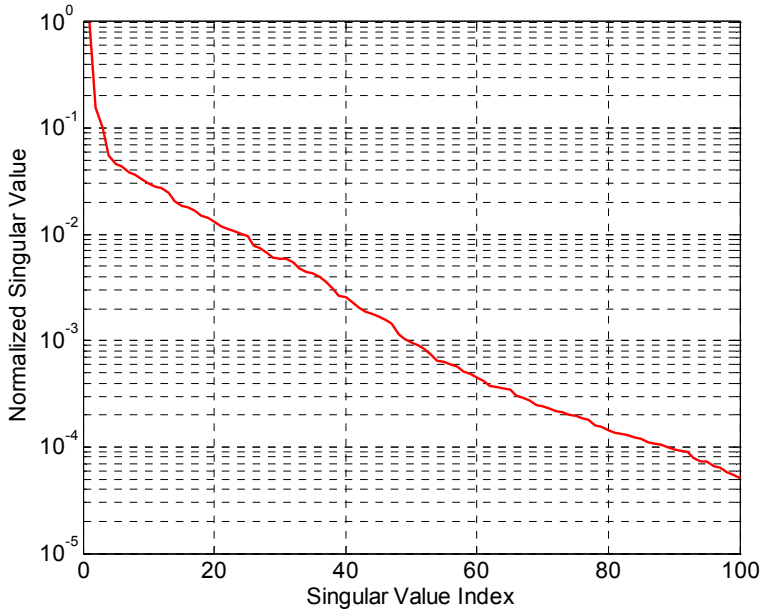

Figure 6-46. Singular Value Spectrum

Table 6-8. Atom Density Variations in BPRs

Description	Material	Variations in Atom Density (atoms/cm·barn)
BPRs	o-16	0.0 ~ 4.1979E-02
	b-10	0.0 ~ 1.7941E-04
	b-11	0.0 ~ 3.6046E-03
	na-23	0.0 ~ 1.5369E-03
	al-27	0.0 ~ 8.1645E-04
	si	0.0 ~ 1.6791E-02
	k	0.0 ~ 1.0577E-04

The E_PGPT is executed and is tested for a perturbed case, i.e. atom densities perturbations in BPRs and microscopic cross sections perturbations. The exact perturbed neutron angular flux values are calculated using direct forward calculation which requires a full NEWT forward execution. To study the performance of E_PGPT for different sizes of the active subspace, the *rms* metric defined in Eq. (6.2.1) is employed. Figure 6-47 shows *rms* errors of neutron angular flux against the different sizes of the active subspace. As can be observed from Figure 6-47, first-order perturbation theory breaks down for this case study, since non-linear effects generated by BPRs insertion will have a significant impact on the flux variations. One can either perform the perturbation analysis by using two direct forward calculations or by using higher-order perturbation theory. The former approach is certainly preferable if only a small number of perturbations are examined. On the other hand, if a very large number of nonlinear perturbations are of interest, then a higher-order perturbation theory may be considered. Another important observation from Figure 6-47 is that higher-

order EPGPT will consistently provide more and more accurate estimations for neutron flux as the size of the active subspace continues to increase.

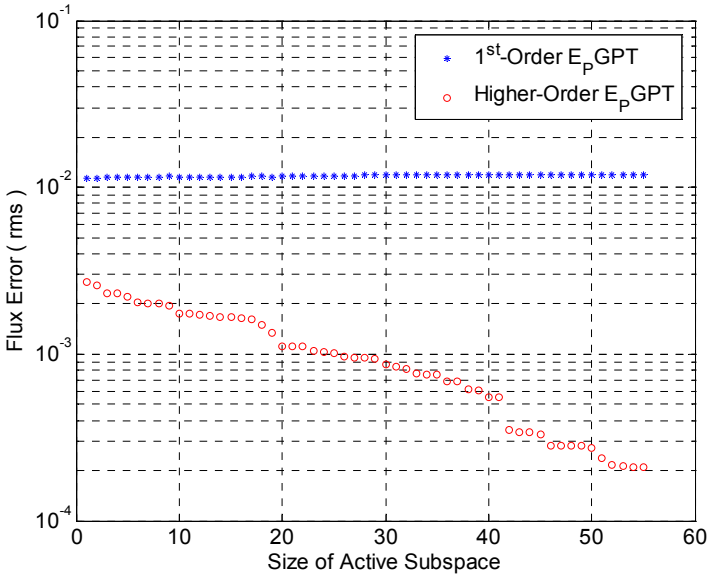

Figure 6-47. Analysis of EPGPT Errors versus *r*

Figure 6-48 shows eigenvalue error, defined in Eq. (6.5.1), against different sizes of the active subspace. For reference, the eigenvalue error calculated by first-order GPT is shown on the same graph as a horizontal line. The exact variation in the eigenvalue is equal to 262.58pcm, and the value obtained with only first-order terms is -1256.18pcm. In this case, first-order perturbation theory does not even predict the correct sign of the variation. The estimated eigenvalue variation by higher-order EPGPT is equal to 255.39pcm, and the absolute error is 7.19pcm if one employs only 55 basis vectors for this case. One may observe that the exact eigenvalue variation is much smaller compared to the preceding case

study, although one has inserted the BPRs. This is because the first-order term $\Delta\mathbf{P}\phi$ nearly cancels the contribution of the term $\mathbf{P}\Delta\phi$. This effect has been denoted as the first-order cancellation in (Williams 1986).

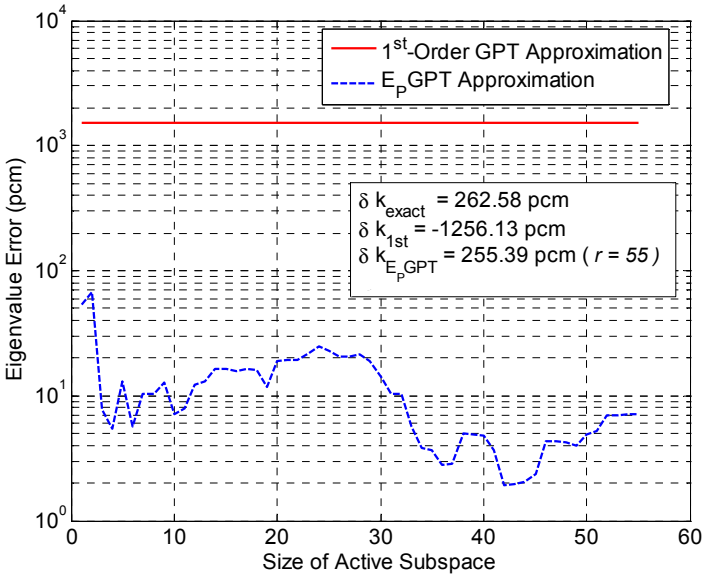

Figure 6-48. Eigenvalue Tolerance versus *r*

We will calculate the 44 responses variations using the EPGPT, where the responses are defined in Eq. (6.5.3), and the discrepancies are defined in Eq. (6.5.4). For comparison, the exact variations in these responses are calculated by NEWT forward. The results presented in Figure 6-49, Figure 6-50 and Figure 6-51 show that higher-order EPGPT consistently provides accurate estimations for user-defined responses, whereas first-order perturbation theory breaks down. For reference, the exact variations in the responses are also shown in these three figures.

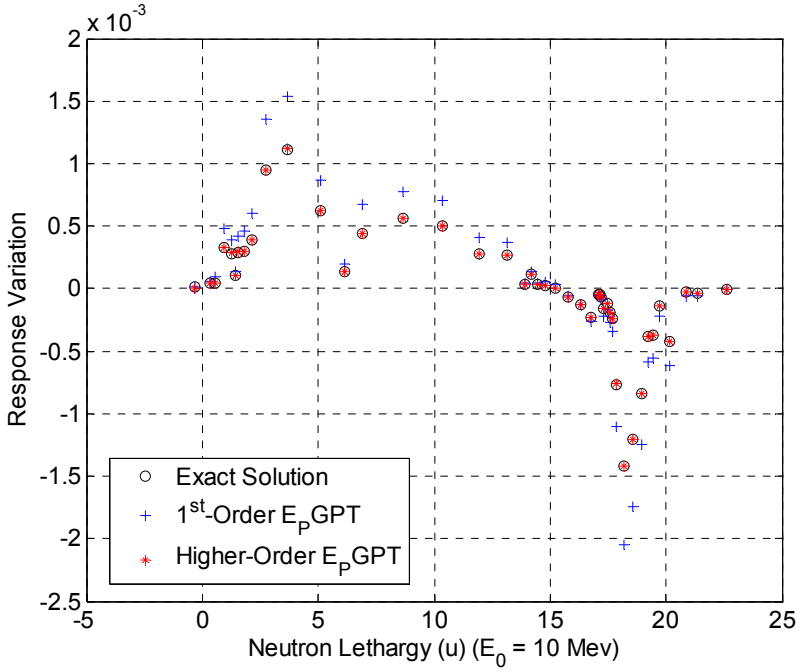

Figure 6-49. Estimation of Response Variations (*r* = 55)

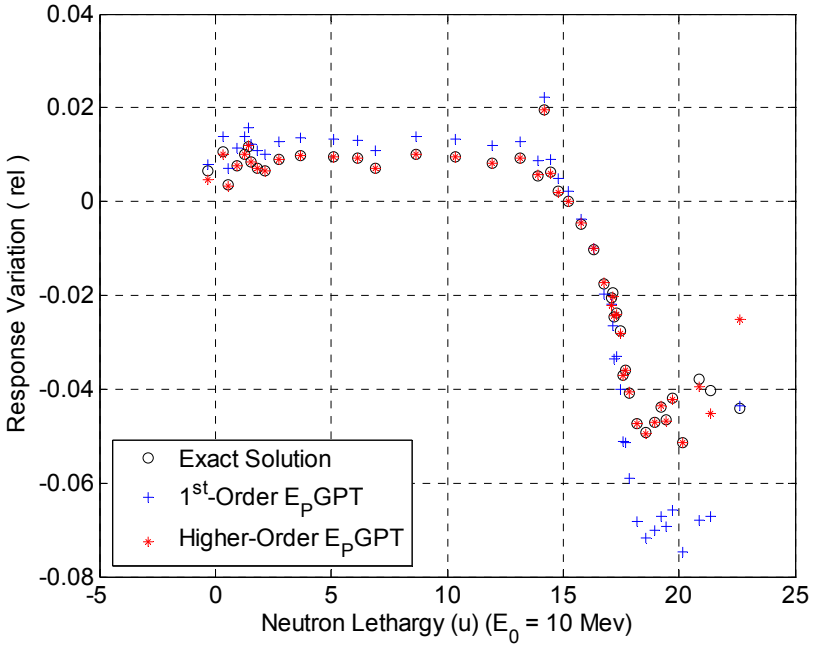

Figure 6-50. Estimation of Response Variations (Relative and *r* = 55)

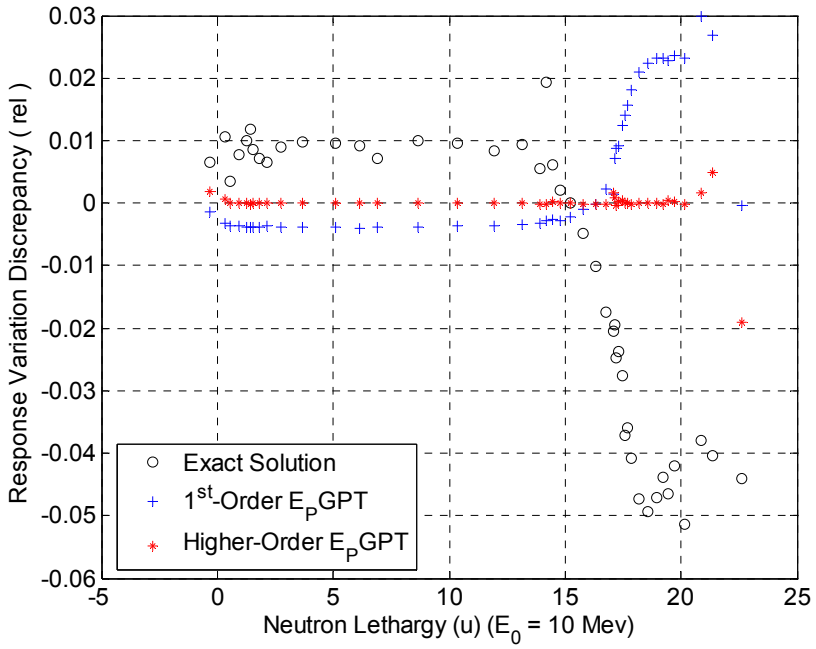

Figure 6-51. Comparison of Response Estimation Accuracy (r = 55)

Moreover, the estimation accuracy is examined by using 30 test samples (i.e., t = 30). As can be seen in Figure 6-52, the higher-order E$_P$GPT using 55 basis vectors can evaluate the k-eigenvalue (or k_{eff}) variation much more accurately than the first-order GPT approximation. Roughly speaking, the maximum exact variation in the eigenvalue is around 6% (or 6,000pcm), the maximum discrepancy between first order and exact variation is around 2% of reference eigenvalue (or 2,000pcm), whereas the maximum discrepancy between higher-order E$_P$GPT and exact variation is around 0.007% of reference eigenvalue (or 7pcm). In addition, Figure 6-53 shows the neutron flux *rms* error defined in Eq. (6.2.1) for all 30 test samples. Both Figure 6-52 and Figure 6-53 indicate that first-order perturbation theory breaks down when strongly absorbing rods are inserted.

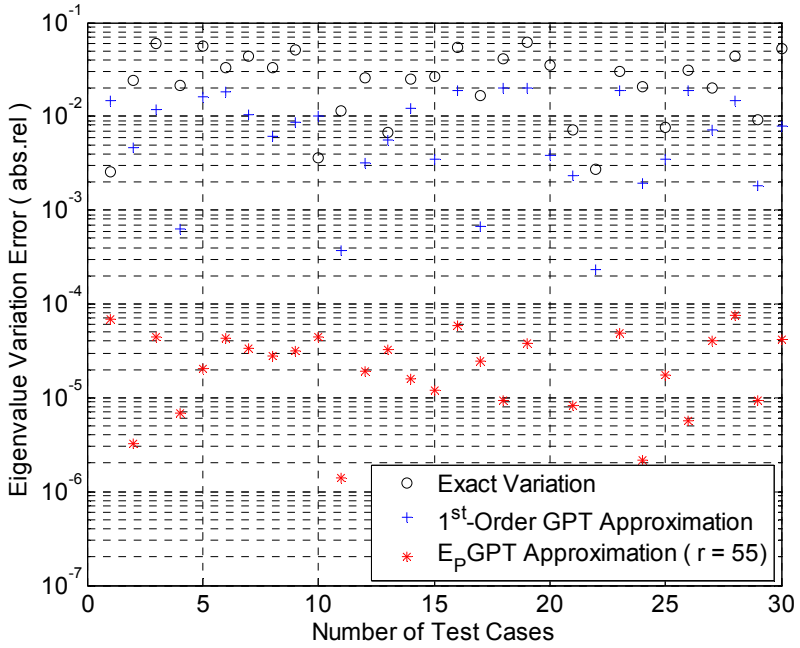

Figure 6-52. Comparison of Estimation Accuracy for Eigenvalue Variation (t = 30)

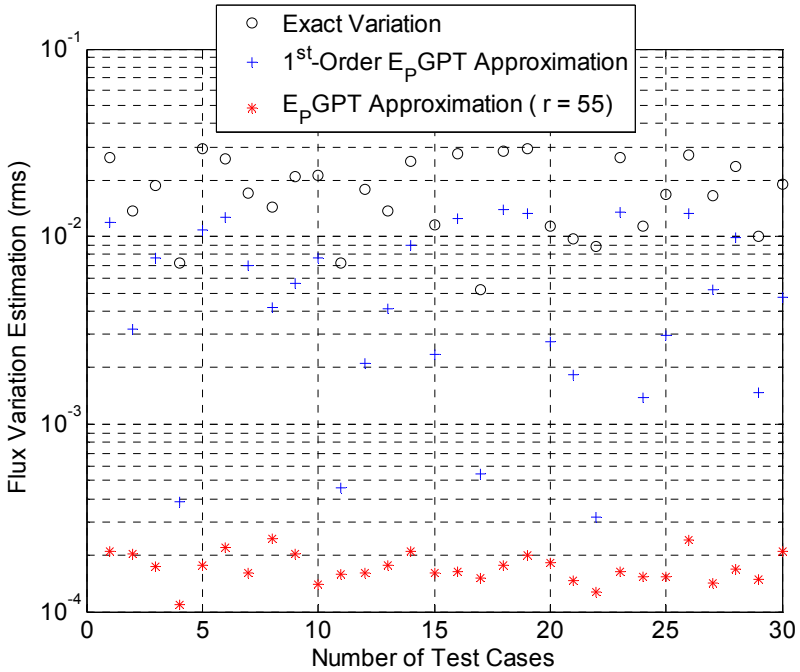

Figure 6-53. Analysis E_PGPT Errors for Angular Flux (t = 30)

CASE III: This case study is based on a lattice model with a large reflector region. This model is modified from input file of NEWT sample 5 (Jessee, Dehart 2011). Table 6-9 provides the design characteristics and Figure 6-54 depicts the model analyzed. In this model, seven UO_2 pin-cells are adjacent to eight MOX pin-cells, which, in turn, are adjacent to a large reflector region. The outer boundary of the reflector is vacuum. Reflection on the top and bottom boundaries makes the problem infinite in the y-direction. The same sequence, i.e. TSUNAMI-2D (reference) – NEWT forward (identify active subspace) – Modified NEWT GPT (adjoint solutions) – Modified SAMS (E_PGPT) – Post-processing, is employed here to calculate the flux/response variations. In this model, the v5-44 (or 44GROUPNDF5) cross section library, S-6 quadrature, P-1 scattering (P-2 in the moderator), spatial and eigenvalue stopping criteria of 1.0E-9 are used for NEWT forward calculation. The eigenvalue at the reference condition for this case is given by $k_{eff} = 1.167126$. For the adjoint and generalized adjoint calculations, the spatial and eigenvalue stopping criteria of 1.0E-7 are employed. There're total 652 computational cells for this lattice model. Thus, the dimension of neutron angular flux space is $652 \times 44 \times 24 = 688212$, i.e., $\phi \in \mathbb{R}^{688512}$. Additionally, 13 different isotopes are adopted for this model. The microscopic multigroup cross sections – fission, radiation capture, ν – of all isotopes are randomly perturbed by $\pm 30\%$. The dimension of the perturbed parameters space is $\alpha \in \mathbb{R}^{1364}$. In Figure 6-55, the singular value spectrum of 150 flux variations is presented, and one can observe that the spectrum of the singular values is decaying rapidly.

Table 6-9. Lattice Design for Case II

Parameters	**Data**
Fuel Lattice	
Lattice	15×1
Number of fuel rod	15
Fuel rod	
Type fuel pellet	MOX
Initial fuel composition (atom/(cm.barn))	
U-235	4.1308E-04
U-234	3.3155E-06
U-236	2.6710E-06
U-238	1.9961E-02
Pu-238	3.6128E-05
Pu-241	1.7037E-05
Pu-242	2.4477E-06
Pu-240	9.6144E-05
Pu-239	4.4708E-04
Rod pitch (cm)	1.26
Rod outer diameter (cm)	0.978
Rod inner diameter (cm)	0.902
Clad material	SS304
Clad temperature (K)	620
Type fuel pellet	UO2
Initial fuel composition (atom/(cm.barn))	
U-235	9.2756E-04
U-234	7.1799E-06
U-236	5.2818E-06
U-238	2.1843E-02
Rod pitch (cm)	1.26
Rod outer diameter (cm)	0.978
Rod inner diameter (cm)	0.8926
Clad material	SS304
Clad temperature (K)	620

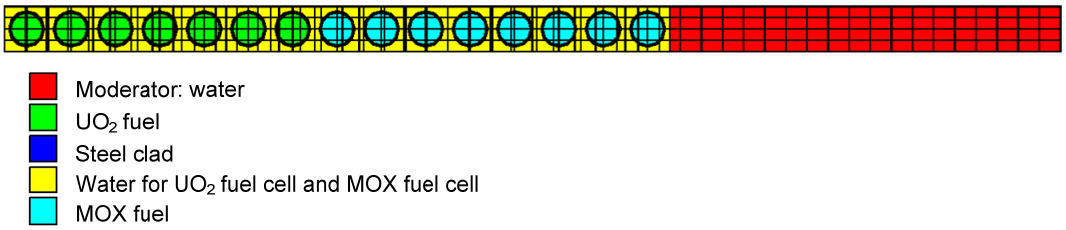

Figure 6-54. Model Layout with Grid Structure

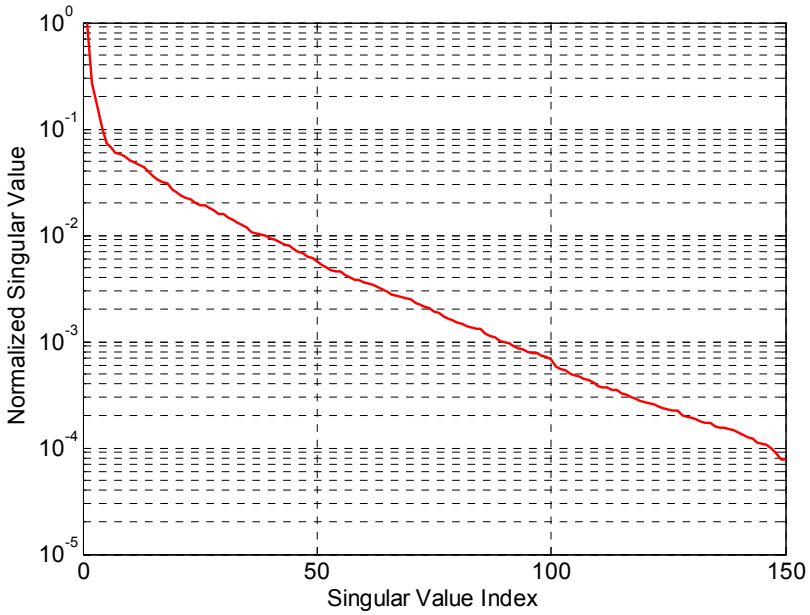

Figure 6-55. Singular Value Spectrum

The EPGPT is executed and is tested for a perturbed case with respect to microscopic multigroup cross sections perturbations. The exact values of perturbed neutron angular flux are calculated using direct forward calculation. To study the performance of EPGPT for different sizes of the active subspace, the *rms* metric defined in Eq. (6.2.1) are employed.

Figure 6-56 shows *rms* errors of neutron angular flux against different sizes of the active subspace.

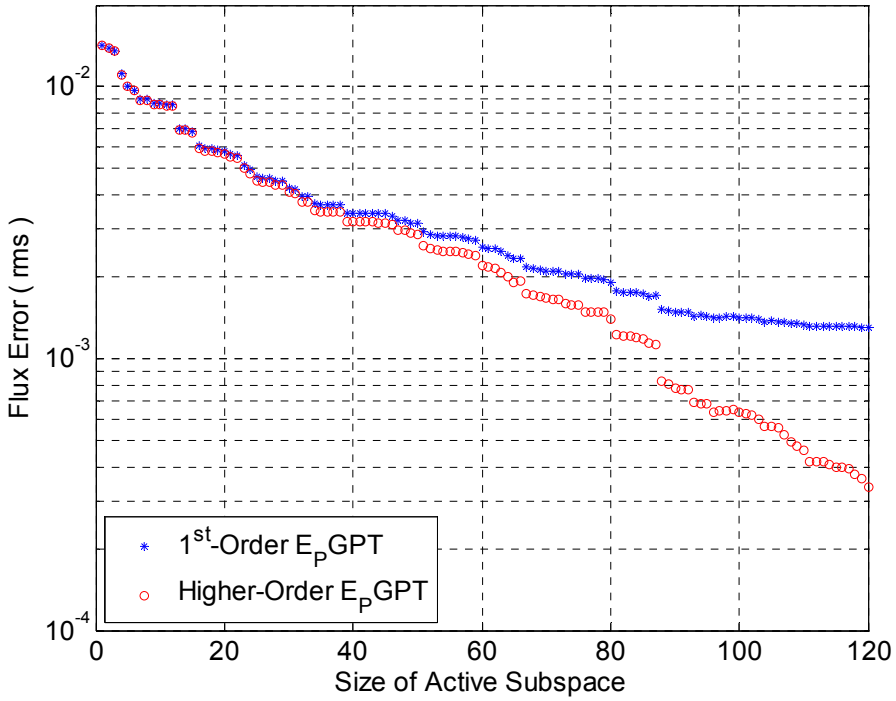

Figure 6-56. Analysis of E_PGPT Errors versus *r*

Similar characteristics can be observed from Figure 6-56. The first-order E_PGPT errors are comparable to E_PGPT when the active subspace is too small to properly capture all possible flux variations. As the size of the subspace is increased, it starts to capture larger portions of flux variations, and the associated errors are reduced accordingly. Figure 6-57 shows eigenvalue error, defined in Eq. (6.5.1), against different sizes of the active subspace.

The perturbed eigenvalue is 1.181381 for this case. For reference, the eigenvalue error calculated by first-order GPT is shown on the same graph as a horizontal line.

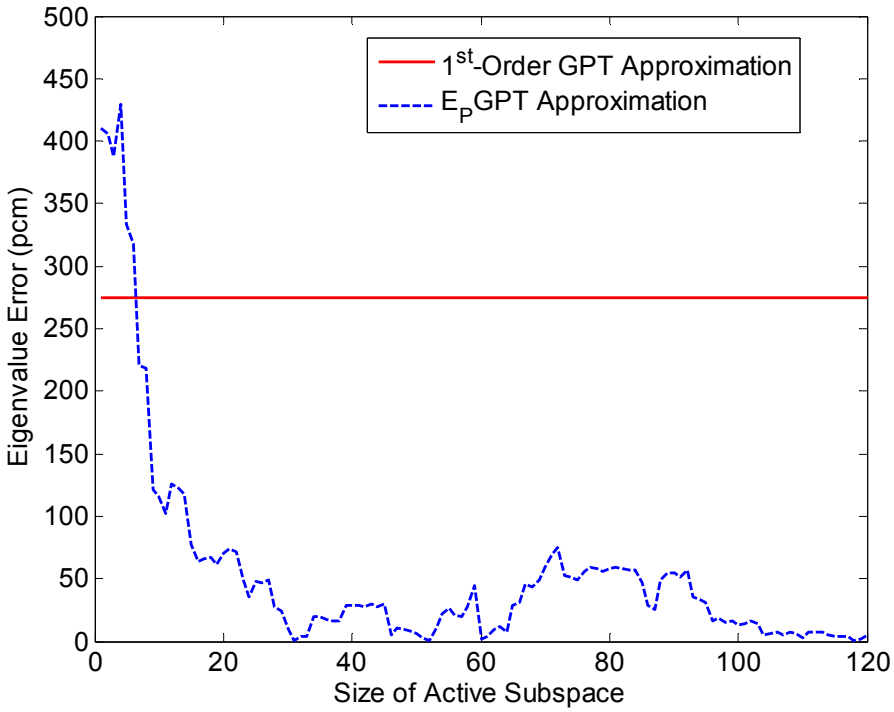

Figure 6-57. Eigenvalue Tolerance versus *r*

As like before, the responses variations are analyzed in Figure 6-58, Figure 6-59, and Figure 6-60 from different point of view. For comparison, the exact variations in these responses are calculated by NEWT forward. Moreover, the estimation accuracy of E_PGPT is examined in Figure 6-61 and Figure 6-62 by using 30 test samples (i.e., t = 30) with 120 basis vectors.

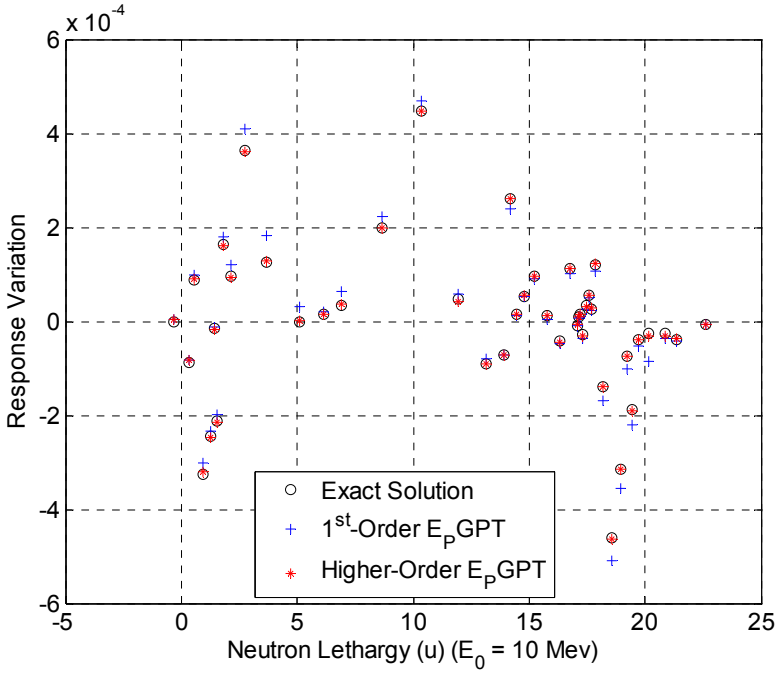

Figure 6-58. Estimation of Response Variations (*r* = 120)

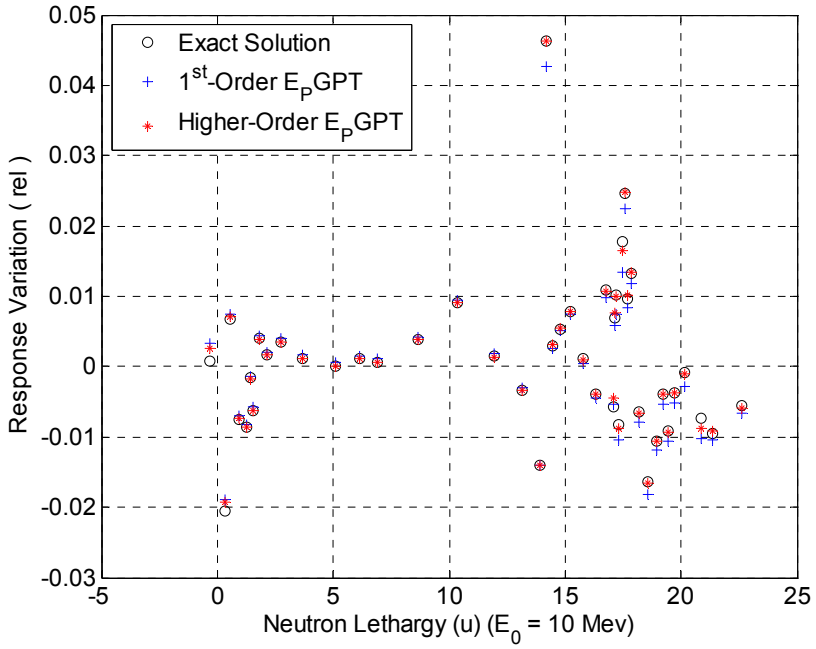

Figure 6-59. Estimation of Response Variations (Relative and *r* = 120)

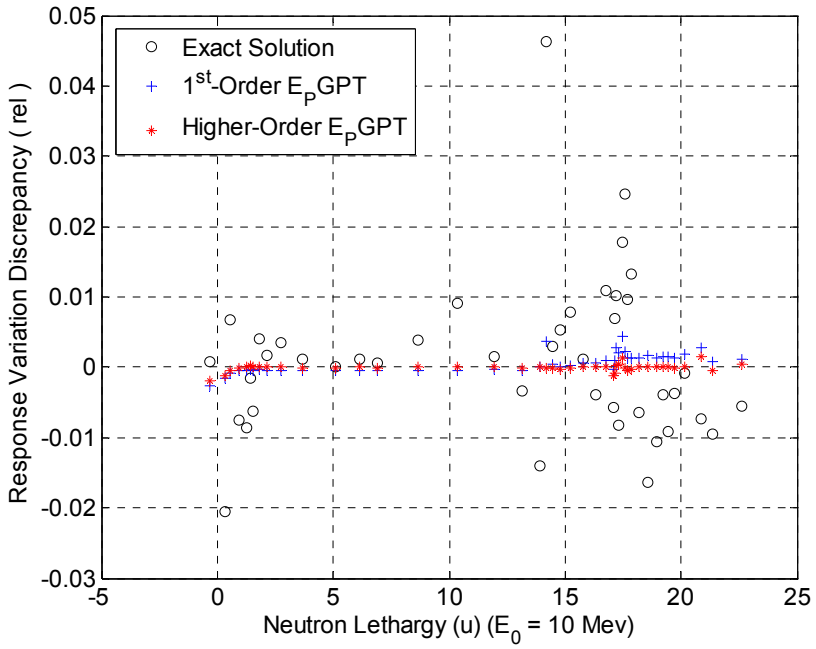

Figure 6-60. Comparison of Response Estimation Accuracy (r = 44)

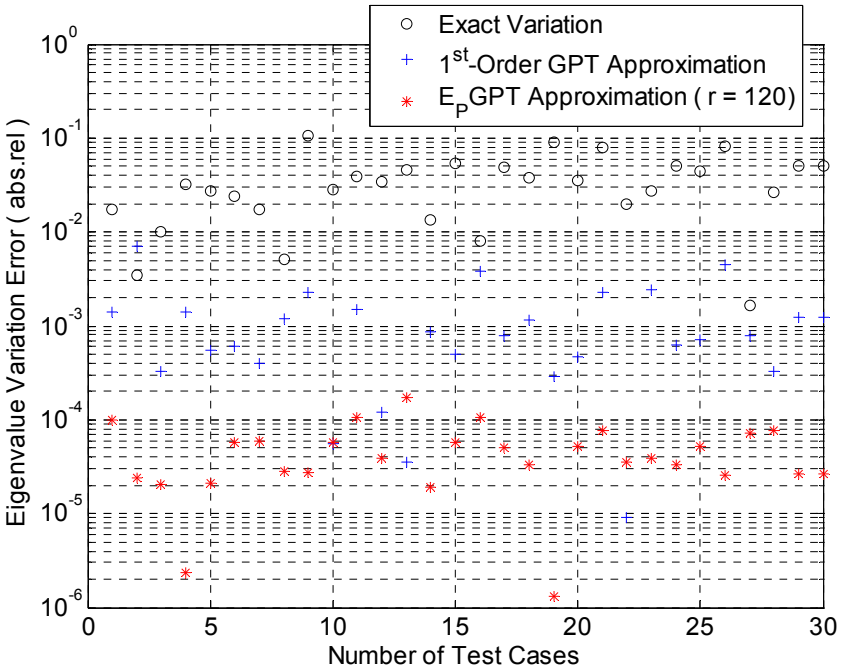

Figure 6-61. Comparison of Estimation Accuracy for Eigenvalue Variation (t = 30)

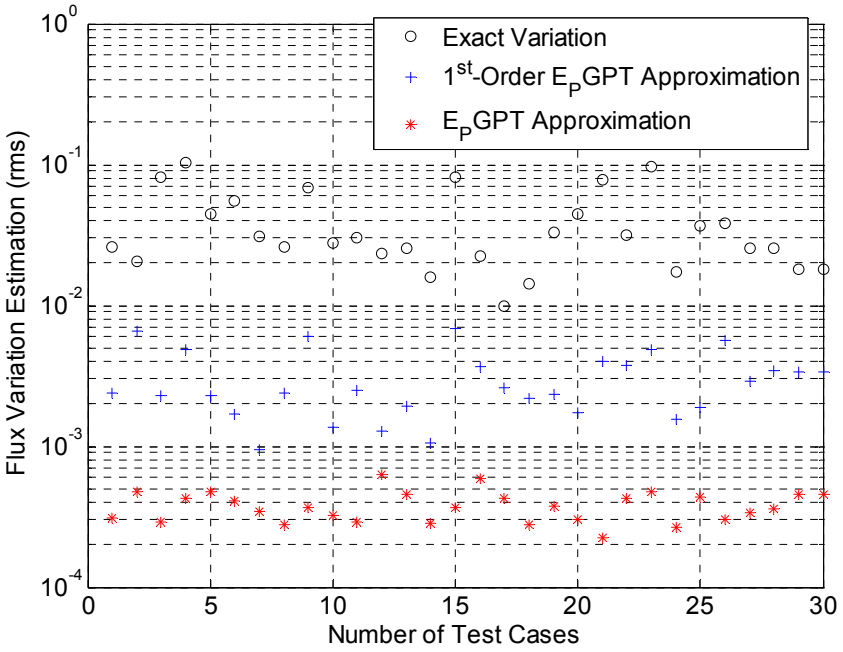

Figure 6-62. Analysis E_PGPT Errors for Angular Flux (t = 30)

6.6 E_PGPT for Neutron Depletion Calculations

Fuel depletion calculation is used to predict the changes in fuel composition during the reactor operation. Such changes will have significant impact on reactor's stability, control and operating life. Therefore, fast and accurate analysis of fuel depletion is always required for reactor design and analysis. The purpose of this case study is to examine the performance of the proposed E_PGPT in the realistic lattice model depletion calculations.

The E_PGPT is exercised on depletion calculations of H. B. Robinson Lattice BO-5 as described in case II study of previous section. The modeling detail for depletion is provided in Figure 6-63 for one-quarter H. B. Robinson Lattice BO-5 with different grid structure compared to Figure 6-36. A reflective boundary condition was applied to the outer boundary

of this configuration. Individual depleting mixtures were specified for the burnable poison rod and its nearest neighbor fuel rod N-9, as illustrated in Figure 6-63; all other fuel rods in the lattice were treated as a single depletion material with uniform composition. The lattice model with initial fuel is depleted in 20 steps by SCALE 6.1 TRITON module. Each depletion step is chosen to 20 days with the power of fuel rod N-9 is normalized to 20.86 MW/MTHM. For a single depletion step calculation, the sequence of BONAMI – CENTRM – NEWT – ORIGEN (Nuclide depletion calculation) is conducted. The fuel compositions are collected after each depletion step, and there're 21 values for each fuel composition in the entire depletion range. These values will be fitted by a polynomial of degree five to the depletion step. The input for each perturbed case is achieved as follows: first sample the depletion step randomly, and then evaluate the fuel compositions using the pre-calculated polynomials of degree five at randomly selected depletion step. These evaluated fuel compositions will be employed as initial input of resonance calculations, i.e. BONAMI – CENTRM, to generate the self-shielded microscopic multigroup cross sections. Both fuel compositions and self-shielded microscopic multigroup cross sections will be considered as the input for the neutron transport calculations. Then, the NEWT forward is employed to generate the active subspace with respect to perturbed input microscopic multigroup cross sections and fuel compositions. The modified NEWT generalized adjoint (or GPT) is utilized to calculate the generalized adjoint solutions with respect to pseudo responses. The modified SAMS will perform first-order GPT calculation by employing fundamental forward and adjoint solution and E_PGPT calculations utilizing the active subspace and generalized adjoint

solutions. Furthermore, the control module TSUNAMI-2D is utilized to perform the reference calculation with fuel compositions and self-shielded microscopic multigroup cross sections evaluated at 200 days, i.e., fundamental forward and adjoint calculations, using v5-44 cross section library.

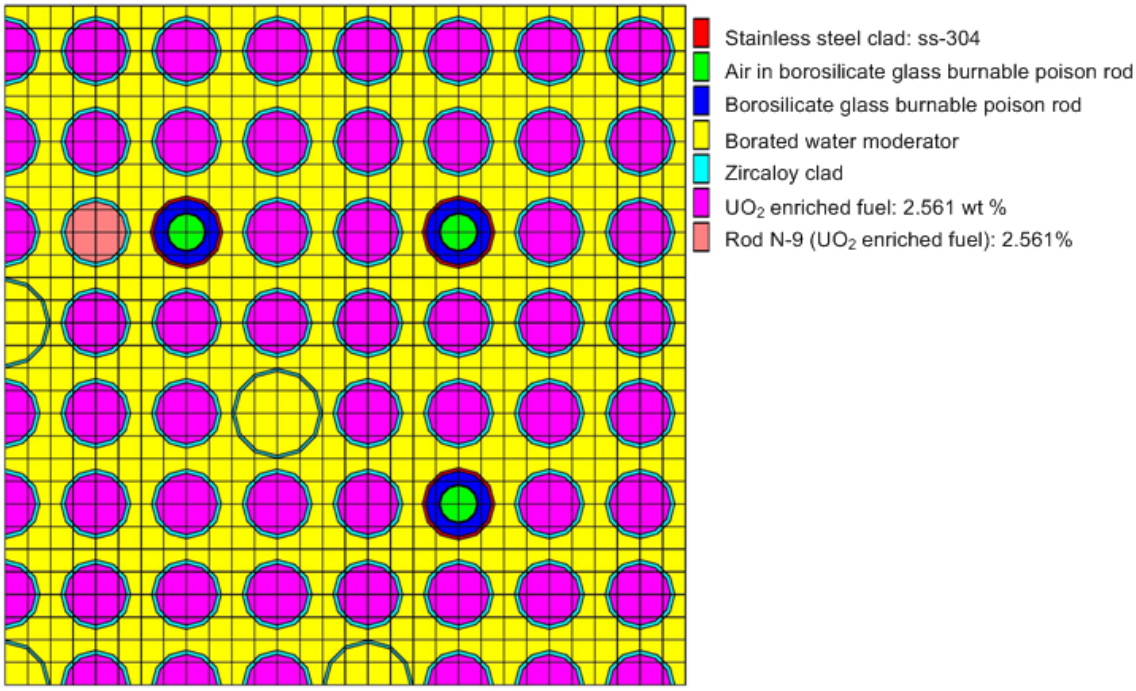

Figure 6-63. Model Layout with Grid Structure

The long-term depletion process will change the materials number densities significantly which will lead to large perturbations in the resonance self-shielded microscopic multigroup cross sections. Considering that both materials densities and cross sections will be changed during depletion, the input parameter space is particular large for this case study. However, the perturbations in input parameters are highly correlated as can be observed in Figure 6-64.

In Figure 6-64, the singular value spectrum of 100 flux variations is presented. One can observe that the spectrum of the singular values is decaying much faster than spectrum shown in Figure 6-46.

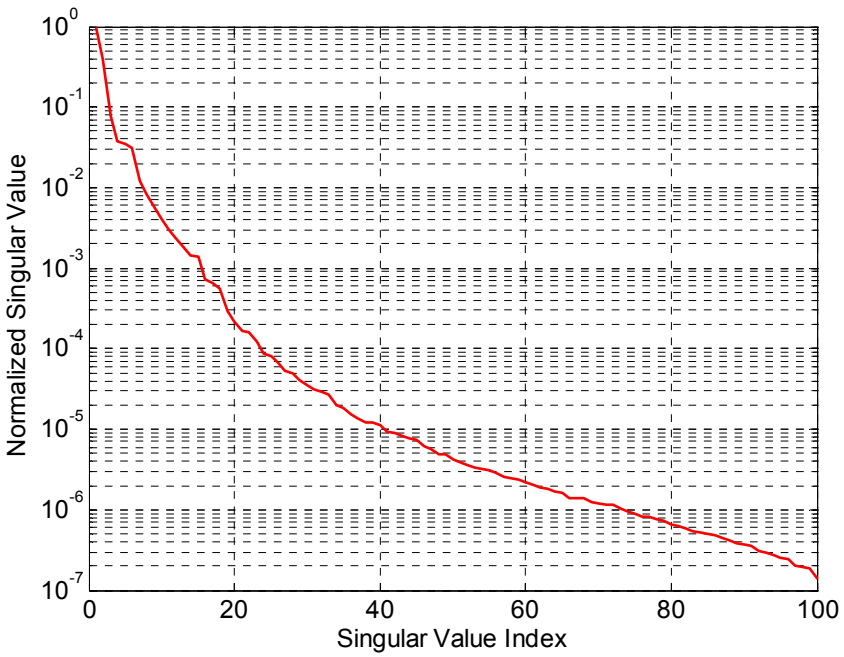

Figure 6-64. Singular Value Spectrum

The EPGPT is executed and is tested for a perturbed case, i.e. perturbed fuel compositions and the consequently generated perturbed microscopic multigroup cross sections. The exact values of perturbed neutron angular flux are calculated using NEWT forward. To study the performance of EPGPT for different sizes of the active subspace, the *rms* metric defined in Eq. (6.2.1) is employed. Figure 6-65 shows *rms* errors of neutron angular flux against the different sizes of the active subspace. As can be observed from

Figure 6-65, there is a significant discrepancy between the first-order E_PGPT and higher-order E_PGPT. Figure 6-65 indicates that first-order approaches, i.e., first-order GPT and first-order E_PGPT, will not provide reliable results for this case study, since non-linear effects generated by depletion will have a significant impact on the flux variations. However, higher-order E_PGPT will consistently provide very accurate approximation for neutron flux and eigenvalue as can be seen from Figure 6-65 and Figure 6-66.

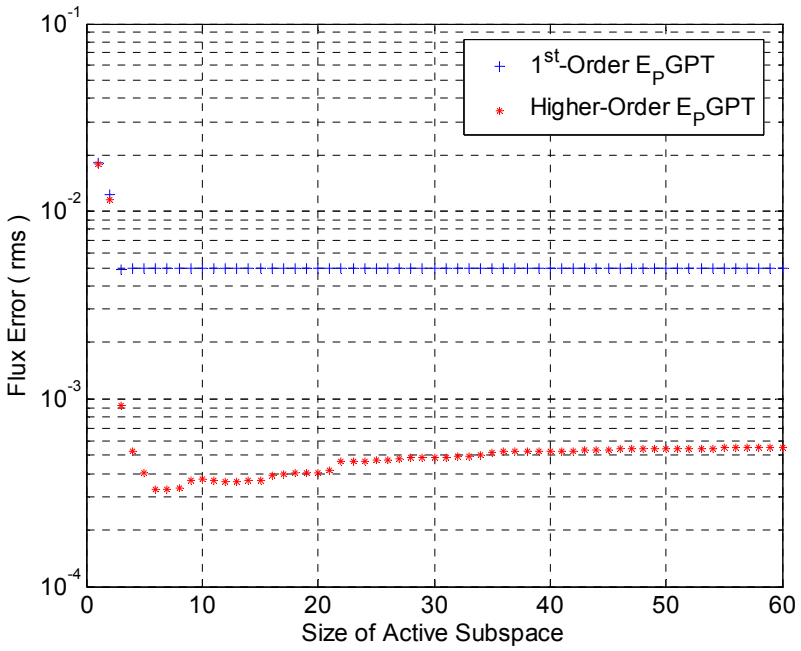

Figure 6-65. Analysis of E_PGPT Errors versus *r*

Figure 6-66 shows eigenvalue error, defined in Eq. (6.5.1), against the size of the active subspace. The exact variation in the eigenvalue is equal to 4398.97pcm (4.30%), the value obtained with only first-order term is 3612.88pcm (3.53%), and the value obtained by higher-

order E_PGPT with r = 60 is 4330.99pcm (4.23%). In this case, only 0.07% of reference eigenvalue cannot be captured by higher-order E_PGPT. For reference, the eigenvalue error calculated by first-order GPT is shown on the same graph as a horizontal line.

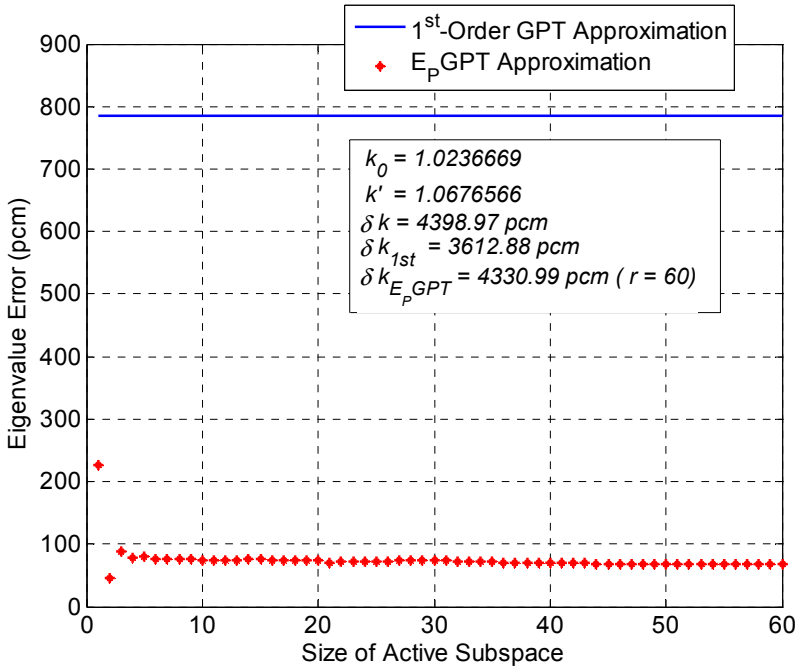

Figure 6-66. Eigenvalue Tolerance versus *r*

We have examined the accuracy for responses variations estimated by using the E_PGPT in Figure 6-68, Figure 6-69 and Figure 6-70. For comparison, the exact variations in these responses are calculated by NEWT forward, and Figure 6-67 shows the 44 responses values at the reference condition against neutron lethargy. In addition, the responses are defined in Eq. (6.5.3), and the discrepancies are defined in Eq. (6.5.4). As known to all, depletion will change materials compositions significantly which will introduce non-linear behaviors into

the model. These non-linear effects can be observed in neutron thermal range in Figure 6-69, which will make first-order approximation inaccurate. However, higher-order E_PGPT consistently provides accurate estimations for user-defined responses as can be observed in Figure 6-68, Figure 6-69 and Figure 6-70.

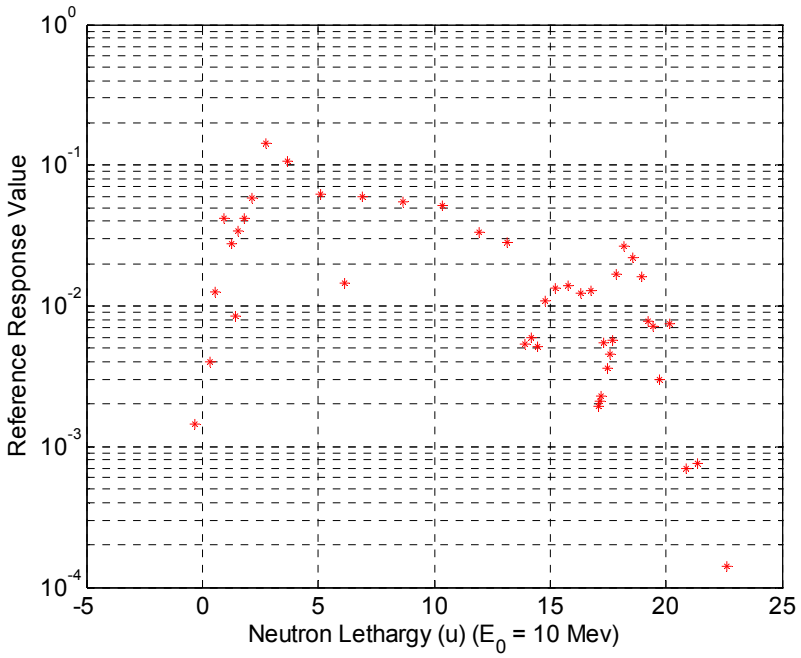

Figure 6-67. Reference Response Values

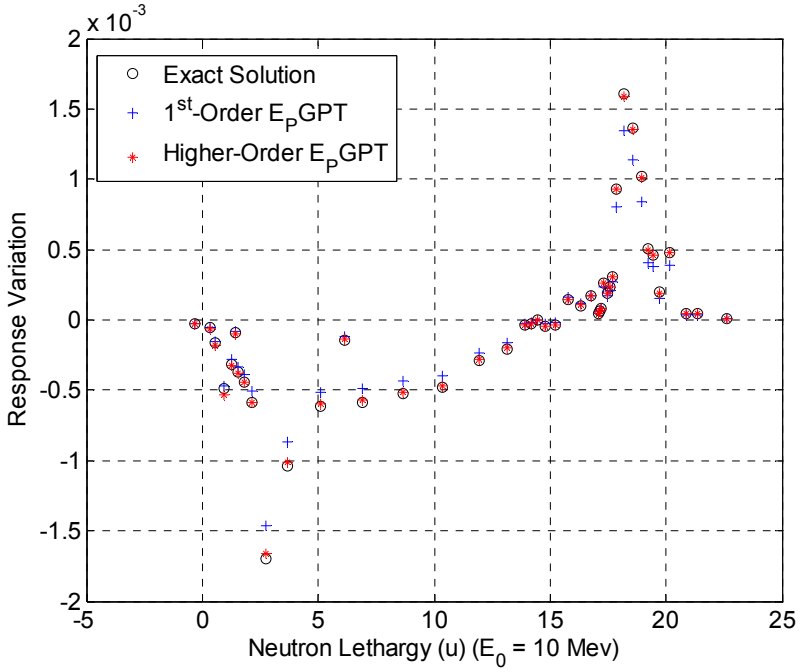

Figure 6-68. Estimation of Response Variations (*r* = 60)

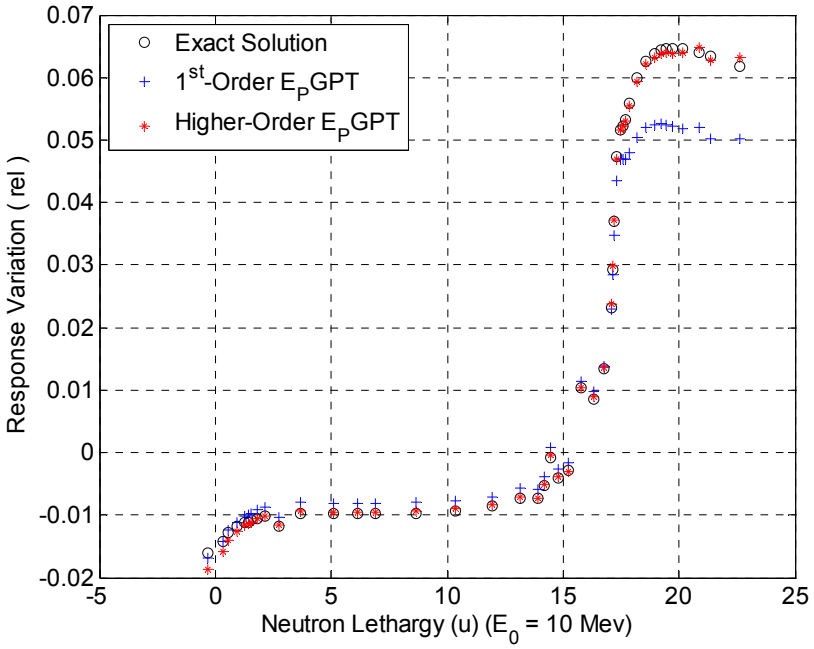

Figure 6-69. Estimation of Response Variations (*r* = 60)

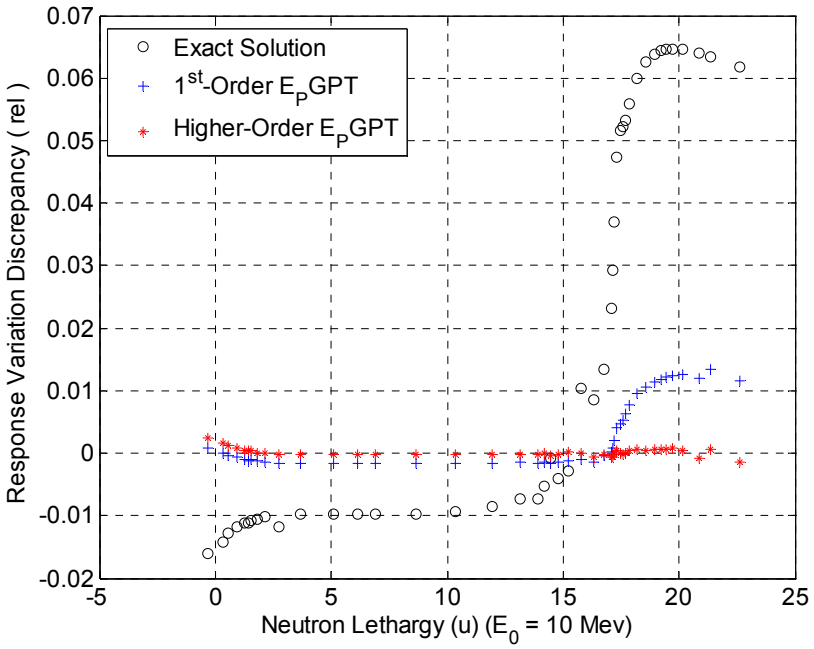

Figure 6-70. Comparison of Response Estimation Accuracy (r = 60)

Moreover, the estimation accuracy is examined by using 25 test samples (i.e., t = 25). As can be seen in Figure 6-71, the higher-order E_PGPT using 30 basis vectors can evaluate the k-eigenvalue (or k_{eff}) variation much more accurately than the first-order GPT approximation. Figure 6-72 shows the *rms* error defined in Eq. (6.2.1) for all 30 test samples. The active subspace for this case is much smaller than the one employed in case II study of section 6.5. This is because the fuel compositions perturbations and the self-shielded microscopic multigroup cross sections perturbations are highly correlated. Additionally, the results presented in Figure 6-71 and Figure 6-72 indicate that first-order perturbation theory will break down for depletion calculations.

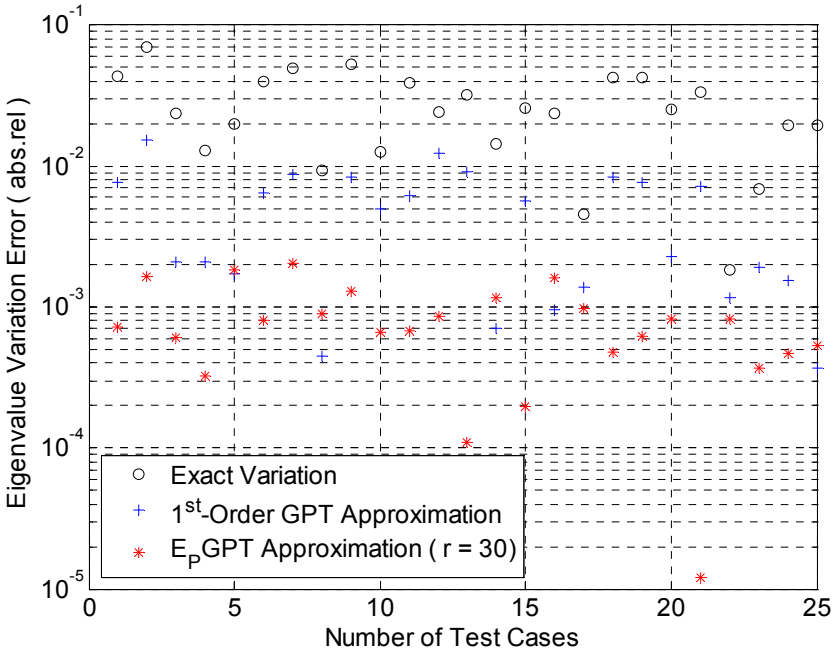

Figure 6-71. Comparison of Estimation Accuracy for Eigenvalue Variation (t = 25)

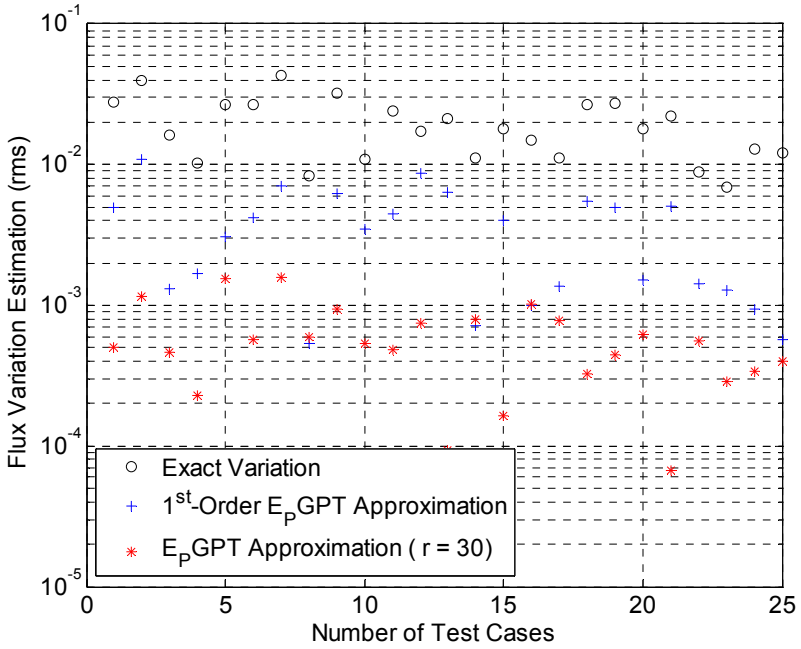

Figure 6-72. Analysis E_PGPT Errors for Angular Flux (t = 25)

CHAPTER 7. EPGPT FOR UNCERTAINTY QUANTIFICATION

7.1 Overview

Reactor design and safety calculations are computationally expensive due to the complexity of the associated physics models which are typically nonlinear and tightly or loosely coupled with many input parameters and output responses. The repeated execution of the various models is essential to completing uncertainty quantification where one is interested in propagating the uncertainties in the simulation to understand the impact on the macroscopic behavior of the system. We restrict our discussion here to uncertainties in the parameters which are the independent variables input to the models. For radiation transport, the most prominent input parameters are the nuclear cross sections which are experimentally evaluated and processed through several pre-processing codes before they are used in core design and safety calculations.

Mathematically, the prior parametric uncertainties are described by probability density functions (PDFs) which can be used to calculate the probability of finding the respective parameters in a given interval. The objective of uncertainty quantification (UQ) is to propagate the parameters PDFs throughout the physics model to determine the responses PDFs. Designers employ responses PDFs to identify the design and safety space. For example, in safety analysis, one needs to calculate the probability that a given response, say fuel temperature, exceeds a given value, e,g., melting point. The PDF for the maximum fuel temperature can be used to calculate this probability, often referred to as tail probability.

Determining tail probabilities represents one of the most difficult tasks in UQ. This is because the responses PDFs are often very different in shape from the parameters PDFs.

Given the need to estimate the responses PDFs, one must have the capability to execute the model as many times as needed to ensure the impact of all possible parameters perturbations is quantified and understood. Understanding the impact implies the ability to determine the key parameters that contribute the most to the propagating uncertainties. In the simplest case, where the model is linear with k parameters whose uncertainties are described by Gaussian distributions, one needs to execute the model k additional times to understand the impact of all parameters. As the model becomes nonlinear, one must take into account the interaction between the parameters which increases the number of possible parameters perturbations that must be considered. The situation becomes even more complex as the parameters increase in number. This follows as the number of possible parameters perturbations becomes exponentially dependent on the number of parameters, which is commonly referred to as the curse of dimensionality.

Therefore to enable UQ for a realistic nuclear engineering model, expected to have many parameters, one must devise a fast yet accurate capability to approximate the action of the forward model. Generalized perturbation theory (GPT) proved to provide such capability. GPT achieves that by solving the adjoint model, the mathematical dual of the forward model. The adjoint solution can be combined with the unperturbed forward solution to calculate first order of responses variations with respect to parameters perturbations (also known as first-order derivatives) without having to re-execute the forward model. The computational cost to

calculate the variations is trivial as it only involves the inner products between the adjoint and forward solutions. The result is all the derivatives of a given response with respect to all parameters. When more responses are required, one must execute the adjoint model again for every given response.

Over the past four decades, the GPT theory has been rigorously extended to describe the higher-order derivatives of responses. Unfortunately, as higher-order derivatives are sought, the computational cost becomes dependent either on the number of input parameters or the dimension of the space used to describe the forward solution, i.e., the flux solution, depending on the higher-order GPT approach employed. These challenges have limited the use of GPT to linear models and investigative studies only.

7.2 EPGPT for Uncertainty Quantification

The EPGPT is based on a hybrid methodology that combines both the forward and adjoint solutions to reduce the number of model executions and allows one calculate the higher orders of variations within user-defined accuracy. The computational cost is also inexpensive as it only involves simple inner products operations. This provides an enabling tool to analyze the impact of parameters perturbations on the responses variations as many times as needed.

In this dissertation, we assume the uncertainties in parameters α can be characterized by assigning a uniform distribution and/or Gaussian distribution with the same expectation

and variance. This is to illustrate the importance of the prior parameters PDF on the responses uncertainties.

An EPGPT-based UQ algorithm involves the following four steps:

1. Define the probability distributions describing the prior knowledge about the uncertain input parameters;

2. Use the distributions in step 1 to generate multiple samples of input parameters;

3. Use EPGPT to calculate the responses variations for each of the samples generated in step 2;

4. Perform statistical analysis, e.g., moments evaluations, tail probability, etc., for the responses of interest.

7.3 Preliminary Numerical Results

The main objective here is to show that the EPGPT can be extended to do uncertainty quantification when the responses variations are nonlinear and the input parameters are non-Gaussian. Moreover, the surrogate model constructed by EPGPT is able to predict the responses variations to the tolerance prescribed by the user. A simple model used in a previous case study is employed here for the demonstration.

Table 7-1 provides the cross sections for the model depicted in Figure 7-1.

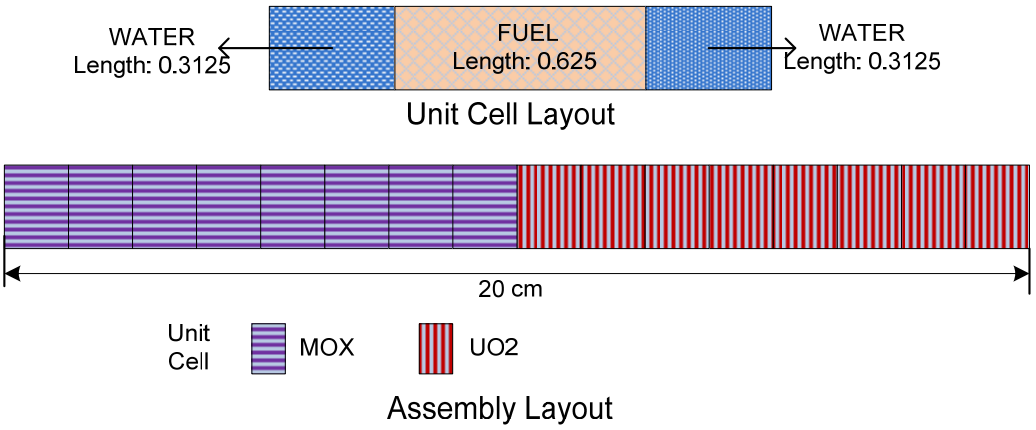

Figure 7-1. Model Layout

Table 7-1. Cross Section Data *

Materials	Input Parameters							
	Σ_t^1	$\Sigma_{s,0}^{1\to1}$	$\Sigma_{s,0}^{1\to2}$	χ^1	Σ_t^2	$\Sigma_{s,0}^{2\to2}$	Σ_f^2	ν_f^2
MOX	0.2	0.185	0.015	1	1.2	0.9	0.3	1.5
UO2	0.2	0.185	0.015	1	1.0	0.9	0.1	1.5
Water	0.2	0.17	0.03	0	1.1	1.1	0	0

* $\Sigma_f^1, \nu_f^1, \overline{\mu}_0^1, \Sigma_{s,0}^{2\to1}, \chi^2, \overline{\mu}_0^2$ are all zeros, and diffusion coefficient is defined as $D^g = \frac{1}{3\Sigma_{tr}^g}$, where $\Sigma_{tr}^g = \Sigma_t^g - \overline{\mu}_0^g \Sigma_s^g$ and g is the energy group index .

In this model, the flux has 256 dimensions representing 128 spatial nodes with equal spatial intervals and 2 energy groups per node. The first 128 values of ϕ denote the fast group flux, the last 128 values of ϕ denote the thermal group flux. The responses are the flux values evaluated everywhere in the space-energy phase space, i.e., $R_i = [\phi]_i$, for i = 1, …, 256.

First, the EPGPT-based algorithm is executed for the perturbed models such that cross sections perturbations, i.e., scattering, fission, and ν, were randomly selected from uniform distributions with 10% standard deviation relative to their reference values. The exact perturbed responses are calculated using direct forward perturbation (in brief, direct method) which requires the full forward model execution. To study the performance of EPGPT-based uncertainty quantification method for different sizes of the active subspace, Figure 7-2 and Figure 7-3 show the Mean (*rms*) and StDev (*rms*) error for responses variations against the size of active subspace, where the *rms* is defined as follows:

$$\text{Mean: } rms = \sqrt{\frac{1}{m}\sum_{i=1}^{m}\left(\frac{\mu\left(\Delta R_{i,\text{exact}}\right)-\mu\left(\Delta R_{i,\text{approx}}\right)}{\mu\left(\Delta R_{i,\text{exact}}\right)}\right)^2} \tag{7.3.1}$$

$$\text{StDev: } rms = \sqrt{\frac{1}{n}\sum_{i=1}^{n}\left(\frac{\sigma\left(\Delta R_{i,\text{exact}}\right)-\sigma\left(\Delta R_{i,\text{approx}}\right)}{\sigma\left(\Delta R_{i,\text{exact}}\right)}\right)^2} \tag{7.3.2}$$

where m is the total number of responses, μ and σ represent the mean value and standard derivation of the responses variations, respectively. We should emphasis here that the quantities defined in Eqs. (7.3.1) and (7.3.2), as one can recognize, are the 'residuals' between the proposed method and the direct method. To wit, all the results shown in (*rms*) can be viewed as the accuracy of the proposed method compared to the direct method.

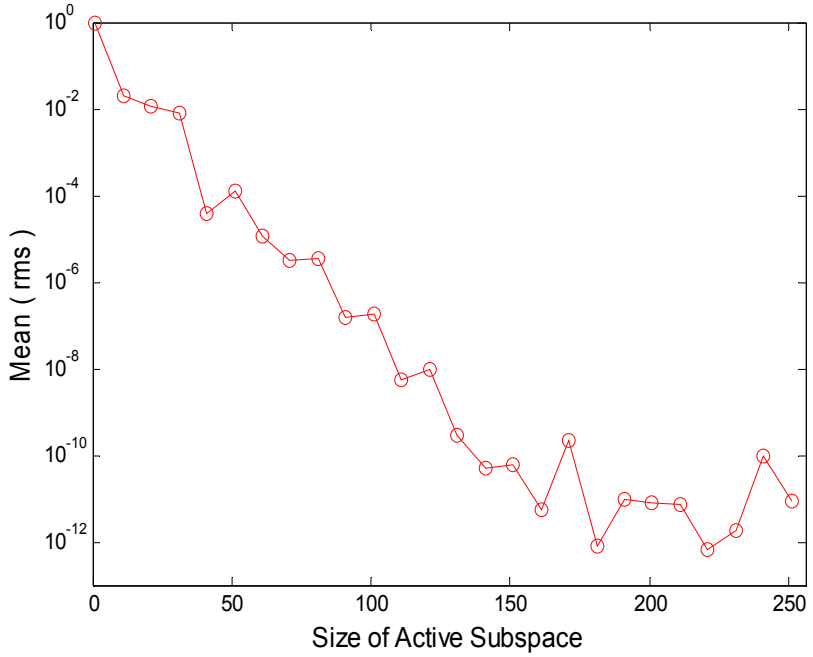

Figure 7-2. Analysis of E_PGPT Errors versus *r* (*with 100 Uniform Samples*)

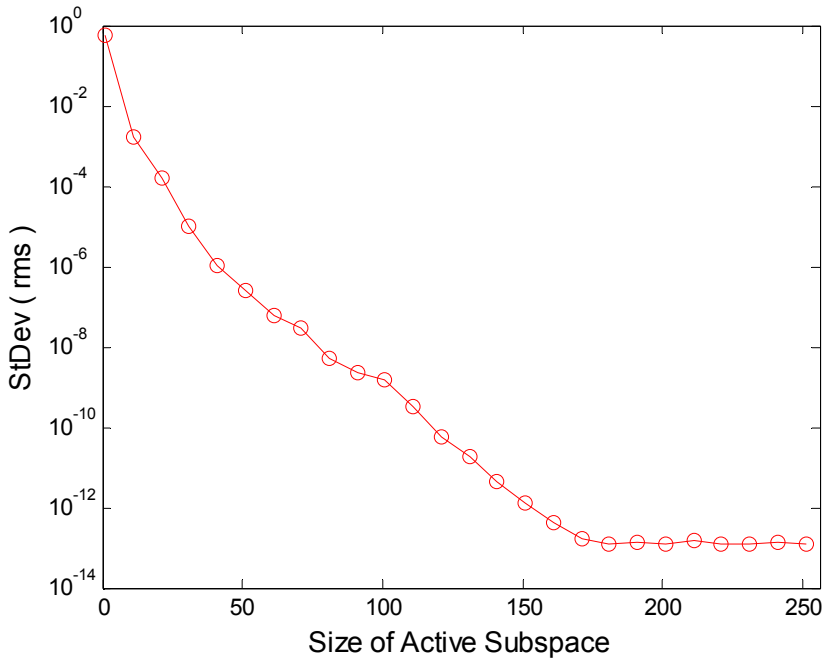

Figure 7-3. Analysis of E_PGPT Errors versus *r* (*with 100 Uniform Samples*)

Second, let us pick a user-defined error tolerance, say Mean: $rms = 10^{-4}$, we can determine the size of the active subspace r is around 50. Choose $r = 50$, and then we assume the uncertainties in the input parameters are characterized by uniform distribution with relative uncertainties within 10%. Table 7-2 shows the accuracy of EPGPT-based method. The relative eigenvalue variations distribution and the relative discrepancy of the eigenvalue variations distribution are shown in Figure 7-4. The results in Figure 7-4 demonstrate that the EPGPT-based method could predict the eigenvalue variations within user-defined tolerance, although there are large variations in the eigenvalue (maximum 20%). The relative output distributions at certain points in the space are shown in Figure 7-5 and Figure 7-6, where R_0 denotes the unperturbed response value, ΔR_{exact} and ΔR_{EpGPT} are the exact response variation calculated by the direct method and the evaluated response variation obtained by EPGPT algorithm, respectively. Although the distribution for the input is uniform, the distribution for the output is non-uniform and non-Gaussian.

Table 7-2. Accuracy of EPGPT-Based Method vs. the Number of Samples

Num. of Samples	100	1000	5000	10000
Mean (*rms*)	1.451e-05	7.656e-06	1.281e-05	6.326e-06
StDev (*rms*)	5.816e-07	4.016e-07	3.991e-07	3.908e-07

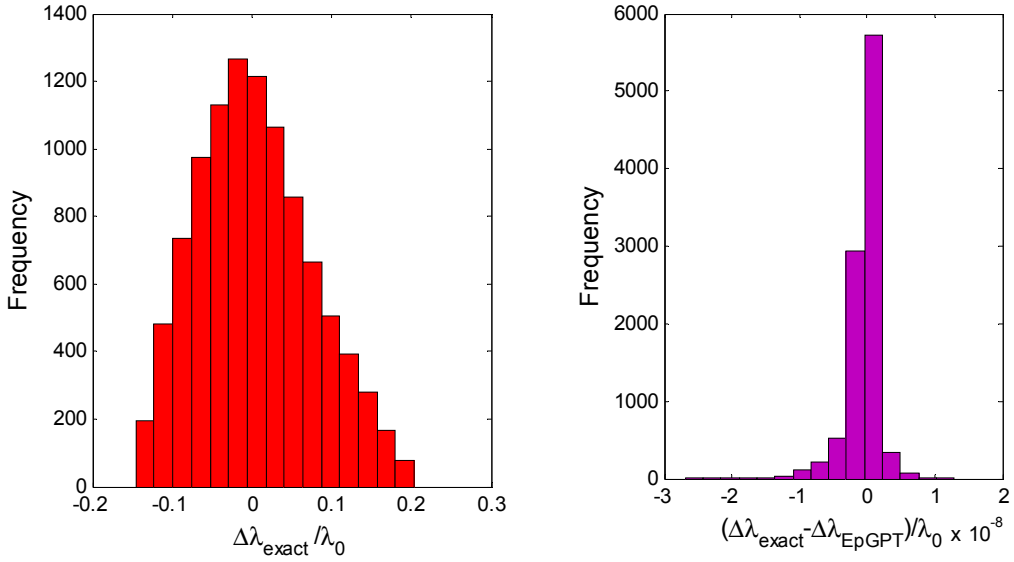

Figure 7-4. Relative Variations Distribution (Left) and Relative Discrepancy of Variations Distribution (Right) (*λ-Eigenvalue with 10000 Uniform Samples*)

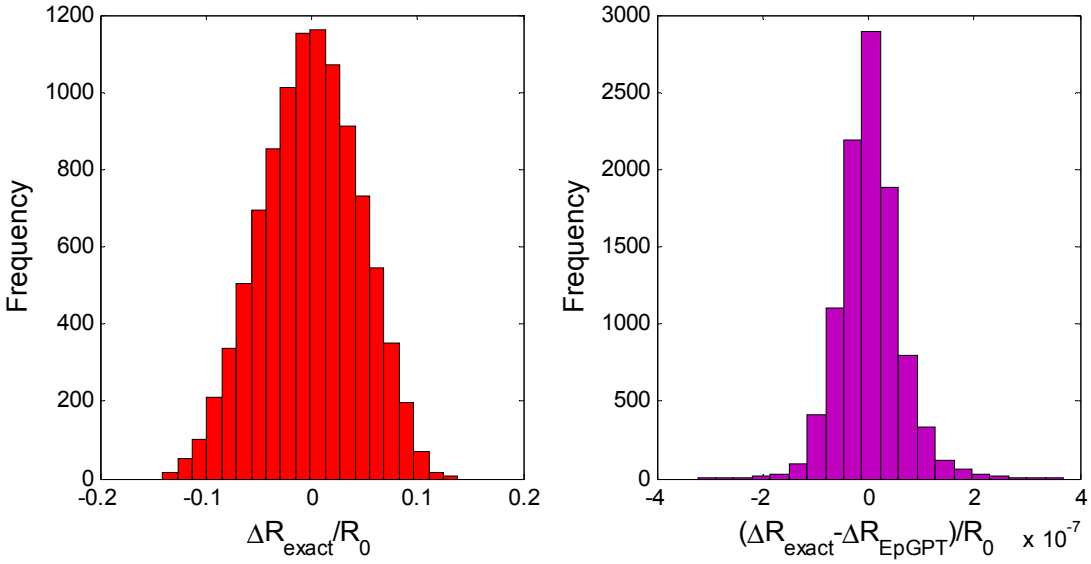

Figure 7-5. Relative Variations Distribution (Left) and Relative Discrepancy of Variations Distribution (Right) (*Response at Point 3.047cm in Group 1 with 10000 Uniform Samples*)

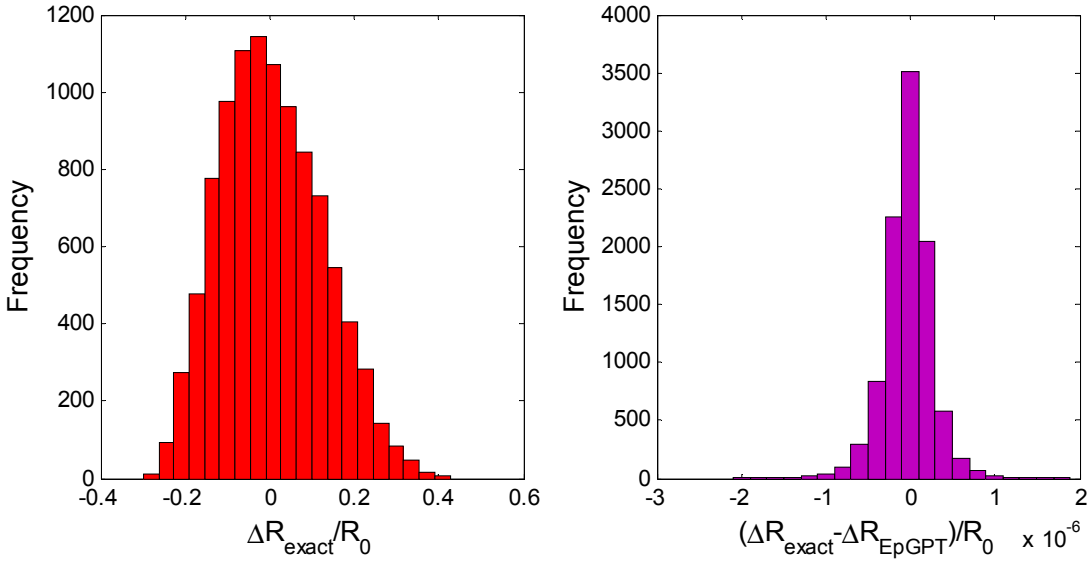

Figure 7-6. Relative Variations Distribution (Left) and Relative Discrepancy of Variations Distribution (Right) (*Response at Point 3.047cm in Group 2 with 10000 Uniform Samples*)

Third, to demonstrate the nonlinearity of the model, Gaussian distributions for the input parameters are employed with the same expectations and standard derivations as the uniform distribution employed in the first test case. Table 7-3, Figure 7-7, Figure 7-8 and Figure 7-9 show the similar results as before. If the model is linear, the relative response variations are expected to follow a Gaussian distribution which is not the case for the thermal flux shown in Figure 7-9. Simple inspection of Figure 7-6 and Figure 7-9 show that the two distributions are quite different especially at the tails, which are particularly important for safety related calculations.

Table 7-3. Accuracy of EpGPT-Based Method vs. the Number of Samples

Num. of Samples	100	1000	5000	10000
Mean (*rms*)	6.169e-05	3.093e-05	5.084e-06	5.452e-06
StDev (*rms*)	5.527e-07	5.914e-07	5.563e-07	6.081e-07

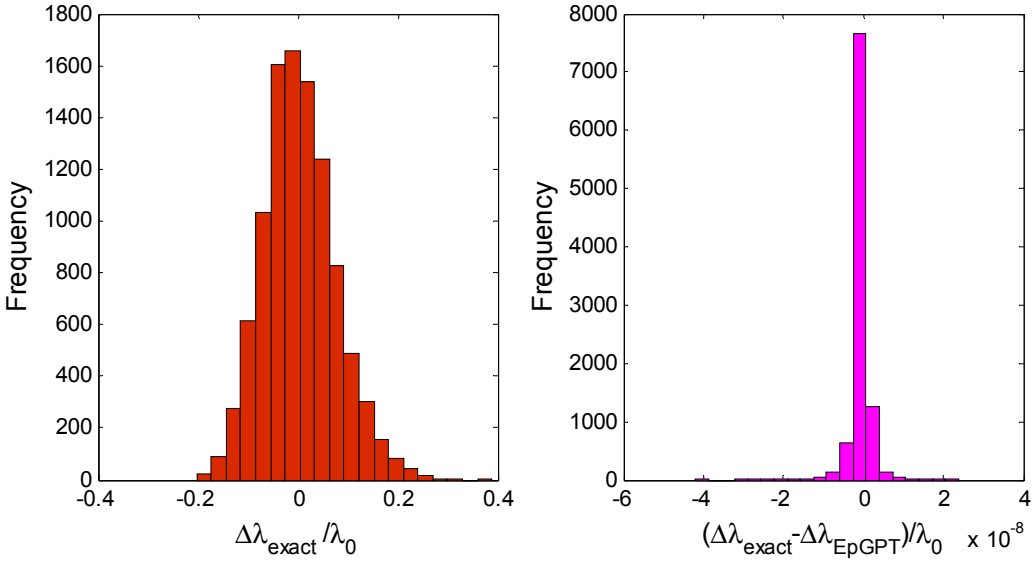

Figure 7-7. Relative Variations Distribution (Left) and Relative Discrepancy of Variations Distribution (Right) (*λ-Eigenvalue with 10000 Gaussian Samples*)

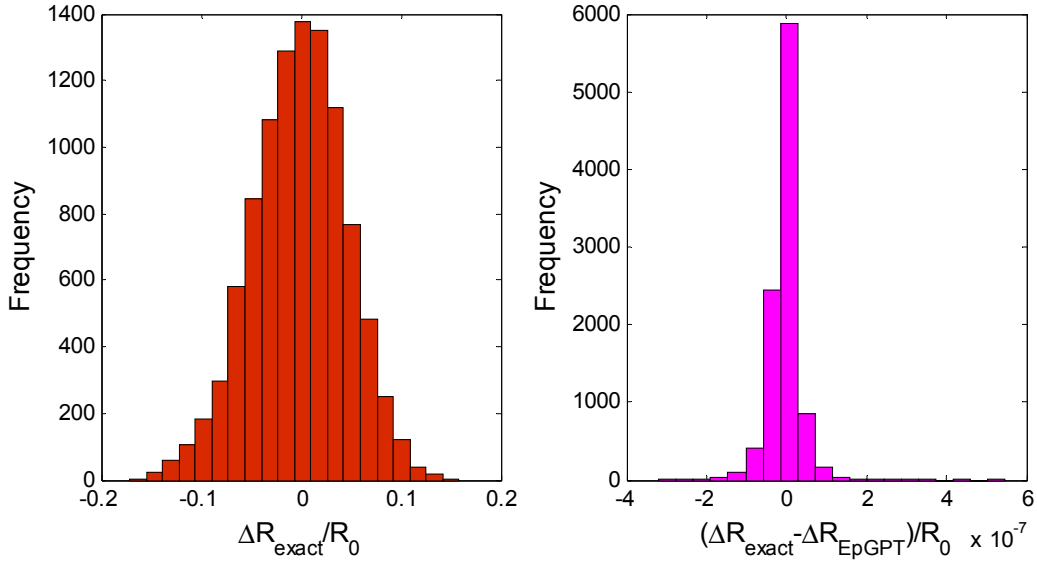

Figure 7-8. Relative Variations Distribution (Left) and Relative Discrepancy of Variations Distribution (Right) (*Response at Point 3.047cm in Group 1 with 10000 Gaussian Samples*)

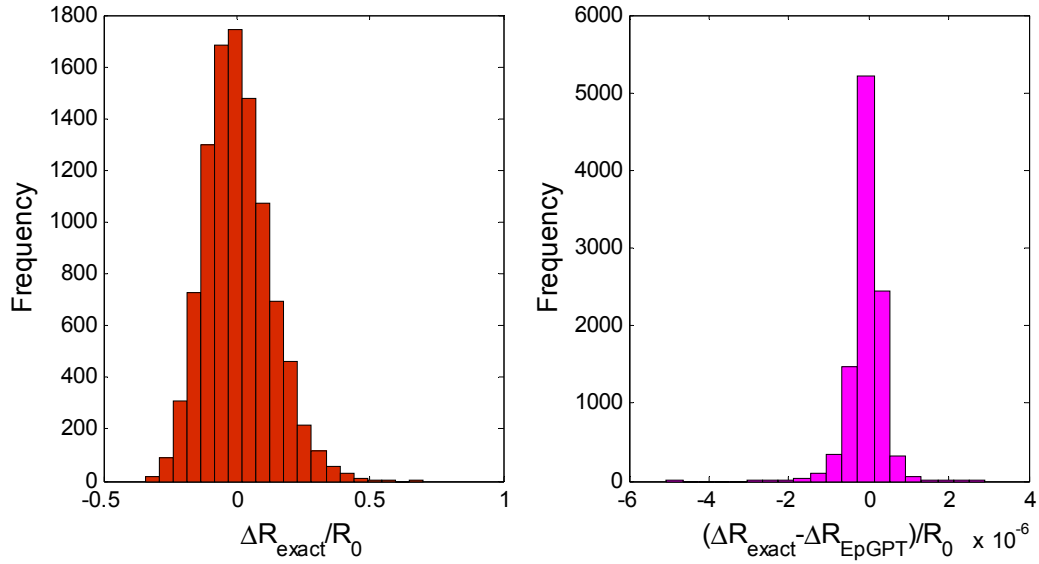

Figure 7-9. Relative Variations Distribution (Left) and Relative Discrepancy of Variations Distribution (Right) (*Response at Point 3.047cm in Group 2 with 10000 Gaussian Samples*)

CHAPTER 8. CONCLUSIONS AND FUTURE WORK

8.1 Conclusions

Generalized perturbation theory is well developed for nuclear reactor design and analysis during the last fifty years. Moreover, it has been successfully applied to reactor critical eigenvalue calculations, depletion calculations, shielding design, kinetics problems, and sensitivity analysis and uncertainty quantification. The most common implementation of GPT estimates the first order of variations for a given response with respect to input parameters perturbations. The first-order GPT has found its way into standardized computer package SCALE 6.1 (RSICC 2011) developed by Oak Ridge National Laboratory (ORNL). In performing reactor analysis and design calculations, first-order GPT can significantly reduce the computational cost through bypassing the repeated executions of forward calculations, which is facilitated via adjoint calculations. Although very efficient, the accuracy is degraded when the parameters are outside the range that renders linear approximation acceptable, e.g., control rod/burnable poison rod insertions, fuel rod burnup, and fuel lattice shuffling. Higher-order GPT has been well developed in theory. Unfortunately, as higher-order derivatives are sought, the computational cost, e.g. the total number of model simulations involving forward and/or adjoint simulations, becomes dependent either on the number of input parameters or the dimension of the space used to describe the forward solution depending on the higher-order GPT approach employed. In this

dissertation, this difficulty in computational cost is properly addressed by E_PGPT via the reduced basis technique.

The objective of the reduced basis technique is to achieve significant computational reduction and improvement in computational performances whenever one is interested in real-time simulation and/or repeated output evaluations for sensitivity analysis and uncertainty quantification. The fundamental idea of the reduced basis technique employed in this dissertation is to represent the state variations using a linear combination of basis vectors spanning the reduced basis space for the high-dimensional input parameters space. The 'snapshots' of forward model simulations corresponding to input parameters perturbations is used to identify the reduced basis space, i.e., the Lagrange reduced basis spaces. To date, the essential approach utilized to explore the best basis functions for the reduced basis space is proper orthogonal decomposition (POD) of snapshots. The basic premise behind POD of snapshots is that the variability of the state can be well approximated by a subspace which may be spanned by the reduced basis. This characteristic can be observed in all the case studies in this dissertation. Furthermore, this kind of basis vectors can be pre-computed and stored for real-time simulations and sensitivity analysis and uncertainty quantification calculations. In this case, the computational cost for higher-order E_PGPT becomes only dependent on the size of the active subspace rather than the original state space or input parameter space. This idea has led to tremendous saving in computational overhead especially for complex large-scale problems where a detailed description of the state must be calculated.

Another limitation of first-order GPT is the difficulty in tackling multi-responses or distributed responses, e.g., few-group cross sections generated by the lattice calculations for full-core simulations, and space-dependent power density in lattice or reactor core calculations. This is because a separate adjoint model simulation is required for each response of interest which can lead to significant computational cost. Traditionally, one can adopt multi-modal approach or use coarse region averaged responses. However, both methods are limited to linear approximation of responses of interest, and furthermore the applicability of multi-modal approach is limited to problem with smooth distributed responses only. This issue could be well addressed by E_PGPT based on the premise that the state variations lie in a small size of active subspace. Moreover, if the response functions are smooth or one is only interest in small perturbations of input parameters, one can employ only first-order E_PGPT to efficiently and accurately calculate the variations in the responses of interest. Of course, higher-order E_PGPT has also been demonstrated by numerical studies to capture both linear and non-linear behaviors of responses of interest.

Thus far, the challenges in the current GPT approach have been properly overcome in this dissertation such that E_PGPT proves to be practical for the realistic reactor calculations. In this dissertation, an efficient computational algorithm has been also proposed to address the explosion in dimensionality whether at the input parameter level or at the response level.

Another distinct characteristic of E_PGPT is the capability to establish a rigorous *a posteriori* upper error bound to describe the accuracy of the responses variations as they compare to exact responses variations calculated using direct forward model perturbations.

Moreover, different error bounds for different responses could also be defined by the user depending on the design specifications. This is achieved by employing range-finding algorithm with only a small number of oversampling to identify the active subspace for EPGPT.

And furthermore, the EPGPT consists of two phases: (1) the *pre-computation phase* involving all necessary forward and adjoint model executions to identify the active subspace and establish a rigorous *a posteriori* upper error bound; (2) the *evaluation phase* calculates the exact variation in the response using only inner products operations which are computationally inexpensive compared to the execution cost of forward and adjoint models.

In conclusion, the essential ingredients of EPGPT method are: (*i*) GPT formalism employed for the response variation calculations with high efficiency; (*ii*) reduced basis technique, in particular, POD of snapshots enabling to generate the best basis functions; and (*iii*) a rigorous *a posteriori* error estimator used for both the basis selection and the certification of the solution. Moreover, the combination of these three factors yields substantial computational savings which are at the basis of an efficient model order reduction, ideally suited for SA/UQ, system optimization and real-time simulation. Moreover, the *posteriori* error estimator is essential to guarantee efficiency, reliability, and accuracy. They allow us to explore efficiently the parameter spaces in search of most representative basis functions, and to identify active subspace. To some extent, EPGPT has extended the applicability of generalized perturbation theory to calculate with quantifiable accuracy the exact variations in models with many responses and many parameters.

8.2 Future Work Recommendations

Although we are focusing only on the derivation of the EPGPT for neutron diffusion and/or transport theory and demonstrating the applicability for the reactor physics calculations, the proposed methods and algorithms can be readily extended to other nuclear reactor problems or even further to other engineering problems. First of all, one can employ EPGPT to efficiently and accurately (accounting for higher orders of variations) replace the lattice calculations, currently executed using transport models. In practice, the lattice calculations must be executed for a range of different conditions to account for neutronics and thermal-hydraulics conditions. One could treat all types of changes in all assemblies as the input parameters perturbations, apply the range-finding algorithm to identify the active subspace, and then employ the EPGPT to accurately evaluate the few group constants. By employing EPGPT, the cost of these lattice calculations could be minimized. Second, the first-order EPGPT can be readily applied into sensitivity analysis and uncertainty quantification, since one could obtain the explicit form for neutron flux variations. To wit,

$$\textbf{Source-driven problem}:\ \Delta\phi\big|_{1st}=\sum_{i=1}^{r}\left(\beta_i(\Delta\alpha)\big|_{1st}\right)q_i=-\sum_{i=1}^{r}\left\langle\Gamma_i^*,\left(\Delta\mathbf{P}\phi-\Delta q_{\text{ex}}\right)\right\rangle q_i$$

$$\textbf{Eigenvalue problem}:\ \Delta\phi\big|_{1st}=\sum_{i=1}^{r}\left(\beta_i(\Delta\alpha)\big|_{1st}\right)q_i=-\sum_{i=1}^{r}\left\langle\Gamma_i^*,\Delta\mathbf{P}\phi\right\rangle q_i$$

Thus, one can calculate the first-order derivatives of the neutron flux with respect to input parameter α :

$$\textbf{Source-driven problem}:\ \frac{\partial\phi}{\partial\alpha}=-\sum_{i=1}^{r}\left\langle\Gamma_i^*,\left(\frac{\partial\mathbf{P}}{\partial\alpha}\phi-\frac{\partial q_{\text{ex}}}{\partial\alpha}\right)\right\rangle q_i$$

$$\textbf{Eigenvalue problem}: \frac{\partial \phi}{\partial \alpha} = -\sum_{i=1}^{r} \left\langle \Gamma_i^*, \frac{\partial \mathbf{P}}{\partial \alpha} \phi \right\rangle q_i$$

Considering the response defined in Eq. (2.5.1), one can calculate the sensitivity coefficients by

$$\frac{\alpha}{R}\frac{\partial R}{\partial \alpha} = \frac{\alpha}{R}\left\langle \frac{\partial \Sigma_d}{\partial \alpha}, \phi \right\rangle + \frac{\alpha}{R}\left\langle \Sigma_d, \frac{\partial \phi}{\partial \alpha} \right\rangle$$

The first term in the RHS denoted as the direct term which can be readily calculated, while the second term in the RHS could be rewritten as:

$$\textbf{Source-driven problem}: \begin{aligned} \frac{\alpha}{R}\left\langle \Sigma_d, \frac{\partial \phi}{\partial \alpha} \right\rangle &= \frac{\alpha}{R}\left\langle \Sigma_d, \left(-\sum_{i=1}^{r} \left\langle \Gamma_i^*, \left(\frac{\partial \mathbf{P}}{\partial \alpha}\phi - \frac{\partial q_{\text{ex}}}{\partial \alpha} \right) \right\rangle q_i \right) \right\rangle \\ &= -\frac{\alpha}{R}\sum_{i=1}^{r} \left\langle \Gamma_i^*, \left(\frac{\partial \mathbf{P}}{\partial \alpha}\phi - \frac{\partial q_{\text{ex}}}{\partial \alpha} \right) \right\rangle \langle \Sigma_d, q_i \rangle \end{aligned}$$

or

$$\textbf{Eigenvalue problem}: \begin{aligned} \frac{\alpha}{R}\left\langle \Sigma_d, \frac{\partial \phi}{\partial \alpha} \right\rangle &= \frac{\alpha}{R}\left\langle \Sigma_d, \left(-\sum_{i=1}^{r} \left\langle \Gamma_i^*, \left(\frac{\partial \mathbf{P}}{\partial \alpha}\phi \right) \right\rangle q_i \right) \right\rangle \\ &= -\frac{\alpha}{R}\sum_{i=1}^{r} \left\langle \Gamma_i^*, \frac{\partial \mathbf{P}}{\partial \alpha}\phi \right\rangle \langle \Sigma_d, q_i \rangle \end{aligned}$$

Considering that SCALE has the ability to calculate the inner product $\left\langle \Gamma^*, \frac{\partial \mathbf{P}}{\partial \alpha}\phi \right\rangle$ in SAMS module, this idea can be readily implemented into SCALE. Near term goals include implementing first-order EPGPT and higher-order EPGPT into SCALE, examining larger spatial region at full core level, demonstrating the convergence for eigenvalue iterative method, and understanding the errors for depletion problems. Long-term goal is to extend EPGPT for fuel loading pattern optimization.

REFERENCES

Abdel-Khalik, H.S. 2012, "Adjoint-based sensitivity analysis for multi-component models", *Nuclear Engineering and Design,* vol. 245, pp. 49-54.

Abdel-Khalik, H.S., Bang, Y. & Wang, C. 2013, "Overview of hybrid subspace methods for uncertainty quantification, sensitivity analysis", *Annals of Nuclear Energy,* vol. 52, pp. 28-46.

Abdel-Khalik, H.S. 2004, *Adaptive core simulation*, PhD Dissertation, North Carolina State University.

Almroth, B.O., Brogan, F.A. & Stern, P. 1978, "Automatic choice of global shape functions in structural analysis", *AIAA Journal,* vol. 16, pp. 525-528.

Anistratov, D.Y. 2005, "Consistent spatial approximation of the low-order quasi-diffusion equations on coarse grids", *Nuclear Science and Engineering,* vol. 149, no. 2, pp. 138-161.

ArfKen, G. 1985, *Mathematical methods for physicists*, 3rd edn, Academic Press, Orlando, FL.

Ball, M.R. 2012, *Uncertainty analysis in lattice reactor physics calculations*, McMaster University Library.

Bang, Y. 2012, *Hybrid reduced order modeling algorithms for reactor physics calculations*, North Carolina State University.

Bang, Y., Abdel-Khalik, H.S. & Hite, J.M. 2012, "Hybrid reduced order modeling applied to nonlinear models", *International Journal for Numerical Methods in Engineering,* vol. 91, no. 9, pp. 929-949.

Bashir, O., Willcox, K., Ghattas, O., van Bloemen Waanders, B. & Hill, J. 2008, "Hessian-based model reduction for large-scale systems with initial-condition inputs", *International Journal for Numerical Methods in Engineering,* vol. 73, no. 6, pp. 844-868.

Bell, G.I. 1979, *Nuclear reactor theory,* R. E. Krieger Pub. Co., Huntington, N. Y.

Bui-Thanh, T., Damodaran, M. & Willcox, K. 2003, "Proper orthogonal decomposition extensions for parametric applications in transonic aerodynamics", *Proceedings of the 15th AIAA Computational Fluid Dynamics Conference*, pp. 4213.

Bui-Thanh, T., Willcox, K. & Ghattas, O. 2008, "Model reduction for large-scale systems with high-dimensional parametric input space", *SIAM Journal on Scientific Computing,* vol. 30, no. 6, pp. 3270-3288.

Cacuci, D.G. 2003, *Sensitivity and uncertainty analysis: theory,* CRC Press.

Cacuci, D.G. 1981a, "Sensitivity theory for nonlinear systems. I. Nonlinear functional analysis approach", *Journal of Mathematical Physics,* vol. 22, no. 12, pp. 2794.

Cacuci, D.G. 1981b, "Sensitivity theory for nonlinear systems. II. Extensions to additional classes of responses", *Journal of Mathematical Physics,* vol. 22, no. 12, pp. 2803.

Cacuci, D.G., Weber, C.F., Oblow , E.M. & Marable, J.H. 1980, "Sensitivity theory for general systems of nonlinear equations", *Nuclear Science and Engineering,* vol. 75, pp. 88.

Cacuci, D.G., Ionescu-Bujor, M. & Navon, I.M. 2005, *Sensitivity and uncertainty analysis, Volume II: applications to large-scale systems,* CRC.

Carlberg, K., Bou-Mosleh, C. & Farhat, C. 2011, "Efficient non-linear model reduction via a least-squares Petrov-Galerkin projection and compressive tensor approximations", *International Journal for Numerical Methods in Engineering,* vol. 86, no. 2, pp. 155-181.

Chaturantabut, S. & Sorensen, D.C. 2010, "Nonlinear model reduction via discrete empirical interpolation", *SIAM Journal on Scientific Computing,* vol. 32, no. 5, pp. 2737-2764.

Dubi, A. & Dudziak, D. 1981, *Higher-order terms in sensitivity analysis through a differential approach*, LA-8813-MS, Los Alamos National Laboratory.

Duderstadt, J.J. & Hamilton, L.J. 1976, *Nuclear reactor analysis*, John Wiley and Sons, Inc., New York.

Fink, P.J. & Rheinboldt, W.C. 1985, "Local error estimates for parametrized nonlinear equations", *SIAM journal on numerical analysis,* vol. 22, no. 4, pp. 729-735.

Galbally, D., Fidkowski, K., Willcox, K. & Ghattas, O. 2010, "Non-linear model reduction for uncertainty quantification in large-scale inverse problems", *Int.J.Numer.Meth.Engng.,* vol. 81, no. 12, pp. 1581-1608.

Ganapathysubramanian, B. & Zabaras, N. 2007, "Sparse grid collocation schemes for stochastic natural convection problems", *Journal of Computational Physics,* vol. 225, no. 1, pp. 652-685.

Gandini, A. 2001, "HGPT based sensitivity time-dependent methods for the analysis of subcritical systems", *Annals of Nuclear Energy,* vol. 28, pp. 1193.

Gandini, A. 1990, "Importance & sensitivity in assessing system reliability", *IEEE Transactions on Reliability,* vol. 39, pp. 61.

Gandini, A. 1988, *Uncertainty analysis and experimental data transposition methods based on perturbation theory In uncertainty analysis,* Y. Ronen Ed., CRC Press, Boca Taton.

Gandini, A. 1981, "Generalized perturbation theory (GPT) for nonlinear systems from the Importance conservation Principle", *Nuclear Science and Engineering,* vol. 77, pp. 316.

Gandini, A. 1978a, "Higher order time-dependent generalized perturbation theory", *Nuclear Science and Engineering,* vol. 67, pp. 91.

Gandini, A. 1978b, "Implicit and explicit higher order perturbation methods for nuclear reactor analysis", *Nuclear Science and Engineering,* vol. 67, pp. 347.

Gandini, A. 1967, "A generalized perturbation method for bilinear functionals of the real and adjoint neutron fluxes", *Journal of Nuclear Energy,* vol. 21, pp. 755.

Georgiou, I.T. & Schwartz, I.B. 1999, "Dynamics of large scale coupled structural/mechanical systems: A singular perturbation/proper orthogonal decomposition approach", *SIAM Journal on Applied Mathematics,* vol. 59, no. 4, pp. 1178-1207.

Gheorghiu, H.N.M. & Rahnema, F. 1998, "Variational principles for steady-state neutron flux functionals", *Transport theory and statistical physics,* vol. 27, no. 1, pp. 67-95.

Golub, G.H. & Van Loan, C.F. 1996, *Matrix computations,* Johns Hopkins University Press.

Greenspan, E. 1975, *Nuclear Science and Engineering,* vol. 57, pp. 250.

Greenspan, E. & Gilai, D. 1978, "Second-order generalized perturbation theory for source-driven systems", *Nuclear Science and Engineering,* vol. 68, pp. 1.

Greenspan, E., Kami, Y. & Gilai, D. 1979, *Higher order effects in cross-section sensitivity analysis*, Oak Ridge National Laboratory.

Halko, N., Martinsson, P.G. & Tropp, J.A. 2011, "Finding structure with randomness: probabilistic algorithms for constructing approximate matrix decompositions", *Journal of Society for Industrial and Applied Mathematics,* vol. 53, no. 2, pp. 217-288.

Holmes, P., Lumley, J.L. & Berkooz, G. 1996, *Turbulence, coherent structures, dynamical systems and symmetry,* Cambridge University Press, Cambridge, NY.

Ito, K. & Ravindran, S.S. 1998, "A reduced-order method for simulation and control of fluid flows", *Journal of computational physics,* vol. 143, no. 2, pp. 403-425.

Ivanov, K., Avramova, M., Kodeli, I. & Sartori, E. 2007, *Benchmark for Uncertainty Analysis in Modelling (UAM) for Design, Operation and Safety Analysis of LWRs, Specification and Support Data for the Neutronics Cases (Phase I),* NEA/NSC/DOC(2007)23.

Jessee, M.A., Williams, M.D. & Dehart, M.D. 2009, "Development of generalized perturbation theory capability within the scale code package", *International Conference on Mathematics*Saratoga Springs, NY.

Jessee, M.A. 2008, *Cross-section adjustment techniques for BWR adaptive simulation*, North Carolina State University.

Jessee, M.A. & Dehart, M.D. 2011, "NEWT: A new transport algorithm for two-dimensional discrete-ordinates analysis in non-orthogonal geometries" in *Scale: A comprehensive modeling and simulation suite for nuclear safety analysis and design*, ORNL/TM-2005/39, Version 6.1, Available from Radiation Safety Information Computational Center at Oak Ridge National Laboratory as CCC-785, Oak Ridge, TN, pp. 2783-2913.

Kappagantu, R.V. & Feeny, B.F. 2000, "Part 2: Proper orthogonal modal modeling of a frictionally excited beam", *Nonlinear Dynamics,* vol. 23, no. 1, pp. 1-11.

Kerschen, G., Golinval, J., Vakakis, A.F. & Bergman, L.A. 2005, "The method of proper orthogonal decomposition for dynamical characterization and order reduction of mechanical systems: an overview", *Nonlinear Dynamics,* vol. 41, no. 1, pp. 147-169.

Kropaczek, D.J. & Turinsky, P.J. 1991, "In-core nuclear fuel management optimization for pressurized water reactors utilizing simulated annealing", *Nuclear Technology,* vol. 95, pp. 9.

Lewins, J.D. 1965, *Importance, the Adjoint Function; the Physical Basis of Variational and Perturbation Theory in Transport and Diffusion Problems,* Pergamon, Oxford.

Lewis, E.E., Smith, M.A., Tsoulfanidis, N., Palmiotti, G., Taiwo, T.A. & Blomquist, R.N. 2001, *Benchmark specification for deterministic 2-D/3-D MOX fuel assembly transport calculations without spatial homogenization (C5G7 MOX),* OECD/NEA document, NEA/NSC/DOC(2001)4.

Liang, Y.C., Lee, H.P., Lim, S.P., Lin, W.Z., Lee, K.H. & Wu, C.G. 2002, "Proper orthogonal decomposition and its applications--part I: theory", *Journal of Sound and Vibration,* vol. 252, no. 3, pp. 527-544.

Lumley, J.L. 1970, *Stochastic tools in turbulence, vol. 12 of Applied Mathematics and Mechanics*, Academic Press, New York.

Maldonado, G.I. & Turinsky, P.J. 1995, "Application of nonlinear nodal diffusion generalized perturbation theory to nuclear fuel reload optimization", *Nuclear Technology,* vol. 110, pp. 198.

Maldonado, G.I., Turinsky, P.J. & Kropaczek, D.J. 1995, "Employing nodal generalized perturbation theory for the minimization of feed enrichment during pressurized water reactor in-core nuclear fuel management optimization", *Nuclear Science and Engineering,* vol. 121, pp. 312.

McKinley, M.S. & Rahnema, F. 2002, "Higher-order boundary condition perturbation theory for the neutron transport equation", *Nuclear Science and Engineering,* vol. 140, pp. 285-294.

McKinley, M.S. & Rahnema, F. 2000, "Higher-order boundary condition perturbation theory for the diffusion approximation", *Nuclear Science and Engineering,* vol. 136, pp. 15-33.

McKinley, M.S. & Rahnema, F. 1999, "A second-order accurate eigenvalue expression for boundary condition perturbation", *Proceedings of International Conference on Mathematics and Computation, Reactor Physics and Environmental Analysis in Nuclear Applications,* Madrid, Spain, September 27-30.

Mitani, H. 1973, "Higher order perturbation method in reactor calculations", *Nuclear Science and Engineering,* vol. 51, pp. 180-188.

Moore, B.R. & Turinsky, P.J. 1998, "Higher order generalized perturbation theory for boiling water reactor in-core fuel management optimization", *Nuclear Science and Engineering,* vol. 130, pp. 98-112.

Nair, P.B. 2001, "On the theoretical foundations of stochastic reduced basis methods", *Proceedings of the 42nd AIAA/ASME/ASCE/AHS/ASC Structures, Structural Dynamics*

and Materials Conference and Exhibition, American Institute of Aeronautics and Astronautics, pp. 1677.

Nair, P.B. & Keane, A.J. 2000, "Reduced basis representation of large-scale random eigenvalue problems", *Proceedings of the 41st AIAA/ASME/ASCE/AHS/ASC Structures, Structural Dynamics and Materials Conference and Exhibition,* American Institute of Aeronautics and Astronautics, pp. 1828.

Nobile, F., Tempone, R. & Webster, C.G. 2008a, "An anisotropic sparse grid stochastic collocation method for partial differential equations with random input data", *SIAM Journal on Numerical Analysis,* vol. 46, no. 5, pp. 2411-2442.

Nobile, F., Tempone, R. & Webster, C.G. 2008b, "A sparse grid stochastic collocation method for partial differential equations with random input data", *SIAM Journal on Numerical Analysis,* vol. 46, no. 5, pp. 2309-2345.

Noor, A.K. & Peters, J.M. 1983, "Multiple-parameter reduced basis technique for bifurcation and post-buckling analyses of composite plates", *International Journal for Numerical Methods in Engineering,* vol. 19, no. 12, pp. 1783-1803.

Noor, A.K. & Peters, J.M. 1981a, "Bifurcation and post-buckling analysis of laminated composite plates via reduced basis technique", *Computer Methods in Applied Mechanics and Engineering,* vol. 29, no. 3, pp. 271-295.

Noor, A.K. & Peters, J.M. 1981b, "Tracing post-limit-point paths with reduced basis technique", *Computer Methods in Applied Mechanics and Engineering,* vol. 28, no. 2, pp. 217-240.

Oblow , E.M. 1976, "Sensitivity theory from a differential viewpoint", *Nuclear Science and Engineering,* vol. 59, pp. 187-189.

Oblow, E.M. 1978, "Sensitivity theory for reactor thermal-hydraulics problems", *Nuclear Science and Engineering,* vol. 68, pp. 322-337.

Patera, A.T. & Rozza, G. 2007, *Reduced basis approximation and a posteriori error estimation for parametrized partial differential equations,* MIT Pappalardo Graduate Monographs in Mechanical Engineering.

Pomraning, G.C. 1986, "A variational treatment of the mixed boundary condition for the equilibrium diffusion equation", *Journal of Quantitative Spectroscopy and Radiative Transfer,* vol. 36, no. 5, pp. 471-481.

Pomraning, G.C. 1965, "A variational principle for linear systems", *Journal of Society for Industrial and Applied Mathematics,* vol. 13, no. 2, pp. 511-519.

Porsching, T. 1985, "Estimation of the error in the reduced basis method solution of nonlinear equations.", *Mathematics of Computation,* vol. 45, no. 172, pp. 487-496.

Radulescu, G., Gauld, I.C. & Ilas, G. 2010, *SCALE 5 predictions of PWR spent nuclear fuel isotopic compositions,* ORNL/TM-2010/44, Oak Ridge National Laboratory, Oak Ridge, TN.

Rahnema, F. & McKinley, M.S. 2002, "Higher-order cross section homogenization method", *Annals of Nuclear Energy,* vol. 29, no. 7, pp. 875-899.

Rahnema, F. 1981, *Generalized Boundary Perturbation Theory and GCFR Disruptive Core Parameterization*, University of California, Los Angeles.

Rathinam, M. & Petzold, L.R. 2004, "A new look at proper orthogonal decomposition", *SIAM Journal on Numerical Analysis,* vol. 41, no. 5, pp. 1893-1925.

Rearden, B.T. 2011, *TSUNAMI-1D: Control module for one-dimensional cross-section sensitivity and uncertainty analysis,* Version 6.1, ORNL/TM-2005/39, Oak Ridge National Laboratory, Oak Ridge, TN.

Rearden, B.T. 2004, "Perturbation theory eigenvalue sensitivity analysis with Monte Carlo techniques", *Nuclear Science and Engineering,* vol. 146, no. 3, pp. 367-382.

Rheinboldt, W.C. 1993, "On the theory and error estimation of the reduced basis method for multi-parameter problems", *Nonlinear Analysis: Theory, Methods & Applications,* vol. 21, no. 11, pp. 849-858.

Rowley, C.W. 2005, "Model reduction for fluids, using balanced proper orthogonal decomposition", *International Journal of Bifurcation Chaos in Applied Sciences and Engineering,* vol. 15, no. 3, pp. 997-1014.

Rozza, G. 2011, "Reduced basis approximation and error bounds for potential flows in parametrized geometries", *Communication in Computational Physics,* vol. 9, pp. 1-48.

Rozza, G. & Veroy, K. 2007, "On the stability of the reduced basis method for Stokes equations in parametrized domains", *Computer Methods in Applied Mechanics and Engineering,* vol. 196, no. 7, pp. 1244-1260.

RSICC 2011, *Scale: A comprehensive modeling and simulation suite for nuclear safety analysis and design,* ORNL/TM-2005/39, Version 6.1, Available from Radiation Safety Information Computational Center at Oak Ridge National Laboratory as CCC-785, Oak Ridge, TN.

Sachdeva, S.K., Nair, P.B. & Keane, A.J. 2006, "Hybridization of stochastic reduced basis methods with polynomial chaos expansions", *Probabilistic Engineering Mechanics,* vol. 21, no. 2, pp. 182-192.

Slesarev, I.S. & Sirotkin, A.M. 1971, "Use of variational functionals with variable boundaries for constructing approximate methods of solving the neutron transport equation", *USSR Computational Mathematics and Mathematical Physics,* vol. 11, no. 2, pp. 281-288.

Stacey, W.M. 1974, *Variational methods in nuclear reactor physics,* Academic Press, New York.

Su, B. & Pomraning, G.C. 1994, "A variational approach to stochastic transport", *Journal of Quantitative Spectroscopy and Radiative Transfer,* vol. 51, no. 3, pp. 467-483.

Usachev, L.N. 1964, "Perturbation theory for the breeding ratio and for other number ratios pertaining to various reactor process", *Journal of Nuclear Energy,* vol. 18, no. 10, pp. 571-583.

Van Geemert, R. 2001, "Development of parallelized higher-order generalized depletion perturbation theory for application in equilibrium cycle optimization", *Annals of Nuclear Energy,* vol. 28, no. 14, pp. 1377-1411.

Van Geemert, R. & Tani, F. 2005, "A polynomial form for higher-order accurate quantification of perturbation effects in nuclear systems", *Nuclear Science and Engineering,* vol. 149, no. 1, pp. 74-87.

White, J.R. & Swanbon, G.A. 1990, "Development of a technique for practical implementation of higher order perturbation theory", *Nuclear Science and Engineering,* vol. 105, pp. 160.

Wigner, E.P. 1992, "Effect of small perturbations on pile period" in *Nuclear Energy*, ed. A.M. Weinberg, Springer Berlin Heidelberg, pp. 540-552.

Willcox, K., Peraire, J. & Paduano, J.D. 2002, "Application of model order reduction to compressor aeroelastic models", *Journal of Engineering for Gas Turbines and Power,* vol. 124, no. 2, pp. 332-339.

Williams, M.L. 1986, "Perturbation theory for nuclear reactor analysis" in *CRC Handbook of Nuclear Reactors Calculations, Volume III*, ed. Y. Ronen, CRC Press, pp. 63-188.

Williams, M.L. 1978, *Development of depletion perturbation theory for coupled neutron/nuclide fields,* ORNL/TM-5958, Department of Energy, Oak Ridge National Laboratory, Oak Ridge, TN.

APPENDICES

Appendix A

MATLAB Code for Analytic Example

```
clear; clc;
% Define Operators;
A=[5.0 0.0; -1.0 2.0];
B=[3.0 1.5; 1.0 0.5];
% Solve Forward Equation;
[refflux k_ref]=eigs(B,A,1);
refflux=abs(refflux)/norm(refflux,1);
% Solve Adjoint Equation;
[aflux ka]=eigs(B',A',1);
% Define Perturbed Operator;
alpha=1;
dA=[alpha 0.0; 0.0 0.0];
% Perturb Input Parameters and Calculate the Flux Variations;
np=2;ng=2;nr=2;
mflux=zeros(ng,np);
for i=1:np
    alpha=rand(1)*2-1;
    dA=[alpha 0.0; 0.0 0.0];
    Ap=A+dA;
    [pflux kp]=eigs(B,Ap,1);
    pflux=abs(pflux)/norm(pflux,1);
    mflux(:,i)=pflux-refflux;
end
% Generate the Basis;
[Q S V]=svd(mflux,0);
gmflux=zeros(ng,nr);
% Solve the Generalized Adjoint Equation and Record the Solution:
gmflux;
Pa=A'-1/k_ref*B';
for i=1:1
    gmflux(:,i)=(Pa)\(Q(:,i)-Q(:,i)'*refflux(:)*ones(ng,1));
    beta=(gmflux(:,i)'*B*refflux)/(aflux'*B*refflux);
    gmflux(:,i)=gmflux(:,i)-beta*aflux;
end
% 100 Random Test Cases
Sigma_c1=3;
for i=1:100
    alpha=(rand(1)*2-1)*0.2*Sigma_c1;
    dA=[alpha 0.0; 0.0 0.0];
    Ap=A+dA;
    [pflux kp]=eigs(B,Ap,1);
    pflux=abs(pflux)/norm(pflux,1);
    lambda0=0;lambda1=0.00001;eta=1e-16;
```

```
    while (abs(lambda1-lambda0)>eta)
        dPa=dA-lambda1*B;
        Uk=dPa*Q;
        dPflx=-Uk*((eye(nr)+gmflux'*Uk)\(gmflux'*dPa*refflux));
        lambda0 = lambda1;
        lambda1=(aflux'*dA*refflux+aflux'*dPflx)/(aflux'*B*refflux);
    end
    dPa=dA-lambda1*B;
    Uk=dPa*Q;
    dpflux_epgpt=-Q*gmflux'*dPa*refflux
          +Q*gmflux'*Uk*((eye(nr)+gmflux'*Uk)\(gmflux'*dPa*refflux));
    dpflux_e=pflux-refflux;
    err_ka(i)=(kp-1/(1/k_ref+lambda1))*1e5;
    lbd_st=(aflux'*dA*refflux)/(aflux'*B*refflux);
    err_k0(i)=(kp-k_ref)*1e5-(-lbd_st*k_ref^2*1e5);
end
%
x=(1:100);
%plots
set(0,'DefaultAxesFontName', 'Arial');
set(0,'DefaultAxesFontSize', 12);
% Change default text fonts.
set(0,'DefaultTextFontname', 'Arial');
set(0,'DefaultTextFontSize', 12);
figure(1)
plot(x,err_k0,'ro',x,err_ka,'b.', 'LineWidth',2);
xlabel('Test Case'); ylabel('K_{eff}  Variational Error (pcm)');
h_legend=legend('1^{st}-Order GPT Approximation','E_PGPT
Approximation',3);
axis([0 100 0 2000]);
```

Appendix B

Higher-Order Generalized Perturbation (Rahnema's Method)

This Appendix explains how the method proposed by Rahnema for boundary conditions perturbations for eigenvalue problem is applied to cross sections perturbations for source-driven problem. Consider a source-driven diffusion model described by:

$$\mathbf{P}(\alpha)\phi = q_s(\alpha)$$

Perturbing the input parameters by some amounts where the flux variations are expanded in terms of powers of a small dimensionless parameter β :

$$\left(\mathbf{P}+\beta\Delta\mathbf{P}\right)\left(\phi+\beta\Delta\phi_1+\beta^2\Delta\phi_2+\cdots+\beta^i\Delta\phi_i+\cdots\right)=q_s+\beta\Delta q_s$$

Combining terms with common powers of β results in a series of higher-order perturbed equations given by:

$$\mathbf{P}\phi = q_s$$

$$\mathbf{P}\Delta\phi_1 = \Delta q_s - \Delta\mathbf{P}\phi$$

$$\mathbf{P}\Delta\phi_2 = -\Delta\mathbf{P}\Delta\phi_1$$

$$\mathbf{P}\Delta\phi_i = -\Delta\mathbf{P}\Delta\phi_{i-1}$$

As defined by Rahnema, ψ_j^* is the solution to

$$\mathbf{P}^*\psi_j^* = G_j$$

where $G_j \equiv \delta\left(x - x_j\right)\delta\left(E - E_j\right)$, we operate on the higher-order perturbed system with $\left\langle \psi_j^*, . \right\rangle$, we arrive at the following equations:

$$\left\langle \psi_j^*, \mathbf{P}\Delta\phi_1 \right\rangle = \left\langle \psi_j^*, \left(\Delta q_s - \Delta\mathbf{P}\phi_0\right) \right\rangle \Rightarrow \Delta\phi_1\left(x_j, E_j\right) = \left\langle G_j, \Delta\phi_1 \right\rangle = \left\langle \psi_j^*, \left(\Delta q_s - \Delta\mathbf{P}\phi_0\right) \right\rangle$$

$$\left\langle \psi_j^*, \mathbf{P}\Delta\phi_2 \right\rangle = \left\langle \psi_j^*, \left(-\Delta\mathbf{P}\Delta\phi_1\right) \right\rangle \Rightarrow \Delta\phi_2\left(x_j, E_j\right) = \left\langle G_j, \Delta\phi_2 \right\rangle = -\left\langle \psi_j^*, \Delta\mathbf{P}\Delta\phi_1 \right\rangle$$

$$\left\langle \psi_j^*, \mathbf{P}\Delta\phi_i \right\rangle = \left\langle \psi_j^*, \left(-\Delta\mathbf{P}\Delta\phi_{i-1}\right) \right\rangle \Rightarrow \Delta\phi_i\left(x_j, E_j\right) = \left\langle G_j, \Delta\phi_i \right\rangle = -\left\langle \psi_j^*, \Delta\mathbf{P}\Delta\phi_{i-1} \right\rangle$$

Finally, we can obtain the higher-order terms for the perturbed flux

$$\Delta\phi_n\left(x_j, E_j\right) = -\left\langle \psi_j^*, \Delta\mathbf{P}\Delta\phi_{n-1} \right\rangle$$

which can be summed to calculate the exact perturbed flux (which represents the response in our case study) as:

$$\tilde{\phi} = \phi + \Delta\phi_1 + \Delta\phi_2 + \cdots + \Delta\phi_i + \cdots$$